The Dissertation Committee for Abraham Levy Taicher
certifies that this is the approved version of the following dissertation:

Mixed Framework for Darcy-Stokes Mixtures

Committee:

Todd Arbogast, Supervisor

Marc Hesse, Co-Supervisor

Clint Dawson

Leszek Demkowicz

Omar Ghattas

Mixed Framework for Darcy-Stokes Mixtures

by

Abraham Levy Taicher, B.S., B.A.

DISSERTATION

Presented to the Faculty of the Graduate School of

The University of Texas at Austin

in Partial Fulfillment

of the Requirements

for the Degree of

DOCTOR OF PHILOSOPHY

THE UNIVERSITY OF TEXAS AT AUSTIN

May 2015

Dedicated to my parents, Gersh and Mery Taicher.

Acknowledgments

I wish to thank my advisors, Todd Arbogast and Marc Hesse, for spending countless hours with me. We really pounded our heads against parts of this project, but in the end we made some serious progress. I'd also like to thank Matthew Knepley and Jed Brown for their help introducing me to PETSc at Argonne National Labs. Though the final form of this project does not use PETSc explicitly, I borrowed a great deal of inspiration from their coding ideas.

Mixed Framework for Darcy-Stokes Mixtures

Publication No. _____

Abraham Levy Taicher, Ph.D.
The University of Texas at Austin, 2015

Supervisors: Todd Arbogast
Marc Hesse

We consider the system of equations arising from mantle dynamics introduced by McKenzie (J. Petrology, 1985). In this multi-phase model, the fluid melt velocity obeys Darcy's law while the deformable "solid" matrix is governed by a highly viscous Stokes equation. The system is then coupled through mass conservation and compaction relations. Together these equations form a coupled Darcy-Stokes system on a continuous *single-domain* mixture of fluid and matrix where the porosity ϕ, representing the relative volume of fluid melt to the bulk volume, is assumed to be much smaller than one. When coupled with solute transport and thermal evolution in a time-dependent problem, the model transitions dynamically from a non-porous single phase solid to a two-phase porous medium. Such mixture models have an advantage for numerical approximation since the free boundary between the one and two-phase regions need not be determined explicitly. The equations of mantle dynamics apply to a wide range of applications in deep earth physics such as mid-ocean ridges, subduction zones, and hot-spot volcanism, as well as to glacier dynamics and other two-phase flows in porous media.

In particular, mid-ocean ridges form when viscous corner flow of the solid mantle focuses fluid toward a central ridge. Melt is believed to migrate upward until it reaches the lithospheric "tent" where it then moves toward the ridge in a high porosity band. Simulation of this physical phenomenon requires confidence in numerical methods to handle highly heterogeneous porosity as well as the single-phase to two-phase transition.

In this work we present a standard mixed finite element method for the equations of mantle dynamics and investigate its limitations for vanishing porosity. While stable and optimally convergent for porosity bounded away from zero, the stability estimates we obtain suggest, and numerical results show, the method becomes unstable as porosity approaches zero. Moreover, the fluid pressure is no longer a physical variable when the fluid phase disappears and thus is not a good variable for numerical methods.

Inspired by the stability estimates of the standard method, we develop a novel stable mixed method with uniqueness and existence of solutions by studying a linear degenerate elliptic sub-problem akin to the Darcy part of the full model: $\mathbf{u} = -a(\phi)\nabla p$ and $\nabla \cdot (b(\phi)\mathbf{u}) + \phi p = \phi^{1/2} f$, where a and b satisfy $a(0) = b(0) = 0$ and are otherwise positive, and the *porosity* $\phi \geq 0$ may be zero on a set of positive measure. Using scaled variables and mild assumptions on the regularity of ϕ, we develop a practical mass-conservative method based on lowest order Raviart-Thomas finite elements.

Finally, we adapt the numerical method for the sub-problem to the full system of equations. We show optimal convergence for sufficiently smooth solutions

for a compacting column and mid-ocean ridge-like corner flow examples, and investigate accuracy and stability for less regular problems.

Table of Contents

List of Tables

List of Figures

Chapter 1

Introduction

The goal of the work presented here and my thesis project as a whole is to develop a mixed finite element method for the equations of mantle dynamics introduced by McKenzie [38]. In this multi-phase model, the fluid melt velocity obeys Darcy's law while the deformable "solid" matrix is governed by a highly viscous Stokes equation. The system is then coupled through mass conservation and compaction relations. Together these equations form a coupled Darcy-Stokes system on a continuous *single-domain* mixture of fluid and matrix where the porosity ϕ, representing the relative volume of fluid melt to the bulk volume, is assumed to be much smaller than one. The coupled equations are given by

$$\frac{\mu_f}{k_0}\phi^{-2(1+\Theta)}\mathbf{u} = -\nabla q_f, \qquad 0 \leq \Theta \leq \tfrac{1}{2} \tag{1.0.1}$$

$$\mu_m \nabla \cdot \mathbf{u} + \phi(q_f - q_m) = 0. \tag{1.0.2}$$

$$\nabla q_m - \nabla \cdot (2\mu_m(1-\phi)\mathcal{D}\mathbf{v}_m) + \nabla\left(\tfrac{5-2\phi}{3}\mu_m \nabla \cdot \mathbf{v}_m\right) = (1-\phi)\Delta\rho\mathbf{g}, \tag{1.0.3}$$

$$\mu_m \nabla \cdot \mathbf{v}_m - \phi(q_f - q_m) = 0, \tag{1.0.4}$$

where $\mathbf{u} = \phi(\mathbf{v}_f - \mathbf{v}_m)$ is the Darcy velocity (or scaled relative velocity), $\mathbf{v}_m$ is the matrix velocity, and q_f and q_m represent the fluid and matrix pressure potentials, respectively. Equations (1.0.1)–(1.0.2) look like Darcy's law for a compressible fluid,

and (1.0.3)–(1.0.4) resemble Stokes equation for a compressible fluid. When coupled with solute transport and thermal evolution in a time-dependent problem, the model transitions dynamically from a non-porous single phase solid to a two-phase porous medium. Such a mixture model has an advantage for numerical approximation since the free boundary between the one and two-phase regions need *not* be determined explicitly. The equations of mantle dynamics apply to a wide range of problems in deep earth physics [1, 30–32] such as mid-ocean ridges, subduction zones, and hot-spot volcanism, as well as to glacier dynamics [8, 28, 52] and other two-phase flows in porous media [13, 14, 20, 35].

Mid-ocean ridge phenomena is the physical problem that guides this project. Mid-ocean ridges (see Figure 2.1) form when viscous corner flow of the solid mantle focuses fluid toward a central ridge. Melt is believed to migrate upward until it reaches the lithospheric "tent" where it then moves toward the ridge in a high porosity band. Simulation of this physical phenomenon requires confidence in numerical methods to handle highly heterogeneous porosity as well as the single-phase to two-phase transition.

Mixed finite element methods (MFEM) are good candidates to model this system. MFEM have an extensive theory in both limiting cases of Darcy flow and Stokes flow. Moreover, velocity fields computed using MFEM are continuous on each element and have continuous normal component across element boundaries. Thus, MFEM are good candidates to couple with the transport equations since they allow for unambiguous determination of trajectories.

The project began by following the natural approach to modeling Darcy and

Stokes. The Stokes part is well-behaved. For test functions Ψ and w, the Darcy part (for homogeneous conditions) of the variational form looks like

$$\left(\frac{\mu_f}{k_0}\phi^{-2(1+\Theta)}\mathbf{u}, \Psi\right) - (q_f, \nabla\cdot\Psi) = 0, \tag{1.0.5}$$

$$(\nabla\cdot\mathbf{u}, w) + \left(\frac{\phi}{\mu_m}(q_f - q_m), w\right) = 0. \tag{1.0.6}$$

When deriving stability estimates we were only able to show

$$\|\phi^{-(1+\Theta)}\mathbf{u}\| + \|\phi^{-1/2}\nabla\cdot\mathbf{u}\| + \|\phi^{1/2}q_f\| \leq C\Delta\rho. \tag{1.0.7}$$

These bounds suggest that the fluid pressure may be *unbounded* as porosity vanishes. Indeed, the fluid pressure is no longer a physical variable when there is no fluid! Moreover, the condition number of the method is sure to blow up as porosity vanishes in part of the domain since we divide by ϕ in (1.0.5). Numerical results also bear these issues out. We were thoroughly unsatisfied with this approach and stuck without a formulation we could be confident in. This is especially relevant for mid-ocean ridges since we are interested in the high porosity band predicted at the one to two-phase boundary.

Thus began the chase for the exploding pressure. Unfortunately, we were unable to find a solution to the mantle equations where the pressure becomes unbounded as porosity decreases to zero in part of the domain. However, we do show it can blow up numerically. During this span of time, the project also took several tangents. I spent a great deal of time investigating the thermodynamics and phase behavior in the mantle (which is not included in this thesis but is the natural next step for further work). I also developed, with the generous help of Matt Knepely

and Jed Brown at Argonne National Labs, a parallel code for implementing mixed finite element methods in PETSc. This code was later scrapped and replaced with a general FEM code I wrote from scratch in MATLAB. As we did not have a formulation set in stone, the code needed generality and flexibility to handle the many future directions of the project and I felt that PETSc was not the right development direction.

The meandering nature of the project continued until, inspired by the stability estimates in (1.0.7), we derived a new method for scaled variables $\tilde{q}_f = \phi^{1/2} q_f$ and $\tilde{\mathbf{v}}_r = \phi^{1+\Theta}\mathbf{u}$ with uniqueness and existence of solutions. We develop the theory for this method by studying a linear degenerate elliptic problem akin to the Darcy part of the full model:

$$\mathbf{u} = -a(\phi)(\nabla p - \mathbf{g}) \qquad \text{in } \Omega, \tag{1.0.8}$$

$$\nabla \cdot \big(b(\phi)\mathbf{u}\big) + \phi p = \phi^{1/2} f \quad \text{in } \Omega, \tag{1.0.9}$$

where a and b satisfy $a(0) = b(0) = 0$ and are otherwise positive, and the porosity $\phi \geq 0$ may be zero on a set of positive measure (choosing a, b, $\mathbf{g}$, and f appropriately we can recover (1.0.1)–(1.0.2)). Degenerate elliptic equations have been approximated in many works [7, 16, 25, 36, 37], using weighted Sobolev spaces and least squares techniques, but in these works the degeneracies are isolated to the boundary of the domain. With mild assumptions on the regularity of ϕ, we produce a new practical, mass-conservative method based on lowest order Raviart-Thomas finite elements, and adapt the numerical method for (1.0.8)–(1.0.9) to the full system of equations. This new method is *stable* even for zero porosity (i.e., the

one-phase case) where the scaled fluid pressure $\tilde{q}_f$ remains well-defined by (1.0.7). The method also shows optimal convergence for sufficiently smooth solutions for a compacting column and mid-ocean ridge-like corner flow examples, and extends to problems with less regular parameters as well.

The outline for this thesis is as follows. In chapter 2, I give an overview of the physics of mid-ocean ridges, describing the size of the melting region, the characteristic velocities in the mantle, and general properties of the porosity. Then, following the derivation of McKenzie, I arrive at equations (1.0.1)–(1.0.4) from general conservation laws. In chapter 3, I present some general theory for Hilbert spaces. I then present a weak formulation for the mantle equations assuming porosity is bounded away from zero. I obtain stability estimates for general boundary conditions and investigate the behavior as porosity goes to zero. In chapter 4, I present a discrete mixed method to the weak form presented in chapter 3. I show this method is indeed well-behaved for positive porosity, but fails as porosity approaches zero. Chapter 5 is devoted to the degenerate problem (1.0.8)–(1.0.9). In this chapter, I introduce a new Hilbert space as the search space for the relative velocity, and prove unique solvability for new scaled variables. I then present a discrete mixed method to (1.0.8)–(1.0.9) and investigate its properties through various numerical tests. In chapter 6, I prove uniqueness and existence to the full equations (1.0.1)–(1.0.4) with scaled variables. Finally, in chapter 7, I write down a new discrete mixed method for the full system of equations and show it is well-behaved as porosity approaches zero (or becomes zero) for the compacting column.

Chapter 2

Mantle Dynamics

2.1 Melt migration beneath mid-ocean ridges

The processes by which magma is removed from partially molten mantle beneath mid-ocean ridges are of considerable interest to Earth scientists because they lead to formation of oceanic plates. Research into the processes governing melt migration beneath mid-ocean ridges has shed some light on the underlying process, but a great deal still remains a mystery. Geoscientists have investigated mid-ocean ridge phenomena using a variety of techniques including geochemical analysis of samples dredged from mid-ocean ridges, seismic data, laboratory experiments, magnetic measurements, mantle outcrops (ophiolites), and computational models. Put together, these studies have produced constraints on melt and solid velocities, as well as various constraints on porosity.

1. *Geometry of the melting region*

   Seismic data show a low velocity region roughly 100 km deep and 400 km wide (not necessarily symmetric) about the ridge axis, as shown in Fig. 2.1. The major element composition of mid-ocean ridge basalts (MORB), or crystallized magma, indicate that most melting takes place at depths shallower than 60 km. Uranium series disequilibria and trace element compositions

suggest that some melting occurs as deep as 150 *km* [45].

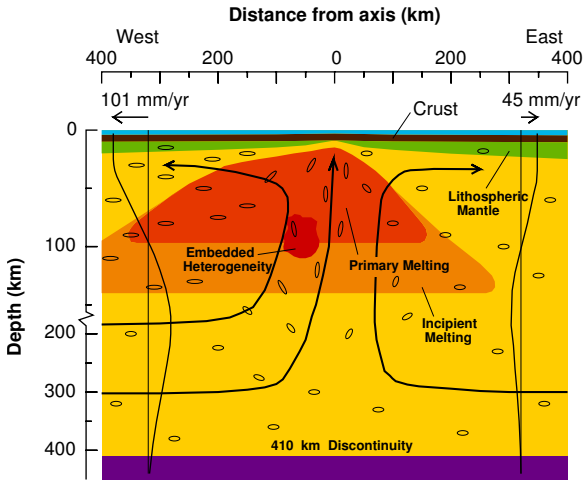

Figure 2.1: Schematic cross-section of the East Pacific Rise at 17^0S. The broad asymmetric region of low seismic velocities is the primary melt production region. The small ellipses represent the direction of preferred long axis alignment of olivine, with flatness increasing with increasing degree of alignment [45].

2. *Mantle porosity is interconnected even for very low porosities and melt extraction is "near-fractional"*

   Melt is believed to form between mantle rock crystal (primarily olivine) boundaries [55]. Three dimensional data obtained using x-ray synchrotron microtomography shows connectivity of the mantle for porosity as low as 2% (see Fig. 2.2). Moreover, melt extraction remains qualitatively similar as porosity increases to 20% [55]. Radioactivity $[^{238}U/^{230}Th]$ ratios point to efficient melt extraction for porosities as low as 0.2% [39]. In fact, A geometry argument presented by Von Bargen [53] shows that the olivine crystal structure, even for infinitesimal porosity, must be connected.

MORBs are not in equilibrium with residual peridotite with respect to orthopyroxene content. This implies that melting is "near-fractional." As soon as melt forms it is extracted. Efficient melt extraction therefore indicates that porosity is not likely to be much larger than 2% anywhere in the mantle [33] which is also in agreement with seismic data predictions of 2% average porosity [45].

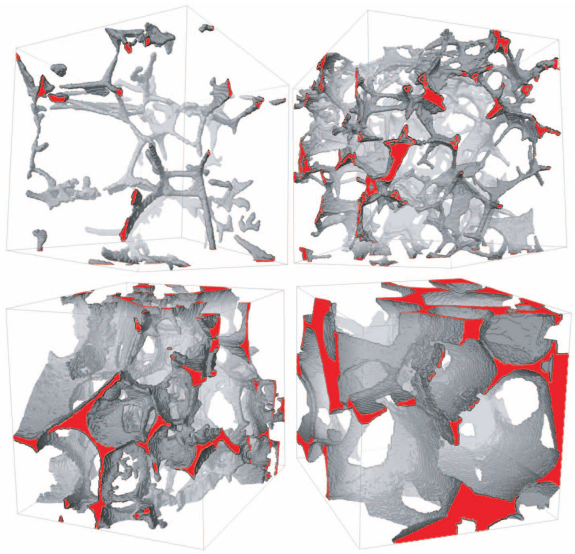

Figure 2.2: 3D melt distribution of olivine-basalt aggregates. The size of each cube is 14 μm^3 with melt fractions (top-left) .02, (top-right) .05, (bottom-left) .10, and (bottom-right) .20. Gray represents interfaces between melt and olivine crystals and red represents interior melt channels. Olivine crystals reside in the hollow space [55].

3. *Porosity is highly heterogeneous and anisotropic*

   MORB disequilibria with residual orthopyroxene implies that mantle melts must travel in high porosity dunite channels. Otherwise, melt in contact with

the solid matrix would re-equilibrate. Dunite channel zones are also visible in the Oman ophiolite (mantle outcrop) [33].

4. *The solid matrix moves by viscous flow*

   For geologic time scales and high temperatures of the deep earth, mantle rock behaves like a highly viscous fluid. Mantle viscosity, estimated to be around 10^{19}–10^{21} $Pa\,s$, has been deduced through study of mineral physics, post-glacial rebound, and large scale mantle flow [50].

5. *Melt and matrix velocity*

   Decompression melting resulting from post-glacial volcanism in Iceland implies melt velocities of about 50 m/yr [33]. In addition, preservation of isotope disequilibria requires melt flow of 10-100 m/yr [33]. Matrix velocities are deduced from the movement of oceanic plates and vary from 2 cm/yr in slow spreading ridges to 10 cm/yr in the fastest spreading ridges (see Fig. 2.1) of the pacific [45].

6. *Melt is focused toward the ridge center*

   While the exact cause of melt focusing remains a source of debate, it has been firmly established that neither lithostatic pressure gradients nor fractures are responsibly for focusing melt toward the ridge axis. Spiegelman [48] proposed that partial crystallization of melt rising in the conductively cooled lithosphere on either side of a ridge may create a permeability barrier that impedes vertical melt flow. Since the base of the lithosphere slopes toward the ridge axis (see Fig. 2.1), ascending melt would migrate toward the ridge

in a high porosity band. Meanwhile, Phipps Morgan [41] suggests anisotropy in permeability due to the orientation of olivine might focus melt toward the ridge axis.

2.2 Governing equations for the mechanical system

The following section follows the derivation of the mechanical equations according to Mckenzie [38]. This and other models of flow in the earth's mantle [1, 30–32] are based on a mixture of fluid melt and matrix solid, where both fluid and solid phases are assumed to exist *at each point* of the domain. Porosity, denoted by ϕ, is defined as the volume fraction of melt and is assumed to be much less than one. The mixture model holds even when one phase disappears (i.e., $\phi = 0$). Such models have an advantage for numerical approximation since the free boundary between the one and two phase regions *need not* be determined explicitly, and, in a time-dependent problem, the equations remain unaltered when a phase disappears or forms in some region of the domain. Though this work does not address solutions to the time-dependent model, the transport equations, including energy and composition, following the derivation by Katz [32], are presented in appendix B.

If Ψ is a conserved quantity within a fixed domain Ω, the change in Ψ must equal the rate Ψ is transported across the boundary $\partial\Omega$ plus the production rate R of Ψ inside Ω. A conservation equation can thus be written as

$$\int_\Omega \frac{\partial \Psi}{\partial t}\, d\mathbf{x} = \frac{\mathrm{d}}{\mathrm{d}t}\int_\Omega \Psi\, d\mathbf{x} = -\int_{\partial\Omega} \Psi\, \mathbf{v}\cdot\boldsymbol{\nu}\, d\mathbf{s} + \int_\Omega R\, d\mathbf{x}, \tag{2.2.1}$$

where $\mathbf{v}$ is the velocity that transports Ψ, ν is the outward pointing normal vector to $\partial\Omega$, and we assume the time derivative in the left-hand side can be moved inside the integral.

2.2.1 Conservation of mass

Assume a continuous *overlying* mixture of melt and solid matrix. If $\Psi = \rho_f \phi$ is the mass of melt per unit volume, an application of the divergence theorem followed by Lebesgue's Lemma (i.e., if (2.2.1) holds for any domain Ω then the integrands must sum to zero) gives

$$\frac{\partial(\rho_f \phi)}{\partial t} + \nabla \cdot (\rho_f \phi \mathbf{v}_f) = m, \tag{2.2.2}$$

where the melting rate m is the rate at which mass is transferred from matrix to fluid and $\mathbf{v}_f$ is the fluid velocity. Similarly, conservation of mass in the matrix, i.e., setting $\Psi = \rho_m(1-\phi)$, leads to

$$\frac{\partial\big(\rho_m(1-\phi)\big)}{\partial t} + \nabla \cdot \big(\rho_m(1-\phi)\mathbf{v}_m\big) = -m, \tag{2.2.3}$$

with $\mathbf{v}_m$ representing the matrix velocity.

2.2.2 Conservation of momentum

To conserve momentum in the matrix take $\Psi = (1-\phi)\rho_m \mathbf{v}_m$. In this case the source term $\mathbf{R}$ consists of three contributions. First is the force due to gravity. Second, denoted by $\mathbf{F}_{\text{int}}$, is the body force per unit volume on the matrix produced by motion in the fluid. Third, denoted by the tensor σ^m, is the stress acting on the

matrix. Equation (2.2.1) is expanded to

$$\int_\Omega \frac{\partial}{\partial t}((1-\phi)\rho_m \mathbf{v}_m)\,d\mathbf{x} = -\int_{\partial\Omega}(1-\phi)\rho_m \mathbf{v}_m \otimes \mathbf{v}_m \cdot \nu\,d\mathbf{s} - \int_\Omega (1-\phi)\rho_m \mathbf{g}\,d\mathbf{x} + \int_\Omega \mathbf{F}_{\text{int}}\,d\mathbf{x} + \int_{\partial\Omega}(1-\phi)\sigma^m \cdot \nu\,d\mathbf{s}, \tag{2.2.4}$$

where $\mathbf{g}$ is the gravitational constant vector pointing downward. Assuming area and volume fraction are equal, the stress tensor σ^m is multiplied by $1-\phi$ in the rightmost term of (2.2.4) since it only acts on the solid surface. For the fluid, take $\Psi = \phi\rho_f \mathbf{v}_f$. A similar equation holds with the stress tensor, σ^f, multiplied by ϕ, and $\mathbf{F}_{\text{int}}$ substituted with $-\mathbf{F}_{\text{int}}$ according to Newton's third law. It is given by

$$\int_\Omega \frac{\partial}{\partial t}(\phi\rho_f \mathbf{v}_f)\,d\mathbf{x} = -\int_{\partial\Omega}\phi\rho_f \mathbf{v}_f \otimes \mathbf{v}_f \cdot \nu\,d\mathbf{s} - \int_\Omega \phi\rho_f \mathbf{g}\,d\mathbf{x} - \int_\Omega \mathbf{F}_{\text{int}}\,d\mathbf{x} + \int_{\partial\Omega}\phi\sigma^f \cdot \nu\,d\mathbf{s}. \tag{2.2.5}$$

In the case of mantle convection, both melt and matrix velocities are small. Thus, the rate of advection of momentum directly through flow (first term of the right-hand side of (2.2.4) and (2.2.5)) and the rate of change of momentum (left-hand side of (2.2.4) and (2.2.5)) are negligible in comparison to momentum diffusion by viscous effects. Therefore, forces maintaining motion must always be balanced by resistive forces. For both fluid and solid phases, this is equivalent to a small Reynolds number

$$Re = \frac{\rho|\mathbf{v}|L}{\mu} \ll 1, \tag{2.2.6}$$

where L is a characteristic length, $|\mathbf{v}|$ is a characteristic velocity, ρ is either matrix or fluid density, and μ is the (dynamic) viscosity. Table 2.1 lists representative value

of parameters for the fluid and matrix phases and shows that *Re* is indeed expected to be small.

Meaning	Variable	Value or Range	Units
Grain size	a	10^{-3}	m
Matrix length scale	L	10^{4}-10^{5}	m
Char. fluid velocity	$\lvert\mathbf{v}_f\rvert$	10^{-6}-10^{-8}	m/s
Ridge spreading rate	$\lvert\mathbf{v}_m\rvert$	10^{-10}-10^{-9}	m/s
Shear viscosity	μ_m	10^{19}	$Pa\ s$
Permeability constant	k_0	10^{-9}-10^{-6}	m^2
Fluid viscosity	μ_f	1	$Pa\ s$
Matrix Density	ρ_m	3300	kg/m^3
Fluid Density	ρ_f	2800	kg/m^3
Gravity	g	9.8	m/s^2

Table 2.1: Representative value of parameters for mantle dynamics. Grain size represents the average size of a matrix grain around which fluid flows. The ridge spreading rate is the rate at which ocean floor is spreading at mid-ocean ridges.

After applying the above assumptions, conservation of momentum for the fluid and matrix reduce to the differential equations

$$(1-\phi)\rho_m\mathbf{g}+\mathbf{F}_{\text{int}}+\nabla\cdot\left((1-\phi)\boldsymbol{\sigma}^m\right)=0, \tag{2.2.7}$$

$$\phi\rho_f\mathbf{g}-\mathbf{F}_{\text{int}}+\nabla\cdot(\phi\boldsymbol{\sigma}^f)=0. \tag{2.2.8}$$

The interphase volume force $\mathbf{F}_{\text{int}}$ can not depend on which frame is used to measure the velocity, whether it is one attached to the matrix or fluid, and $\mathbf{F}_{\text{int}}$ must also account for forces arising from gradients in porosity [24]. The simplest form of $\mathbf{F}_{\text{int}}$ satisfying Darcy's Law (see (2.2.12) below) is therefore given by

$$\mathbf{F}_{\text{int}}=C(\mathbf{v}_f-\mathbf{v}_m)-p_f\nabla\phi. \tag{2.2.9}$$

Meanwhile, assuming negligible deviatoric stress in the fluid,

$$\sigma^f = -p_f \mathbf{I}. \tag{2.2.10}$$

Substituting (2.2.9) and (2.2.10) into (2.2.8), and applying the product rule gives

$$\mathbf{v}_f - \mathbf{v}_m = -\frac{\phi}{C}\nabla(p_f - \rho_f \mathbf{g} z), \tag{2.2.11}$$

where z corresponds to depth. For compatibility with Darcy's Law (i.e., if $\mathbf{v}_m = 0$), (2.2.11) should reduce to

$$\phi \mathbf{v}_f = -\frac{k_\phi}{\mu_f}\nabla(p_f - \rho_f \mathbf{g} z), \tag{2.2.12}$$

where k_ϕ is the porosity dependent permeability and μ_f is the melt viscosity. This requires

$$C = \frac{\mu_f \phi^2}{k_\phi}. \tag{2.2.13}$$

The stress acting on the matrix requires a more complicated expression to account for shear forces and is given by

$$\sigma^m = -p_m \mathbf{I} + \mu_m \Big(\nabla \mathbf{v}_m + \nabla \mathbf{v}_m^T - \frac{2}{3}\nabla \cdot \mathbf{v}_m \mathbf{I} \Big), \tag{2.2.14}$$

where μ_m is the matrix shear viscosity. For a quantity Ψ, define the mixture variable

$$\overline{\Psi} = \phi \Psi_f + (1-\phi)\Psi_m. \tag{2.2.15}$$

Then, adding (2.2.8) and (2.2.7), the mixture obeys Stokes equation

$$\overline{\sigma} = \phi \sigma_f + (1-\phi)\sigma_m = -\overline{p}\mathbf{I} + \mu_m(1-\phi)\Big(\nabla \mathbf{v}_m + \nabla \mathbf{v}_m^T - \frac{2}{3}\nabla \cdot \mathbf{v}_m \mathbf{I} \Big), \tag{2.2.16}$$

$$\nabla \cdot \overline{\sigma} = \overline{\rho}\mathbf{g}. \tag{2.2.17}$$

2.2.3 Compaction

We close the mechanical system by relating the solid and fluid pressures through a compaction relation [46]

$$p_m - p_f = -\zeta_m \nabla \cdot \mathbf{v}_m, \tag{2.2.18}$$

where ζ_m is the matrix bulk viscosity. This equation can be interpreted as the compressibility of the matrix. If the matrix pressure is larger than the fluid pressure, the matrix volume should contract (i.e., $\nabla \cdot \mathbf{v}_m < 0$).

2.2.4 Summary of the mechanical equations

Mantle permeability is calculated according to the standard Kozeny-Carmen relationship [13, 55], simplified for small porosity and constant grain size to

$$k_\phi = k_0 \phi^{2(1+\Theta)}, \qquad 0 \leq \Theta \leq \tfrac{1}{2}. \tag{2.2.19}$$

The shear viscosity is taken to be constant while the matrix bulk viscosity,

$$\zeta_m = \frac{\mu_m}{\phi}, \tag{2.2.20}$$

is proportional to the inverse of porosity.

A total of four equations govern the mechanical system. Adding (2.2.2) and (2.2.3) to eliminate the melting rate m, substituting constitutive relations (2.2.19) and (2.2.20), and applying the *Boussinesq approximation* [47] (constant and equal

densities for non-buoyancy terms) gives

$$\mathbf{v}_f - \mathbf{v}_m = -\frac{k_0 \phi^{1+2\Theta}}{\mu_f} \nabla (p_f - \rho_f g \mathbf{z}), \tag{2.2.21}$$

$$\nabla \cdot \overline{\mathbf{v}} = 0, \tag{2.2.22}$$

$$\nabla \overline{p} - \nabla \cdot (2\mu_m (1-\phi) \mathcal{D}\mathbf{v}_m) + \nabla \left(\frac{2}{3} \mu_m (1-\phi) \nabla \cdot \mathbf{v}_m \right) = \overline{\rho} \mathbf{g}, \tag{2.2.23}$$

$$\phi (p_m - p_f) = -\mu_m \nabla \cdot \mathbf{v}_m, \tag{2.2.24}$$

where $\mathcal{D}\mathbf{v}_m = \frac{1}{2}(\nabla \mathbf{v}_m + \nabla \mathbf{v}_m^T)$ is the symmetric gradient. Equation (2.2.21) describes fluid flow around matrix "grains" with permeability strongly dependent on porosity. Equation (2.2.22) is a balance of mass between the fluid and matrix. Equation (2.2.23) shows that changes in the mixture pressure depend on the shear deformation of the matrix and the mixture buoyancy of the fluid and matrix. Equation (2.2.24) shows the compressibility of the matrix is strongly dependent on porosity.

Chapter 3

A Mixed Formulation for Positive Porosity

In this chapter we develop a mixed finite element method for the mantle equations where we assume *porosity is bounded away from zero*, i.e., $\phi \geq \phi_* > 0$. First, we rewrite the equations in a symmetric form that reveals their Darcy-Stokes nature. We then introduce the essential Hilbert space theory to define appropriate spaces to search for solutions and interpret boundary conditions. Finally, we obtain stability estimates for general boundary conditions and investigate their behavior as porosity vanishes. These observations inspire a novel method developed in chapter 5. In chapter 4 we implement a discrete version method developed in this chapter and observe its limitations as porosity approaches zero.

3.1 Symmetric form of the Darcy-Stokes mixture

Introduce the new variables

$$\mathbf{u} = \phi(\mathbf{v}_f - \mathbf{v}_m),$$

$$q_f = p_f - \rho_f g z,$$

$$q_m = p_m - \rho_f g z,$$

where $\mathbf{u}$ is a scaled relative velocity or Darcy velocity (representing mass flux), q_f is the fluid pressure potential, and q_m is the matrix pressure potential (note that

q_m is defined using the *fluid* density ρ_f). We will refer to the pressure and pressure potential interchangeably when the meaning is clear. Compaction (2.2.18) becomes

$$\mu_m \nabla \cdot \mathbf{v}_m = \phi (q_f - q_m),$$

and substituting into (2.2.22) transforms conservation of mass into

$$\mu_m \nabla \cdot \mathbf{u} + \phi (q_f - q_m) = 0.$$

We have the four equations,

$$\frac{\mu_f}{k_0} \phi^{-2(1+\Theta)} \mathbf{u} = -\nabla q_f, \tag{3.1.1}$$

$$\nabla \cdot \mathbf{u} + \tfrac{\phi}{\mu_m}(q_f - q_m) = 0. \tag{3.1.2}$$

$$\nabla q_m - \nabla \cdot (2\mu_m(1-\phi)\mathcal{D}\mathbf{v}_m) + \nabla\left(\tfrac{5-2\phi}{3}\mu_m \nabla \cdot \mathbf{v}_m\right) = (1-\phi)\Delta\rho \mathbf{g}, \tag{3.1.3}$$

$$\nabla \cdot \mathbf{v}_m - \tfrac{\phi}{\mu_m}(q_f - q_m) = 0, \tag{3.1.4}$$

where $\Delta\rho = \rho_m - \rho_f > 0$ is the density difference between the solid and fluid phases. The variable transformations also changes the matrix stress to

$$\sigma_m = -q_m \mathbf{I} + \mu_m(1-\phi)\left(2\mathcal{D}\mathbf{v}_m - \tfrac{5-2\phi}{3}\mu_m \nabla \cdot \mathbf{v}_m \mathbf{I}\right). \tag{3.1.5}$$

This form of the equations allows us to interpret (3.1.1)–(3.1.2) as compressible Darcy, and (3.1.3)–(3.1.4) as compressible Stokes, coupled by the pressure difference, $q_f - q_m$.

3.1.1 Hilbert spaces

Before building the weak formulation, we establish the Hilbert spaces wherein solutions can be found. Let Ω be a bounded Lipschitz domain in $\mathbb{R}^d$ with outward

pointing normal ν. The space $L^2(\Omega)$ denotes all square integrable functions on Ω. It is equipped with the inner product

$$(u,v) = (u,v)_{L^2(\Omega)} = \int_\Omega uv \, d\mathbf{x} \tag{3.1.6}$$

and associated norm $\|u\| = \|u\|_{L^2(\Omega)} = (u,u)^{1/2}$. Denote by $H^1(\Omega)$ all square integrable functions with square integrable weak derivatives. This space has the corresponding norm

$$\|u\|_1 = \|u\|_{H^1(\Omega)} = \left(\int_\Omega |u|^2 d\mathbf{x} + \int_\Omega |\nabla u|^2 d\mathbf{x} \right)^{1/2}. \tag{3.1.7}$$

Let $H(\mathrm{div};\Omega)$ denote all square integrable vector-valued functions with square integrable weak divergence, and equip it with the norm

$$\|\mathbf{u}\|_{\mathrm{div}} = \|\mathbf{u}\|_{H(\mathrm{div};\Omega)} = \left(\int_\Omega |\mathbf{u}|^2 d\mathbf{x} + \int_\Omega |\nabla \cdot \mathbf{u}|^2 d\mathbf{x} \right)^{1/2}. \tag{3.1.8}$$

Both $L^2(\Omega)$ and $H^1(\Omega)$ extend to spaces on vector-valued (or matrix-valued) functions $(L^2(\Omega))^d$ and $(H^1(\Omega))^d$, respectively, by requiring each component be in its proper space. Note that $(H^1(\Omega))^d \subset H(\mathrm{div};\Omega) \subset (L^2(\Omega))^d$.

For functions defined on the boundary, let $\langle \cdot, \cdot \rangle_{\partial\Omega}$ denote the $L^2(\partial\Omega)$ inner product or duality pairing. We can extend functions in $H^1(\Omega)$ to the boundary $\partial\Omega$ using the trace lemma [2]:

Lemma 3.1.1. *There exists a bounded linear operator $\gamma : H^1(\Omega) \to H^{1/2}(\partial\Omega)$ such that, for a constant C_Ω depending only on the geometry of Ω,*

$$\gamma(u) = u|_{\partial\Omega} \quad \textit{for } u \in H^1(\Omega) \cap C(\overline{\Omega}), \tag{3.1.9}$$

$$\|\gamma(u)\|_{1/2,\partial\Omega} \leq C_\Omega \|u\|_1, \tag{3.1.10}$$

For our purposes, $H^{1/2}(\partial\Omega) \subset L^2(\partial\Omega)$ is simply the image of γ and we leave out a definition of the norm $\|u\|_{1/2,\partial\Omega} = \|u\|_{H^{1/2}(\partial\Omega)}$ as we are only interested in its existence. For functions in $H(\mathrm{div};\Omega)$ a similar lemma holds:

Lemma 3.1.2. *There exists a bounded linear operator $\gamma_\nu : H(div;\Omega) \to H^{-1/2}(\partial\Omega) = (H^{1/2}(\partial\Omega))^*$ such that, for a constant C_Ω depending only on the geometry of Ω,*

$$\gamma_\nu(\mathbf{u}) = \mathbf{u}\cdot\nu|_{\partial\Omega} \quad \textit{for } \mathbf{u} \in H(div;\Omega) \cap (C(\overline{\Omega}))^d, \tag{3.1.11}$$

$$\|\gamma_\nu(\mathbf{u})\|_{-1/2,\partial\Omega} \leq C_\Omega \|\mathbf{u}\|_{div}. \tag{3.1.12}$$

To derive the latter lemma, we use integration by parts to get, for $w \in H^{1/2}(\partial\Omega)$,

$$\langle \gamma_\nu(\mathbf{u}), w\rangle = (\nabla\cdot\mathbf{u}, w) + (\mathbf{u}, \nabla w),$$

where we have extended w to $H^1(\Omega)$.

3.1.2 Boundary conditions in two dimensions

Let τ be the tangent vector to $\partial\Omega$ following the right-hand rule. For the Darcy part, set either Neumann or Robin boundary conditions

$$\begin{cases} \mathbf{u}\cdot\nu = \phi^{1/2} g_f^N, & \text{on } \Gamma_f^N, \\ \phi q_f - \kappa_f^2 \mathbf{u}\cdot\nu = \phi^{1/2} g_f^R, & \text{on } \Gamma_f^R, \end{cases} \quad \overline{\Gamma_f^N} \cup \overline{\Gamma_f^R} = \partial\Omega, \tag{3.1.13}$$

where $\kappa_f \geq 0$ is bounded. The scaling by ϕ will become clear as we develop stability estimates in the following section. For the Stokes part, set either Neumann or Robin boundary conditions for each component,

$$\begin{cases} \mathbf{v}_m\cdot\nu = g_m^{\nu,N}, & \text{on } \Gamma_m^{\nu,N}, \\ \sigma_m(q_m,\mathbf{v}_m)\nu\cdot\nu - \kappa_\nu^2 \mathbf{v}_m\cdot\nu = g_m^{\nu,R}, & \text{on } \Gamma_m^{\nu,R}, \end{cases} \quad \overline{\Gamma_m^{\nu,N}} \cup \overline{\Gamma_m^{\nu,R}} = \partial\Omega, \tag{3.1.14}$$

$$\begin{cases} \mathbf{v}_m \cdot \tau = g_m^{\tau,N}, & \text{on } \Gamma_m^{\tau,N}, \\ \sigma_m(q_m, \mathbf{v}_m)\nu \cdot \tau - \kappa_\tau^2 \mathbf{v}_m \cdot \tau = g_m^{\tau,R}, & \text{on } \Gamma_m^{\tau,R}, \end{cases} \quad \overline{\Gamma_m^{\tau,N}} \cup \overline{\Gamma_N^{\tau,R}} = \partial\Omega, \tag{3.1.15}$$

where $\kappa_\nu, \kappa_\tau \geq 0$ and bounded. Suppose also that we can extend g_f^N to $\mathbf{u}^N$ in Ω such that

$$\mathbf{u}^N \cdot \nu = \phi^{1/2} g_f^N \quad \text{on } \Gamma_f^N, \tag{3.1.16}$$

and similarly let $\mathbf{v}_m^{\nu,N}$ and $\mathbf{v}_m^{\tau,N}$ be extensions into Ω of $g_m^{\nu,N}$ and $g_m^{\tau,N}$, respectively, such that

$$\mathbf{v}_m^{\nu,N} \cdot \nu = g_m^{\nu,N}, \qquad \mathbf{v}_m^{\tau,N} \cdot \nu = 0, \qquad \text{on } \Gamma_m^{\nu,N}, \tag{3.1.17}$$

$$\mathbf{v}_m^{\nu,N} \cdot \tau = 0, \qquad \mathbf{v}_m^{\tau,N} \cdot \tau = g_m^{\tau,N}, \qquad \text{on } \Gamma_m^{\tau,N}. \tag{3.1.18}$$

3.1.3 Weak formulation

Consider the following spaces, each with its natural norm, for the unknown quantities:

$$\begin{aligned} V_r &= H(\text{div};\Omega) \cap \{\mathbf{v} \cdot \nu = 0 \text{ on } \Gamma_f^N\}, \\ V_m &= (H^1(\Omega))^d \cap \{\mathbf{v} \cdot \nu = 0 \text{ on } \Gamma_m^{\nu,N}\} \cap \{\mathbf{v} \cdot \tau = 0 \text{ on } \Gamma_m^{\tau,N}\}, \\ W_m &= W_f = L^2(\Omega). \end{aligned} \tag{3.1.19}$$

Note that if $\Gamma_f^R = \Gamma_m^{\nu,R} = \emptyset$ then the pressures are defined only up to their difference. In this case, we eliminate the constant nullspace by setting $W_f = L_0^2(\Omega) = L^2(\Omega) \cap \left\{ \int_\Omega w = 0 \right\}$ (or alternatively setting the fluid pressure at some point in the domain). For the weak form, we modify the test and trial spaces according to the Neumann boundary conditions while the Robin boundary conditions are naturally inserted into the weak formulation. The weak formulation of equations (3.1.1)–(3.1.4) is

Find $\mathbf{u} \in V_r + \mathbf{u}^N$, $\mathbf{v}_m \in V_m + \mathbf{v}_m^{\nu,N} + \mathbf{v}_m^{\tau,N}$, $q_f \in W_f$, and $q_m \in W_m$ such that

$$\begin{aligned}\left(\frac{\mu_f}{k_0}\phi^{-2(1+\Theta)}\mathbf{u}, \Psi_r\right) - (q_f, \nabla\cdot\Psi_r) + \langle \kappa_f \phi^{-1}\mathbf{u}\cdot\nu, \Psi_r\cdot\nu\rangle_{\Gamma_f^R} \\ = -\langle g_f^R, \phi^{-1/2}\Psi_r\cdot\nu\rangle_{\Gamma_f^R} \qquad \forall \Psi_r \in V_r,\end{aligned} \tag{3.1.20}$$

$$(\nabla\cdot\mathbf{u}, w_f) + \left(\frac{\phi}{\mu_m}(q_f - q_m), w_f\right) = 0 \qquad \forall w_f \in W_f, \tag{3.1.21}$$

$$\begin{aligned}-(q_m, \nabla\cdot\Psi_m) + \left(2\mu_m(1-\phi)\mathcal{D}\mathbf{v}_m, \mathcal{D}\Psi_m\right) - \left(\tfrac{5-2\phi}{3}\mu_m\nabla\cdot\mathbf{v}_m, \nabla\cdot\Psi_m\right) \\ + \langle \kappa_\nu^2 \mathbf{v}_m\cdot\nu, \Psi_m\cdot\nu\rangle_{\Gamma_m^{\nu,R}} + \langle \kappa_\tau^2 \mathbf{v}_m\cdot\tau, \Psi_m\cdot\tau\rangle_{\Gamma_m^{\tau,R}} \\ = \langle g_m^{\nu,R}, \Psi_m\cdot\nu\rangle_{\Gamma_m^{\nu,R}} + \langle g_m^{\tau,R}, \Psi_m\cdot\tau\rangle_{\Gamma_m^{\tau,R}} \\ + \left((1-\phi)\Delta\rho\mathbf{g}, \Psi_m\right) \qquad \forall \Psi_m \in V_m,\end{aligned} \tag{3.1.22}$$

$$(\nabla\cdot\mathbf{v}_m, w_m) - \left(\frac{\phi}{\mu_m}(q_f - q_m), w_m\right) = 0 \qquad \forall w_m \in W_m. \tag{3.1.23}$$

3.2 Stability estimates: degenerate porosity limit

If porosity is allowed to vanish, the standard theory for proving uniqueness and existence of solutions breaks down. Numerically, division by the porosity in the first term of (3.1.20) will cause instability. We will also see that the fluid pressure is no longer a good variable as porosity vanishes. However, we can still obtain stability estimates when a solution exists and investigate the a behavior as porosity approaches zero. Continue to assume porosity is much less than one. In the remainder of this chapter we analyze (3.1.20)–(3.1.23) with homogeneous boundary conditions then address both Neumann and Dirichlet/Robin conditions individually to see their contribution to the stability estimates. Homogeneous conditions are

of course a subset of the non-homogeneous conditions, but we choose to present them because they are notationally easier to follow and build up well to the non-homogeneous cases.

Proceeding formally, assume a solution to (3.1.20)–(3.1.23) exists. Recall the inf-sup condition [10],

$$\|w\| \leq C \sup_{\Psi \in (H_0^1(\Omega))^d} \frac{(w, \nabla \cdot \Psi)}{\|\Psi\|_1}, \quad \forall w \in L^2(\Omega), \tag{3.2.1}$$

where $(H_0^1(\Omega))^d = H^1(\Omega) \cap \{\mathbf{v} = \mathbf{0} \text{ on } \partial\Omega\} \subset V_m$. Substituting (3.1.22) into (3.2.1) gives

$$\begin{aligned} \|q_m\| &\leq C \sup_{\Psi \in V_m} \frac{1}{\|\Psi\|_1} \Big\{ \big| \big(2\mu_m(1-\phi)\mathcal{D}\mathbf{v}_m, \mathcal{D}\Psi\big) \big| \\ &\qquad + \Big| \Big(\tfrac{5-2\phi}{3} \mu_m \nabla \cdot \mathbf{v}_m, \nabla \cdot \Psi \Big) \Big| + \big| \big((1-\phi)\Delta\rho \mathbf{g}, \Psi \big) \big| \Big\} \\ &\leq C(\|\mathcal{D}\mathbf{v}_m\| + \|\nabla \cdot \mathbf{v}_m\| + \Delta\rho) \\ &\leq C(\|\mathbf{v}_m\|_1 + \Delta\rho). \end{aligned} \tag{3.2.2}$$

For the fluid pressure, by the triangle inequality,

$$\begin{aligned} \|\phi^{1/2} q_f\| &\leq \|\phi^{1/2} q_m\| + \|\phi^{1/2}(q_f - q_m)\| \\ &\leq \|q_m\| + \|\phi^{1/2}(q_f - q_m)\|. \end{aligned} \tag{3.2.3}$$

Choosing $w_m = \phi^{-1} \nabla \cdot \mathbf{v}_m$ in (3.1.23), $w_f = \phi^{-1} \nabla \cdot \mathbf{u}$ in (3.1.21) gives

$$\begin{aligned} &(\nabla \cdot \mathbf{v}_m, \phi^{-1} \nabla \cdot \mathbf{v}_m) + (\nabla \cdot \mathbf{u}, \phi^{-1} \nabla \cdot \mathbf{u}) \\ &\quad = \Big(\tfrac{\phi}{\mu_m}(q_f - q_m), \phi^{-1} \nabla \cdot \mathbf{v}_m \Big) - \Big(\tfrac{\phi}{\mu_m}(q_f - q_m), \phi^{-1} \nabla \cdot \mathbf{u} \Big), \end{aligned}$$

and therefore, by Young's inequality

$$\|\phi^{-1/2} \nabla \cdot \mathbf{u}\| + \|\phi^{-1/2} \nabla \cdot \mathbf{v}_m\| \leq C \|\phi^{1/2}(q_f - q_m)\|. \tag{3.2.4}$$

3.2.1 Homogeneous conditions

For homogeneous conditions, let Γ_f^N, $\Gamma_m^{v,N}$, $\Gamma_m^{\tau,N}$ all equal to $\partial\Omega$ and $g_f^N = g_m^{v,N} = g_m^{\tau,N} = 0$ in (3.1.13)–(3.1.15). Testing with $\Psi_r = \mathbf{u}$ in (3.1.20), $\Psi_m = \mathbf{v}_m$ in (3.1.22), $w_f = q_f$ in (3.1.21), $w_m = q_m$ in (3.1.23),

$$\begin{aligned}
&\Big(\frac{\mu_f}{k_0}\phi^{-2(1+\Theta)}\mathbf{u},\mathbf{u}\Big) + \Big(\tfrac{\phi}{\mu_m}(q_f-q_m), q_f-q_m\Big)\\
&+ \big(2\mu_m(1-\phi)\mathcal{D}\mathbf{v}_m, \mathcal{D}\mathbf{v}_m\big) - \Big(\tfrac{5-2\phi}{3}\mu_m\nabla\cdot\mathbf{v}_m, \nabla\cdot\mathbf{v}_m\Big)\\
&\qquad = \big((1-\phi)\Delta\rho\mathbf{g}, \mathbf{v}_m\big).
\end{aligned}$$

Using (3.1.4) to eliminate the negative term on the left-hand side gives

$$\begin{aligned}
&\Big(\frac{\mu_f}{k_0}\phi^{-2(1+\Theta)}\mathbf{u},\mathbf{u}\Big) + \Big(\big(1-\tfrac{5-2\phi}{3}\phi\big)\tfrac{\phi}{\mu_m}(q_f-q_m), q_f-q_m\Big)\\
&\quad + \big(2\mu_m(1-\phi)\mathcal{D}\mathbf{v}_m, \mathcal{D}\mathbf{v}_m\big) = \big((1-\phi)\Delta\rho\mathbf{g}, \mathbf{v}_m\big).
\end{aligned}$$

Then,

$$\|\phi^{-(1+\Theta)}\mathbf{u}\| + \|\phi^{1/2}(q_f-q_m)\| + \|\mathcal{D}\mathbf{v}_m\| \le \varepsilon\|\mathbf{v}_m\| + C_\varepsilon\Delta\rho,$$

for any $\varepsilon > 0$ and some constant C_ε independent of porosity. Finally an application on Korn's inequality,

$$\|\mathbf{v}_m\|_1 \le C\|\mathcal{D}\mathbf{v}_m\|, \tag{3.2.5}$$

results in

$$\|\phi^{-(1+\Theta)}\mathbf{u}\| + \|\phi^{1/2}(q_f-q_m)\| + \|\mathbf{v}_m\|_1 \le C\Delta\rho. \tag{3.2.6}$$

Combining (3.2.2)–(3.2.4) and (3.2.6) we have the following theorem:

Theorem 3.2.1. *There exists a constant $C > 0$ such that, if they exist, the velocity and pressure solutions to the mixed variational form (3.1.20)–(3.1.23) with homogeneous boundary conditions satisfy the stability estimates*

$$\|\phi^{-(1+\Theta)}\mathbf{u}\| + \|\phi^{-1/2}\nabla\cdot\mathbf{u}\| + \|\phi^{1/2}q_f\| + \|\mathbf{v}_m\|_1 + \|\phi^{-1/2}\nabla\cdot\mathbf{v}_m\| + \|q_m\| \leq C\Delta\rho. \tag{3.2.7}$$

While the velocities are stable as $\phi \to 0$, the stability estimates do not guarantee a good bound for the fluid pressure.

3.2.2 Neumann conditions

Let $\Gamma_f^N = \Gamma_m^{\nu,N} = \Gamma_m^{\tau,N} = \partial\Omega$ and $\mathbf{u}^N$, $\mathbf{v}_m^{\nu,N}$, and $\mathbf{v}_m^{\tau,N}$ be defined by (3.1.16)–(3.1.18). Testing with $\Psi_r = \mathbf{u} - \mathbf{u}^N$ in (3.1.20), $\Psi_m = \mathbf{v}_m - \mathbf{v}_m^{\nu,N} - \mathbf{v}_m^{\tau,N}$ in (3.1.22), $w_f = q_f$ in (3.1.21), $w_m = q_m$ in (3.1.23),

$$\begin{aligned}
&\Big(\frac{\mu_f}{k_0}\phi^{-2(1+\Theta)}\mathbf{u},\mathbf{u}\Big) + \Big(\tfrac{\phi}{\mu_m}(q_f - q_m), q_f - q_m\Big) \\
&+ \big(2\mu_m(1-\phi)\mathcal{D}\mathbf{v}_m, \mathcal{D}\mathbf{v}_m\big) - \Big(\tfrac{5-2\phi}{3}\mu_m\nabla\cdot\mathbf{v}_m, \nabla\cdot\Psi_m\Big) \\
&\qquad = \Big(\frac{\mu_f}{k_0}\phi^{-2(1+\Theta)}\mathbf{u},\mathbf{u}^N\Big) - (q_f, \nabla\cdot\mathbf{u}^N) - \big(q_m, \nabla\cdot(\mathbf{v}_m^{\nu,N} + \mathbf{v}_m^{\tau,N})\big) \\
&\qquad + \big(2\mu_m(1-\phi)\mathcal{D}\mathbf{v}_m, \mathcal{D}(\mathbf{v}_m^{\nu,N} + \mathbf{v}_m^{\tau,N})\big) - \Big(\tfrac{5-2\phi}{3}\mu_m\nabla\cdot\mathbf{v}_m, \nabla\cdot(\mathbf{v}_m^{\nu,N} + \mathbf{v}_m^{\tau,N})\Big) \\
&\qquad + \big((1-\phi)\Delta\rho\mathbf{g}, \mathbf{v}_m - \mathbf{v}_m^{\nu,N} - \mathbf{v}_m^{\tau,N}\big).
\end{aligned}$$

Using (3.1.4) to eliminate the negative term on the left-hand side as before,

$$\begin{aligned}
&\|\phi^{-(1+\Theta)}\mathbf{u}\| + \|\phi^{1/2}(q_f - q_m)\| + \|\mathcal{D}\mathbf{v}_m\| \\
&\quad \leq \varepsilon\big\{\|\mathbf{v}_m - \mathbf{v}_m^{\nu,N} - \mathbf{v}_m^{\tau,N}\|_0 + \|q_m\| + \|\mathcal{D}\mathbf{v}_m\| + \|\nabla\cdot\mathbf{v}_m\| + \|\phi^{1/2}(q_f - q_m)\|\big\} \\
&\quad + C_\varepsilon\big\{\|\phi^{-(1+\Theta)}\mathbf{u}^N\| + \|\phi^{-1/2}\nabla\cdot\mathbf{u}^N\| + \|\nabla\cdot(\mathbf{v}_m^{\nu,N} + \mathbf{v}_m^{\tau,N})\| + \|\mathcal{D}(\mathbf{v}_m^{\nu,N} + \mathbf{v}_m^{\tau,N})\| + \Delta\rho\big\},
\end{aligned}$$

and applying Korn's inequality (3.2.5)

$$\|\phi^{-(1+\Theta)}\mathbf{u}\| + \|\phi^{1/2}(q_f - q_m)\| + \|\mathbf{v}_m\|_1 \\ \leq C\big\{\|\phi^{-(1+\Theta)}\mathbf{u}^N\| + \|\phi^{-1/2}\nabla\cdot\mathbf{u}^N\| + \|\mathbf{v}_m^{\nu,N}\|_1 + \|\mathbf{v}_m^{\tau,N}\|_1 + \Delta\rho\big\}, \tag{3.2.8}$$

Combining (3.2.2)–(3.2.4) and (3.2.8) we have the following theorem:

Theorem 3.2.2. *There exists a constant $C > 0$ such that, if they exist, the velocity and pressure solutions to the mixed variational form (3.1.20)–(3.1.23) with Neumann boundary conditions satisfy the stability estimates*

$$\|\phi^{-(1+\Theta)}\mathbf{u}\| + \|\phi^{-1/2}\nabla\cdot\mathbf{u}\| + \|\phi^{1/2}q_f\| + \|\mathbf{v}_m\|_1 + \|\phi^{-1/2}\nabla\cdot\mathbf{v}_m\| + \|q_m\| \\ \leq C\big\{\|\phi^{-(1+\Theta)}\mathbf{u}^N\| + \|\phi^{-1/2}\nabla\cdot\mathbf{u}^N\| + \|\mathbf{v}_m^{\nu,N}\|_1 + \|\mathbf{v}_m^{\tau,N}\|_1 + \Delta\rho\big\}. \tag{3.2.9}$$

with $\mathbf{u}^N$, $\mathbf{v}_m^{\nu,N}$, and $\mathbf{v}_m^{\tau,N}$ defined by (3.1.16)–(3.1.18).

This shows that $g_f^N \in H^{-1/2}(\partial\Omega)$, $g_m^{\nu,N}$, $g_m^{\tau,N} \in H^{1/2}(\partial\Omega)$ for the right-hand side of (3.2.9) to be bounded.

3.2.3 Dirichlet and Robin conditions

Let $\Gamma_f^R = \Gamma_m^{\nu,R} = \Gamma_m^{\tau,R} = \partial\Omega$. Testing with $\Psi_r = \mathbf{u}$ in (3.1.20), $\Psi_m = \mathbf{v}_m$ in (3.1.22), $w_f = q_f$ in (3.1.21), $w_m = q_m$ in (3.1.23),

$$\Big(\frac{\mu_f}{k_0}\phi^{-2(1+\Theta)}\mathbf{u},\mathbf{u}\Big) + \Big(\tfrac{\phi}{\mu_m}(q_f - q_m), q_f - q_m\Big) \\ + \big(2\mu_m(1-\phi)\mathcal{D}\mathbf{v}_m, \mathcal{D}\mathbf{v}_m\big) - \Big(\tfrac{5-2\phi}{3}\mu_m\nabla\cdot\mathbf{v}_m, \nabla\cdot\Psi_m\Big) \\ + \langle g_f^R, \phi^{-1/2}\mathbf{u}\cdot\nu\rangle_{\partial\Omega} + \langle\kappa_f^2\phi^{-1}\mathbf{u}\cdot\nu, \mathbf{u}\cdot\nu\rangle_{\partial\Omega} \\ + \langle g_m^{\nu,R}, \mathbf{v}_m\cdot\nu\rangle_{\partial\Omega} + \langle g_m^{\tau,R}, \mathbf{v}_m\cdot\tau\rangle_{\partial\Omega} + \langle\kappa_\nu^2\mathbf{v}_m\cdot\nu, \mathbf{v}_m\cdot\nu\rangle_{\partial\Omega} + \langle\kappa_\tau^2\mathbf{v}_m\cdot\tau, \mathbf{v}_m\cdot\tau\rangle_{\partial\Omega} \\ = \big((1-\phi)\Delta\rho\mathbf{g}, \mathbf{v}_m\big).$$

Using (3.1.4) to eliminate the negative term on the left-hand as before,

$$\begin{aligned}
&\|\phi^{-(1+\Theta)}\mathbf{u}\| + \|\phi^{1/2}(q_f - q_m)\| + \|\mathcal{D}\mathbf{v}_m\| \\
&+ \|\kappa_f \phi^{-1/2}\mathbf{u}\cdot\nu\|_{\partial\Omega} + \|\kappa_\nu \mathbf{v}_m\cdot\nu\|_{\partial\Omega} + \|\kappa_\tau \mathbf{v}_m\cdot\tau\|_{\partial\Omega} \\
&\leq \varepsilon\big\{\|\mathbf{v}_m\| + \|\phi^{-1/2}\mathbf{u}\cdot\nu\|_{-1/2,\partial\Omega} + \|\mathbf{v}_m\cdot\nu\|_{1/2,\partial\Omega} + \|\mathbf{v}_m\cdot\tau\|_{1/2,\partial\Omega}\big\} \\
&+ C_\varepsilon\big\{\|g_f^R\|_{1/2,\partial\Omega} + \|g_m^{\nu,R}\|_{-1/2,\partial\Omega} + \|g_m^{\tau,R}\|_{-1/2,\partial\Omega} + \Delta\rho\big\}
\end{aligned}$$

For homogeneous Robin conditions, $g_f^R = 0$, or uniform Robin conditions, $\kappa_f \geq \kappa_* > 0$, we can bound the term $\langle g_f^R, \phi^{-1/2}\mathbf{u}\cdot\nu\rangle_{\partial\Omega}$. Otherwise, we must try to bound the edge integral another way. For $w \in H^{1/2}(\partial\Omega)$, integration by parts gives

$$\begin{aligned}
\langle \phi^{-1/2}\mathbf{u}\cdot\nu, w\rangle_{\partial\Omega} &= (\phi^{-1/2}\nabla\cdot\mathbf{u}, w) + \big(\mathbf{u}, \nabla(\phi^{-1/2}w)\big) \\
&= (\phi^{-1/2}\nabla\cdot\mathbf{u}, w) - \Big(\mathbf{u}, \tfrac{1}{2}\phi^{-3/2}\nabla\phi w\Big) + (\mathbf{u}, \phi^{-1/2}\nabla w)
\end{aligned}$$

so *only* when $\phi^{-1/2+\Theta}\nabla\phi$ is well behaved,

$$\|\phi^{-1/2}\mathbf{u}\cdot\nu\|_{-1/2,\partial\Omega} \leq C\{\|\phi^{-1/2}\nabla\cdot\mathbf{u}\| + \|\phi^{-(1-\Theta)}\mathbf{u}\|\}.$$

Moreover, by the trace lemma 3.1.2,

$$\|\mathbf{v}_m\cdot\nu\|_{1/2,\partial\Omega} + \|\mathbf{v}_m\cdot\tau\|_{1/2,\partial\Omega} \leq \|\mathbf{v}_m\|_1,$$

resulting in

$$\begin{aligned}
&\|\phi^{-(1+\Theta)}\mathbf{u}\| + \|\phi^{1/2}(q_f - q_m)\| + \|\mathbf{v}_m\|_1 + \|\kappa_f\phi^{-1/2}\mathbf{u}\cdot\nu\|_{\partial\Omega} \\
&\qquad \leq C\big\{\|g_f^R\|_{1/2,\partial\Omega} + \|g_m^{\nu,R}\|_{-1/2,\partial\Omega} + \|g_m^{\tau,R}\|_{-1/2,\partial\Omega} + \Delta\rho\big\}.
\end{aligned} \tag{3.2.10}$$

Combining (3.2.2)–(3.2.4) and (3.2.10) we have the following theorem:

Theorem 3.2.3. *Let $\nabla\phi$ be bounded, $g_f^R = 0$, or $\kappa_f \geq \kappa_* > 0$ everywhere. There exists a constant $C > 0$ such that, if they exist, the velocity and pressure solutions to the mixed variational form (3.1.20)–(3.1.23) with Robin boundary conditions satisfy the stability estimates*

$$\begin{aligned}\|\phi^{-(1+\Theta)}\mathbf{u}\| + \|\phi^{-1/2}\nabla\cdot\mathbf{u}\| + \|\phi^{1/2}q_f\| + \|\mathbf{v}_m\|_1 + \|\phi^{-1/2}\nabla\cdot\mathbf{v}_m\| + \|q_m\| \\ + \|\kappa_f\phi^{-1/2}\mathbf{u}\cdot\nu\|_{\partial\Omega} \leq C\big\{\|g_f^R\|_{1/2,\partial\Omega} + \|g_m^{\nu,R}\|_{-1/2,\partial\Omega} + \|g_m^{\tau,R}\|_{-1/2,\partial\Omega} + \Delta\rho\big\}.\end{aligned} \tag{3.2.11}$$

3.2.4 Observations

The matrix velocity and pressure as well as the Darcy velocity remain bounded as the porosity approaches zero. Meanwhile, the fluid pressure may be *unbounded*. Indeed, the fluid pressure is no longer a quantity with physical meaning when there is no fluid. This is a significant issue to numerically modeling mid-ocean ridges because we expect a well-defined melting region bounded by the lithosphere. More generally, it is a significant impediment to taking advantage of the general nature of the mantle equations, as they hold even in the case of a phase disappearing.

One could envision several alternatives to (3.1.20)–(3.1.23) (from now on called the standard method) to avoid dividing by the porosity. A commonly used approach introduces an auxiliary velocity variable $\tilde{\mathbf{v}}_r$ [6]. In this case, we add to (3.1.20)–(3.1.23) the equation

$$\left(\phi^{2(1+\Theta)}\tilde{\mathbf{v}}_r, \tilde{\Psi}_r\right) - (\mathbf{u}, \tilde{\Psi}_r) = 0 \qquad \forall \tilde{\Psi}_r \in V_r, \quad (3.2.12)$$

and modify (3.1.20) to

$$\begin{aligned} &\left(\frac{\mu_f}{k_0}\tilde{\mathbf{v}}_r, \Psi_r\right) - (q_f, \nabla\cdot\Psi_r) + \langle \kappa_f \phi^{-1}\mathbf{u}\cdot\nu, \Psi_r\cdot\nu\rangle_{\Gamma_f^R} \\ &\qquad = -\langle g_f^R, \phi^{-1/2}\Psi_r\cdot\nu\rangle_{\Gamma_f^R} \qquad \forall \Psi_r \in V_r, \end{aligned} \quad (3.2.13)$$

We will call this the expanded method. Alternatively, we could keep the symmetric nature of the problem by using a different scaling of the relative velocity $\tilde{\mathbf{v}}_r = \phi^{-\Theta}(\mathbf{v}_f - \mathbf{v}_m)$ and substituting (3.1.20)–(3.1.21) with

$$\begin{aligned} &\left(\frac{\mu_f}{k_0}\tilde{\mathbf{v}}_r, \Psi_r\right) - \left(q_f, \nabla\cdot(\phi^{1+\Theta}\Psi_r)\right) + \langle \kappa_f \phi^{-1}\tilde{\mathbf{v}}_r\cdot\nu, \Psi_r\cdot\nu\rangle_{\Gamma_f^R} \\ &\qquad = -\langle g_f^R, \phi^{-1/2}\Psi_r\cdot\nu\rangle_{\Gamma_f^R} \qquad \forall \Psi_r \in V_r, \end{aligned} \quad (3.2.14)$$

$$\left(\nabla\cdot(\phi^{1+\Theta}\tilde{\mathbf{v}}_r), w_f\right) + \left(\frac{\phi}{\mu_m}(q_f - q_m), w_f\right) = 0 \qquad \forall w_f \in W_f. \quad (3.2.15)$$

While unorthodox to leave porosity with the test functions, this approach, called the symmetry preserving method, should be gentler numerically since it spreads out the porosity over two equations, but now (3.2.15) degenerates to $0 = 0$ as porosity approaches zero. None of these methods address the issue of the unbounded pressure.

The stability estimates suggest, loosely speaking, that we could "transfer" some ϕ-regularity from the Darcy velocity $\mathbf{u}$ to the pressure q_f. A new formulation in terms of a scaled fluid pressure $\phi^{1/2}q_f$, scaled relative velocity $\phi^{1+\Theta}\mathbf{u}$ $(= \phi^{-\Theta}(\mathbf{v}_f - \mathbf{v}_m))$ as in the symmetry preserving method), and a modified divergence space could then be well-behaved. In chapter 6, we show this is in fact the

case by providing an existence and uniqueness proof as well as adequate stability estimates for new scaled variables. For the mantle problem we assume that we never lose the solid phase, and thus the problem of degeneracy (or loss of a phase) lies squarely on the Darcy part of the equations. In chapter 5, we ignore the Stokes part and look carefully at a problem that generalizes the Darcy part. For the numerical results in chapter 4, we continue to model problems with non-zero porosity using the formulation in (3.1.20)–(3.1.23) and omit a proof of existence and uniqueness as it will be a special case of the one presented in chapter 6.

Chapter 4

A Discrete Mixed Method for Positive Porosity

Assume Ω is a union of rectangles in two dimensions. Let $\mathcal{T}_h$ be a rectangular finite element mesh covering Ω with maximal spacing h, let $\mathcal{E}_h$ denote the set of element edges, and let $\mathcal{N}_h$ denote the set of mesh nodes. Let $\mathbb{P}_n$ denote polynomials of degree n, and $\mathbb{P}_{n_1,n_2}$ polynomials of degree n_1 in x and n_2 in z.

4.1 Finite element spaces

To formulate the discrete problem we introduce two sets finite element spaces specially used for mixed methods. First we define the lowest order Raviart-Thomas (RT_0) finite element spaces $V_{RT_0} \times W_{RT_0}$ [18, 42, 43]. On an element $E \in \mathcal{T}_h$,

$$V_{RT_0}(E) = \mathbb{P}_{1,0} \times \mathbb{P}_{0,1}, \tag{4.1.1}$$

$$W_{RT_0}(E) = \mathbb{P}_0. \tag{4.1.2}$$

The degrees of freedom for V_{RT_0} are the normal fluxes on the edges, and the degrees of freedom for W_{RT_0} are the average values over the elements, i.e.,

$$V_{RT_0} = \text{span}\left\{ \mathbf{v}_e : \int_f \mathbf{v}_e \cdot \nu_f \, ds = \delta_{e,f} \quad \forall e, f \in \mathcal{E}_h \right\}, \tag{4.1.3}$$

$$W_{RT_0} = \text{span}\{ w_E : w_E|_F = \delta_{E,F} \quad \forall E, F \in \mathcal{T}_h \}, \tag{4.1.4}$$

where $\delta_{i,j}$ is the Kronecker delta function for indices i and j. Raviart-Thomas spaces are commonly used to solve Darcy's equation and RT_0 is first order accurate in $H(\mathrm{div};\Omega)$ for V_{RT_0} and in $L^2(\Omega)$ for W_{RT_0}. Next, define the finite element space BR [15] used by Arbogast-Wheeler [5], $V_{BR} \times W_{BR}$. On an element $E \in \mathcal{T}_h$,

$$V_{BR}(E) = \mathbb{P}_{1,2} \times \mathbb{P}_{2,1}, \tag{4.1.5}$$

$$W_{BR}(E) = \mathbb{P}_0. \tag{4.1.6}$$

The degrees of freedom for V_{BR} are the normal fluxes on the edges and nodal values of each component, and the degrees of freedom for W_{BR} are the average values over the elements, i.e.,

$$\begin{aligned} V_{BR} = \mathrm{span}\Bigg\{ & \mathbf{v}_e : \int_f \mathbf{v}_e \cdot \nu_f \, ds = \delta_{e,f} \ \forall e, f \in \mathcal{E}_h, \\ & \mathbf{v}_{\mathbf{p},i} : \mathbf{v}_{\mathbf{p},i}(\mathbf{q}) \cdot \mathbf{e}_j = \delta_{\mathbf{p},\mathbf{q}} \delta_{i,j} \ \forall \mathbf{p}, \mathbf{q} \in \mathcal{N}_h, \ i, j = 1, 2 \Bigg\}, \end{aligned} \tag{4.1.7}$$

$$W_{BR} = \mathrm{span}\{ w_E : w_E|_F = \delta_{E,F} \ \forall E, F \in \mathcal{T}_h \}. \tag{4.1.8}$$

The space BR was first introduced to solve Stokes equation, and has also been adapted to solve Darcy's equation with continuous velocities. The space BR is first order accurate in $(H^1(\Omega))^2$ for V_{BR} and in $L^2(\Omega)$ for W_{BR}. Since we will use these elements in conjunction with RT_0, we would not make use of any additional convergence obtained by using more standard Stokes elements such as Taylor-Hood [26]. In exchange, BR has fewer degrees of freedom. For a derivation of a discrete inf-sup condition for BR see appendix A.

4.2 Discrete weak formulation

We use RT_0 For the relative velocity and fluid pressure and BR for the matrix velocity and mixture pressure. That is,

$$\begin{aligned} V_{r,h} &= V_{RT_0} \cap \{\mathbf{v}\cdot\nu = 0 \text{ on } \Gamma_f^N\}, \\ V_{m,h} &= V_{BR} \cap \{\mathbf{v}\cdot\nu = 0 \text{ on } \Gamma_m^{\nu,N}\} \cap \{\mathbf{v}\cdot\tau = 0 \text{ on } \Gamma_m^{\tau,N}\}, \\ W_{m,h} &= W_{f,h} = W_{RT_0} = W_{BR}. \end{aligned} \tag{4.2.1}$$

With boundary conditions given by (3.1.13)–(3.1.15), the discrete form of the mixed formulation (3.1.20)–(3.1.23), is given by

Find $\mathbf{u} \in V_{r,h} + \mathbf{u}^N$, $\mathbf{v}_m \in V_{m,h} + \mathbf{v}_m^{\nu,N} + \mathbf{v}_m^{\tau,N}$, $q_f \in W_{f,h}$, and $q_m \in W_{m,h}$ such that

$$\begin{aligned} &\left(\frac{\mu_f}{k_0}\phi^{-2(1+\Theta)}\mathbf{u}, \Psi_r\right) - (q_f, \nabla\cdot\Psi_r) + \langle \kappa_f \phi^{-1}\mathbf{u}\cdot\nu, \Psi_r\cdot\nu\rangle_{\Gamma_f^R} \\ &\qquad = -\langle g_f^R, \Psi_r\cdot\nu\rangle_{\Gamma_f^R} \qquad \forall \Psi_r \in V_{r,h}, \end{aligned} \tag{4.2.2}$$

$$(\nabla\cdot\mathbf{u}, w_f) + \left(\frac{\phi}{\mu_m}(q_f - q_m), w_f\right) = 0 \qquad \forall w_f \in W_{f,h}, \tag{4.2.3}$$

$$\begin{aligned} &-(q_m, \nabla\cdot\Psi_m) + \left(2\mu_m(1-\phi)\mathcal{D}\mathbf{v}_m, \mathcal{D}\Psi_m\right) - \left(\tfrac{5-2\phi}{3}\mu_m(1-\phi)\nabla\cdot\mathbf{v}_m, \nabla\cdot\Psi_m\right) \\ &\qquad + \langle \kappa_\nu^2 \mathbf{v}_m\cdot\nu, \Psi_m\cdot\nu\rangle_{\Gamma_m^{\nu,R}} + \langle \kappa_\tau^2 \mathbf{v}_m\cdot\tau, \Psi_m\cdot\tau\rangle_{\Gamma_m^{\tau,R}} \\ &\qquad = \langle g_m^{\nu,R}, \Psi_m\cdot\nu\rangle_{\Gamma_m^{\nu,R}} + \langle g_m^{\tau,R}, \Psi_m\cdot\tau\rangle_{\Gamma_m^{\tau,R}} \\ &\qquad + ((1-\phi)\Delta\rho\mathbf{g}, \Psi_m) \qquad \forall \Psi_m \in V_{m,h}, \end{aligned} \tag{4.2.4}$$

$$(\nabla\cdot\mathbf{v}_m, w) - \left(\frac{\phi}{\mu_m}(q_f - q_m), w\right) = 0 \qquad \forall w_m \in W_{m,h}. \tag{4.2.5}$$

with $\mathbf{u}^N$, $\mathbf{v}_m^{\nu,N}$, and $\mathbf{v}_m^{\tau,N}$ defined by (3.1.16)–(3.1.18). Note that for the expanded method, a discrete version of (3.2.12) is added to (4.2.2)–(4.2.5) with search space $V_{r,h}$.

4.3 Numerical results

In this section we introduce two key test problems: compacting column and viscous corner flow. All closed form solutions to these problems are derived in appendix C. We first test the rate of convergence of the three mixed methods introduced in the previous chapter against known closed form solutions. Since the three methods performed similarly, we only present convergence results for the standard method. Next, we explore the methods' behavior for discontinuous porosity. Finally, we analyze the behavior of the condition number for each method as we decrease the porosity. Numerical results presented in the remainder of this chapter are from a general 2D finite element code written in MATLAB and C. The code uses Gauss quadrature to evaluate cell and edge integrals. For code documentation see appendix D.

4.3.1 Benchmark test: constant porosity compacting column

Consider a mantle column [39] as shown in Fig. 4.1(a) for $z \in [-L, L]$ with constant porosity and no flow through the bottom and top boundaries, i.e.,

$$v_m(-L) = v_m(L) = u(-L) = u(L) = 0, \tag{4.3.1}$$

and fluid pressure scaled so $q_f(0) = 0$. In order to best reveal the qualitative nature of the symmetric equations for the compacting column, we non-dimensionalize using the compaction length scale [32]

$$L_c = \left(\frac{k_0 \mu_m}{\mu_f}\right)^{1/2} \approx 10^5 - 10^6 m, \tag{4.3.2}$$

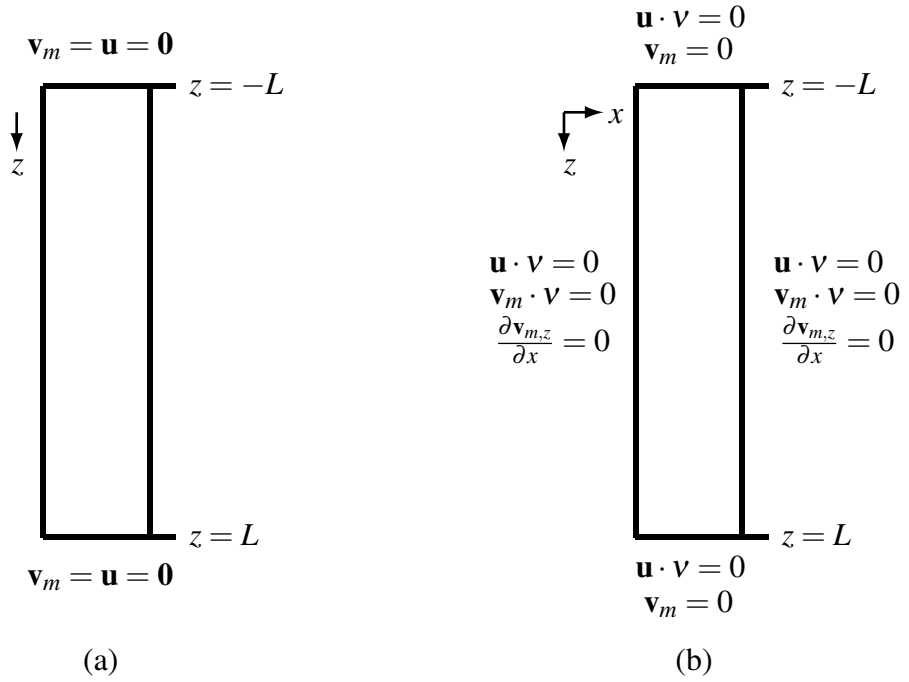

Figure 4.1: (a) Compacting column on a domain $[-L,L]$ with no flow through the top and bottom boundaries. (b) Boundary conditions used to imitate the one dimensional compacting column in two dimensions.

which governs the separation of fluid from matrix. Defining dimensionless variables

$$\begin{aligned} \mathbf{x} &= \tilde{\mathbf{x}} L_c, \\ (q_f,\, q_m) &= (\tilde{q}_f,\, \tilde{q}_m)\Delta\rho g L_c, \\ (\mathbf{u},\, \mathbf{v}_m) &= (\tilde{\mathbf{u}},\, \tilde{\mathbf{u}})\frac{k_0 \Delta\rho g}{\mu_f}, \end{aligned} \tag{4.3.3}$$

reducing to the vertical dimension, taking constant porosity $\phi = \phi_0$, and dropping tildes, (3.1.1)–(3.1.4) become

$$\phi_0^{-2(1+\Theta)} u = -q_f', \tag{4.3.4}$$

$$(q_m - \tfrac{1}{3}(1-4\phi_0)v_m')' = 1-\phi_0, \tag{4.3.5}$$

$$v_m' = \phi_0(q_f - q_m), \tag{4.3.6}$$

$$u' = -\phi_0(q_f - q_m). \tag{4.3.7}$$

Note that in the one-dimensional problem, there is no longer a distinction between shear deformation and compaction. The solution is

$$v_m = -u = \phi_0^{2(1+\Theta)}(1-\phi_0)\big(1 - Ce^{-R(z+L)} - Ce^{R(z-L)}\big), \tag{4.3.8}$$

$$q_f = (1-\phi_0)\Big(z + \tfrac{C}{R}\big(e^{-R(z+L)} - e^{R(z-L)}\big)\Big), \tag{4.3.9}$$

$$q_m = (1-\phi_0)\Big(z - \tfrac{1-4\phi_0}{1-\phi_0+4\phi_0^2}\phi_0 \tfrac{C}{R}\big(e^{-R(z+L)} - e^{R(z-L)}\big)\Big), \tag{4.3.10}$$

with

$$R = R(\phi_0) = \left(\tfrac{1-\phi_0+4\phi_0^2}{3}\phi_0^{1+2\Theta}\right)^{-1/2} \approx \sqrt{3}\phi_0^{-(1+2\Theta)/2},$$

and $C = (1+e^{-2RL})^{-1} \approx 1$.

To solve the compacting column numerically using our code, we imitate the one dimensional problem in a two dimensional domain using boundary conditions according to Figure 4.1(b). Note that $\sigma v \cdot \tau \propto \dfrac{\partial v_{m,z}}{\partial x} + \dfrac{\partial v_{m,x}}{\partial z} = \dfrac{\partial v_{m,z}}{\partial x}$ since $v_{m,x} = 0$ everywhere. Additionally, we remove the constant nullspace from the fluid pressure potential by setting $q_f(0) = 0$. Convergence results in Table 4.1 show the expected convergence, with quadratic convergence for the velocities and linear convergence for the pressures. Convergence rates for the interpolation error in Table 4.2 show super-convergence for the L^2-interpolation-errors of both pressures and for the H^1-interpolation-errors of both velocities. Note that for the $1D$ compacting column, $H^1(\Omega) = H(\mathrm{div};\Omega)$.

4.3.2 Benchmark test: viscous corner flow with no melting

Following Spiegelman [49], consider the viscous corner flow model in the quarter plane $x, z > 0$ shown in Figure 4.2(a), where at the top boundary $z = 0$ we impose a matrix velocity U_0 in the x-direction, and flow symmetry along the left boundary $x = 0$. We take porosity to be constant and disallow melting. Then, (2.2.2) and (2.2.3) reduce to incompressiblity equations for the fluid and matrix,

$$\nabla \cdot \mathbf{v}_m = \nabla \cdot \mathbf{u} = 0\,. \tag{4.3.11}$$

Moreover, the compaction relation (3.1.4) implies the fluid and matrix pressure potentials are identical, i.e.,

$$q_f = q_m = q\,. \tag{4.3.12}$$

	Darcy velocity $\mathbf{u}$				fluid pres. pot. q_f	
n	L^2-error	rate	H^1-error	rate	L^2-error	rate
10	0.0948	—	0.5829	—	0.502	—
20	0.0309	1.6178	0.3641	0.6792	0.0251	1.0008
40	0.0084	1.8743	0.1958	0.8949	0.0125	1.0000
80	0.0022	1.9657	0.0998	0.9714	0.0063	1.0010
160	0.0005	1.9910	0.0502	0.9927	0.0031	1.0007

	matrix velocity $\mathbf{v}_m$				matrix pres. pot. q_m	
n	L^2-error	rate	H^1-error	rate	L^2-error	rate
10	0.0948	—	0.5829	—	0.0525	—
20	0.0309	1.6178	0.3641	0.6792	0.0263	0.9990
40	0.0084	1.8743	0.1958	0.8949	0.0131	1.0004
80	0.0022	1.9657	0.0998	0.9714	0.0066	1.0011
160	0.0005	1.9910	0.0502	0.9927	0.0033	1.0007

Table 4.1: Standard method for a compacting column with constant porosity $\phi_0 = .04$. Relative L^2-errors and convergence rates for $\mathbf{u}$, q_f, $\mathbf{v}_m$, and q_m. Relative H^1-errors and convergence rates for $\mathbf{u}$ and $\mathbf{v}_m$. Solved on an $n \times 1$ ($\approx 6n$ DOF) mesh. $L = 1.5$, $\Theta = .1$.

	Darcy velocity $\mathbf{u}$		fluid pres. pot. q_f	
n	H^1-inter.-error	rate	L^2-inter.-error	rate
80	3.6459e-3	—	2.53e-4	—
160	9.1833e-4	1.9892	7.5096e-5	1.7523
320	2.3001e-4	1.9973	2.0519e-5	1.8618
640	5.7531e-5	1.9993	5.3670e-6	1.9348
1280	1.4384e-5	1.9998	1.3727e-6	1.9671

	matrix velocity $\mathbf{v}_m$		matrix pres. pot. q_m	
n	H^1-inter.-error	rate	L^2-inter.-error	rate
80	3.6459e-3	—	2.4806e-4	—
160	9.1833e-4	1.9892	7.3965e-5	1.7458
320	2.3001e-4	1.9973	2.0248e-5	1.8691
640	5.7531e-5	1.9993	5.3007e-6	1.9335
1280	1.4384e-5	1.9998	1.3563e-6	1.9665

Table 4.2: Standard method for a compacting column with constant porosity $\phi_0 = .04$. Relative L^2-interpolation-errors and convergence rates for q_f and q_m. Relative H^1-interpolation-errors and convergence rates for $\mathbf{u}$ and $\mathbf{v}_m$. Solved on an $n \times 1$ ($\approx 6n$ DOF) mesh. $L = 1.5$, $\Theta = .1$.

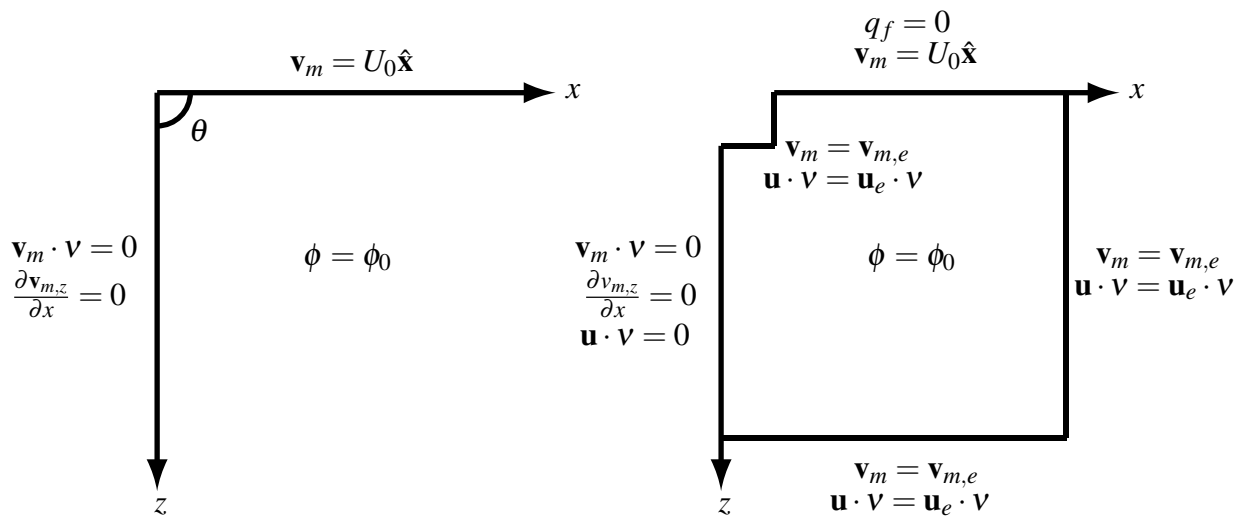

Figure 4.2: (a) Viscous corner flow on a quarter plane with constant velocity equal to U_0 at the top boundary and symmetry condition at the left boundary. (b) Boundary conditions for the numerical method.

Incompressibility of the matrix also reduces Stokes (3.1.3) to

$$\nabla q - \mu_m(1-\phi_0)\nabla^2 \mathbf{v}_m = (1-\phi_0)\Delta\rho\hat{\mathbf{g}}, \tag{4.3.13}$$

where we use the identity $2\nabla \cdot \mathcal{D}\mathbf{v} = \nabla^2\mathbf{v} + \nabla(\nabla \cdot \mathbf{v})$. Note that the four equations (4.3.11), (4.3.13), along with Darcy's law (3.1.1), have only three unknowns, but remain consistent since (4.3.13) implies incompresibilty for the relative velocity. Introduce the length scale

$$L_s = \left(\frac{\mu_m U_0}{\Delta\rho g}\right)^{1/2} \approx 10^3 m, \tag{4.3.14}$$

which governs extraction of fluid by shear forces in the matrix. Defining dimensionless variables

$$\begin{aligned}(x,z) &= (\bar{x},\tilde{z})L_s,\\ q &= \tilde{q}\Delta\rho g L_s,\\ (\mathbf{v}_m,\mathbf{u}) &= (\tilde{\mathbf{v}}_m,\tilde{\mathbf{u}})U_0,\end{aligned} \tag{4.3.15}$$

substituting, and dropping tildes gives

$$\nabla\cdot\mathbf{v}_m = \nabla\cdot\mathbf{u} = 0\,, \tag{4.3.16}$$

$$\nabla q - (1-\phi)\nabla^2\mathbf{v}_m = (1-\phi)\hat{\mathbf{z}}\,, \tag{4.3.17}$$

$$\mathbf{u} = -\frac{w_0}{U_0}\nabla q\,, \tag{4.3.18}$$

where

$$w_0 = \frac{k_0\phi_0^{2(1+\Theta)}\Delta\rho g}{\mu_f}, \tag{4.3.19}$$

is the percolation velocity, which determines the separation of fluid from matrix (and is strongly dependent on porosity). Equations (4.3.16)–(4.3.18) have a stream function solution for $r>0$,

$$\mathbf{v}_m = \frac{2}{\pi}((\theta\sin\theta-\cos\theta)\hat{\mathbf{r}}+\theta\cos\theta\hat{\boldsymbol{\theta}}) \tag{4.3.20}$$

$$q = (1-\phi_0)\Big(-\frac{4}{\pi r}+r\Big)\cos\theta = (1-\phi_0)\Big(-\frac{4}{\pi r}\cos\theta+z\Big), \tag{4.3.21}$$

$$\mathbf{u} = -\frac{w_0}{U_0}(1-\phi_0)\Big(\frac{4}{\pi r^2}(\cos\theta\hat{\mathbf{r}}+\sin\theta\hat{\boldsymbol{\theta}})+\hat{\mathbf{z}}\Big). \tag{4.3.22}$$

Notice that the solution to this simplified system also solves the full equations (3.1.1)–(3.1.4). Since the mixed method has a unique solution, we can use this simplified solution to validate the method.

	Darcy velocity $\mathbf{u}$		fluid pres. pot. q_f	
n	L^2-error	rate	L^2-error	rate
8	0.2445	—	0.0997	—
16	0.1254	0.9519	0.0505	0.9823
32	0.0635	0.9925	0.0253	0.9936
64	0.0318	0.9984	0.0127	0.9982

	matrix velocity $\mathbf{v}_m$				matrix pres. pot. q_m	
n	L^2-error	rate	H^1-error	rate	L^2-error	rate
8	0.0112	—	0.0804	—	0.0990	—
16	0.0031	1.8580	0.0407	0.9836	0.0505	0.9716
32	0.0008	1.9776	0.0200	1.0260	0.0254	0.9940
64	0.0002	1.9937	0.0099	1.0083	0.0127	0.9988

Table 4.3: Viscous corner flow with constant porosity $\phi_0 = .04$. Relative L^2- errors and convergence rates for $\mathbf{u}$, q_f, $\mathbf{v}_m$, and q_m. Relative H^1-errors and convergence rates for $\mathbf{v}_m$. Errors shown for $n \times n$-meshes ($\approx 8n^2$ DOF)

To avoid the singularity at $r = 0$, we test the method on a rectangular mesh with the corner removed, as shown in figure 4.2(b). We set the exact solution as Neumann boundary conditions,

$$\mathbf{v}_m = \mathbf{v}_{m,e},$$

$$\mathbf{u} \cdot \nu = \mathbf{u}_e \cdot \nu$$

at the corner and as far field conditions. Note the condition $q_f = 0$ on the top boundary is consistent with the exact solution (4.3.21). Table 4.3 shows the expected convergence rates for the relative error.

4.3.3 Discontinuous porosity

Consider the compacting column in Figure 4.1(a) with porosity ϕ given by

$$\phi = \begin{cases} \phi_- & \text{if } z \leq 0, \\ \phi_+ & \text{if } z > 0. \end{cases} \tag{4.3.23}$$

We would like to explore the qualitative nature of the numerical solution to the methods in the previous chapter even when the parameters are highly irregular. Figure 4.3 shows computed solutions on a coarse mesh for the three methods. Recall that the velocity calculated in the symmetry preserving method is scaled by the porosity and hence is discontinuous at $z = 0$. This method fails to capture that jump.

4.3.4 Condition number for decreasing porosity

We observe the behavior of the condition number as porosity approaches zero in part of the domain. Consider three porosities on $[-L, L]$

$$\phi_1(z) = \phi_0 + \begin{cases} 0 & \text{if } z \leq 0, \\ z^2 & \text{if } z > 0, \end{cases} \tag{4.3.24}$$

$$\phi_2(z) = \phi_0 + \begin{cases} 0 & \text{if } z \leq 0, \\ \sqrt{z} & \text{if } z > 0, \end{cases} \tag{4.3.25}$$

$$\phi_3(z) = \phi_0 + \begin{cases} 0 & \text{if } z \leq 0, \\ \phi_+ & \text{if } z > 0, \end{cases} \tag{4.3.26}$$

and let $\phi_0 \to 0$. At $z = 0$, ϕ_1 is continuously differentiable, $\phi_2(z)$ is continuous but has unbounded derivative, and $\phi_3(z)$ is discontinuous. For every method the condition number blows up with porosity, as shown in Figure 4.4. Moreover, the

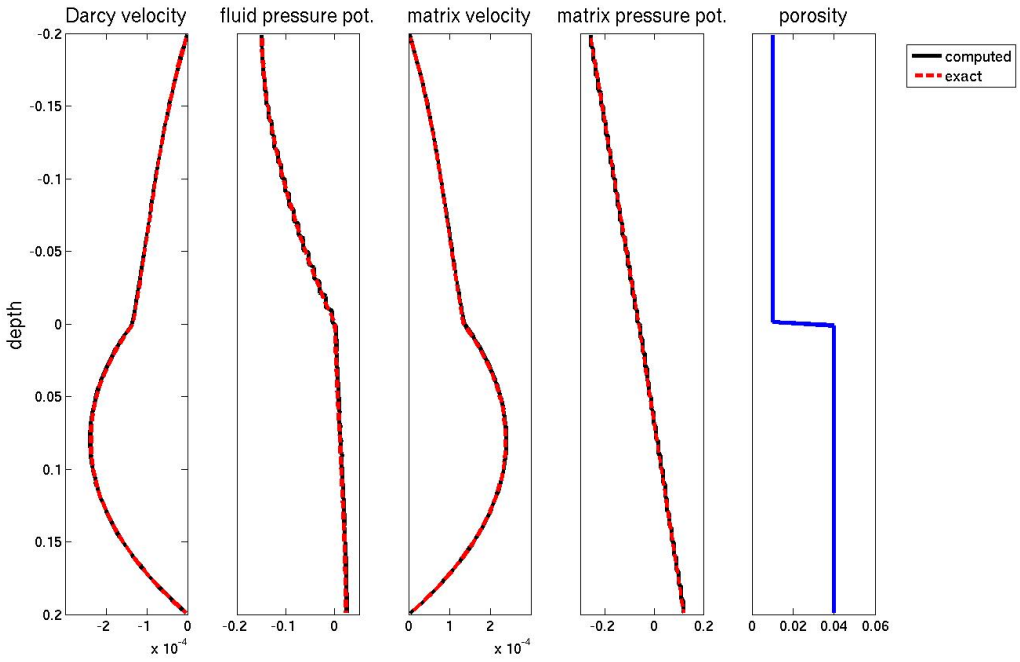
Darcy velocity
fluid pressure pot.
matrix velocity
matrix pressure pot.
porosity
computed
exact
depth
x 10^-4

(a)

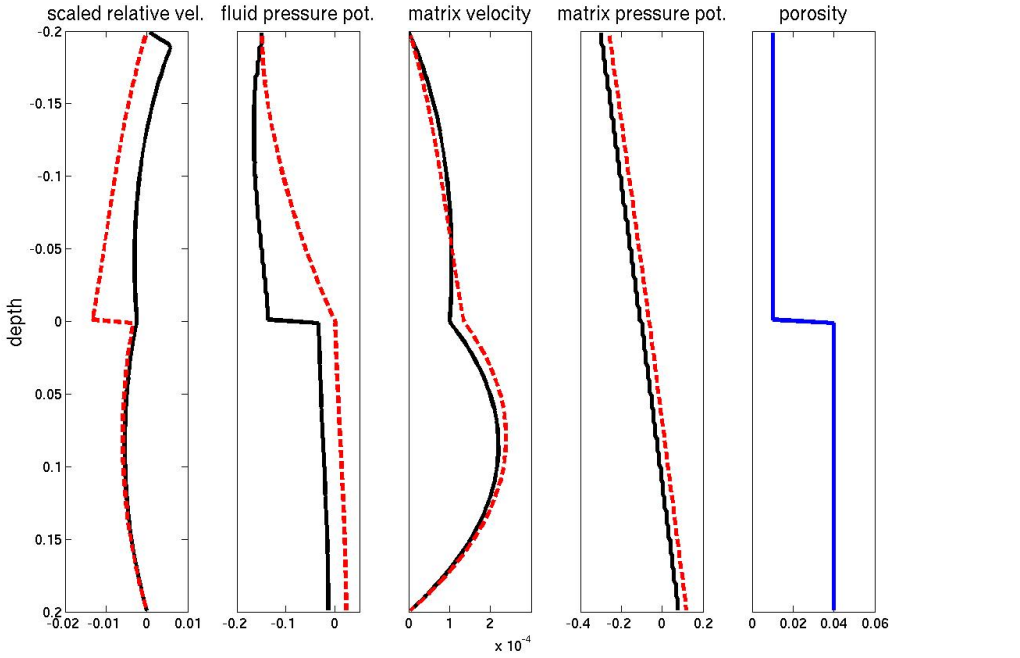
scaled relative vel.
fluid pressure pot.
matrix velocity
matrix pressure pot.
porosity
depth
x 10^-4

(b)

Figure 4.3

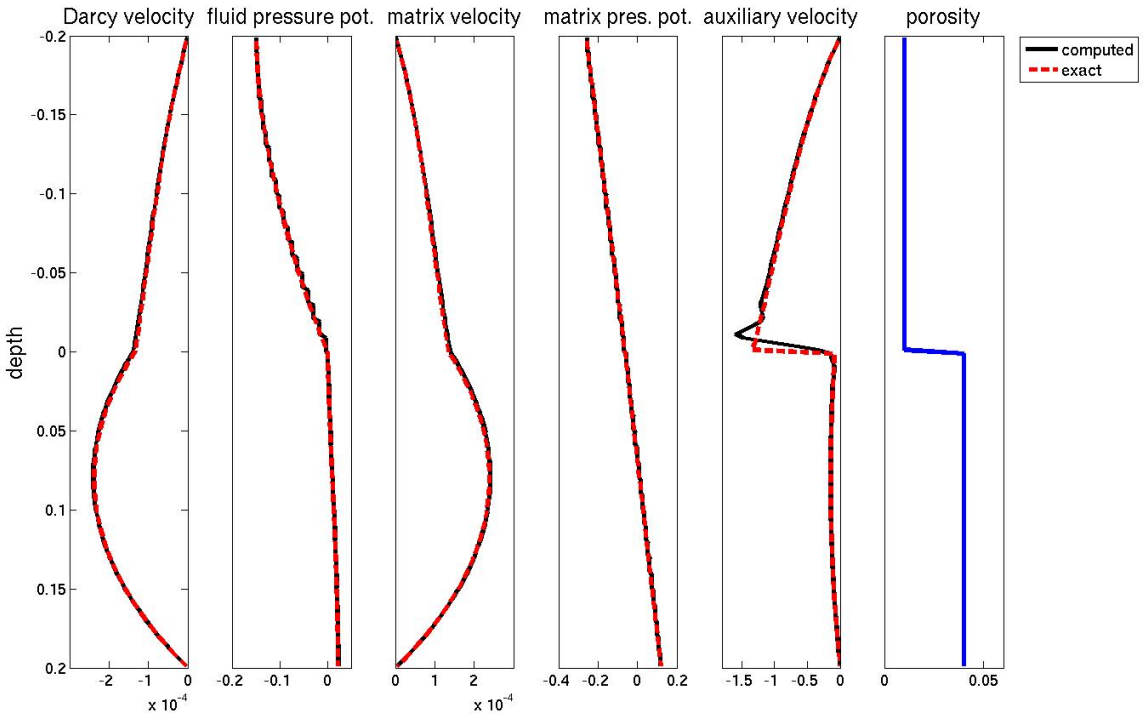

(c)

Figure 4.3: Computed solution on a 40×1-mesh for a compacting column with discontinuous porosity (4.3.23) and $\Theta = 0$. (a) standard method. (b) symmetry preserving method. (c) expanded method.

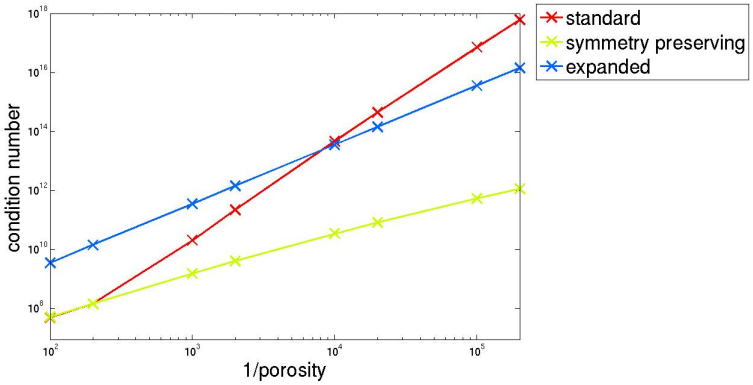

(a)

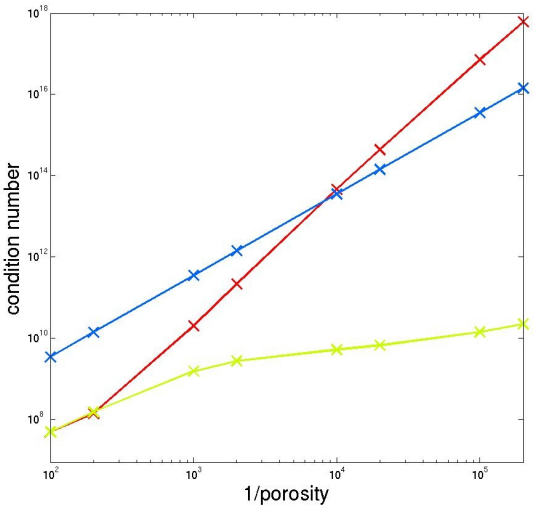

(b)

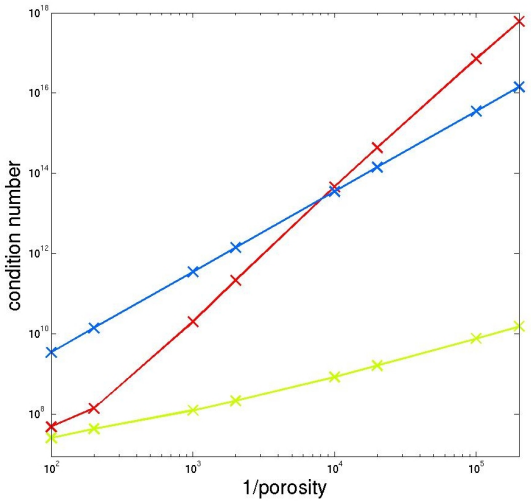

(c)

Figure 4.4: Condition number as $\phi_0 \to 0$ for porosities defined in (4.3.24)–(4.3.26) on a 100×1-mesh. $L = .2$. (a) ϕ_1. (b) ϕ_2. (c) ϕ_3, $\phi_+ = .04$.

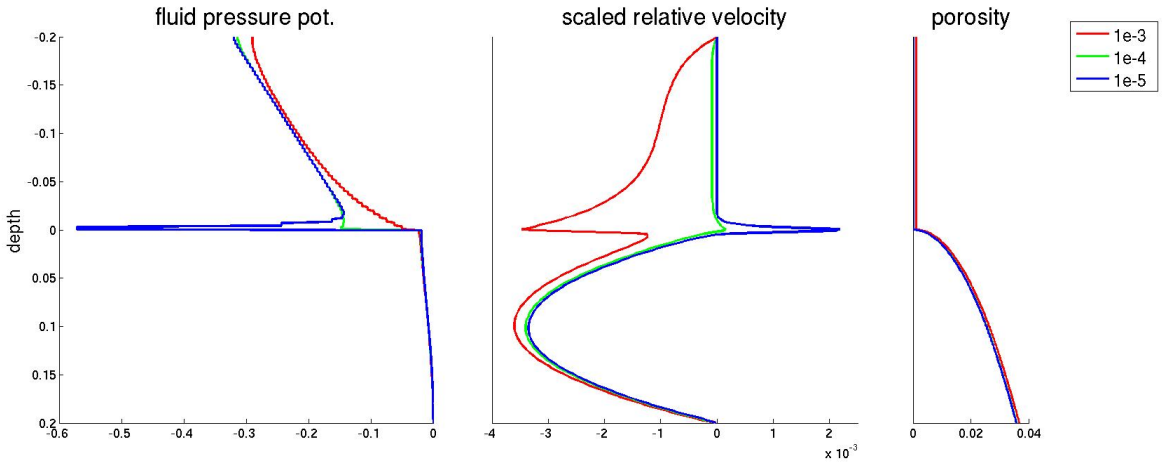

Figure 4.5: Fluid pressure and scaled relative velocity blow up for the symmetry preserving method with porosity defined by (4.3.25), and ϕ_0 decreasing to zero. 100×1- mesh. $L = .2$

regularity (or lack of) of ϕ does not appear to affect the condition number as porosity vanishes. While for the standard method and the expanded method the solutions appear to converge, for the symmetry preserving method, Figure 4.5 shows the fluid pressure actually blows up as $\phi_0 \to 0$ in $\phi_2(z)$ (though surprisingly does converge to the true solution for $\phi_3(z)$). This result shows that we cannot trust the numerical solution using the mixed methods of chapter 3 when the porosity is small. This is especially relevant for mid-ocean ridges, where we are specifically interested in the behavior at the phase boundaries where high-porosity channels form. Following the theory developed in the following chapters, we will develop a new method which, as we shall see in chapter 7 is numerically stable as porosity approaches zero in part of the domain.

Chapter 5

A Linear Degenerate Elliptic Equation

The mantle equations (3.1.1)–(3.1.4) give rise to a degenerate system when the fluid disappears. The Stokes part (3.1.3)–(3.1.4) is well-posed, since there is always matrix present at each point of space (i.e., $\phi \leq \phi^* < 1$). Thus we ignore the matrix part of the problem and define the following degenerate problem.

Let $\Omega \subset \mathbb{R}^d$ be a domain, let the porosity $\phi : \Omega \to [0, \phi^*]$, $0 < \phi^* < \infty$, be a given differentiable function, and let a and b lie in $C^1([0, \phi^*])$, both positive on $(0, \phi^*]$, and non-negative at $x = 0$. For velocity $\mathbf{u}$ and pressure p, we consider the linear degenerate elliptic boundary value problem

$$\mathbf{u} = -a(\phi)(\nabla p - \mathbf{g}) \qquad \text{in } \Omega, \tag{5.0.1}$$

$$\nabla \cdot \big(b(\phi)\mathbf{u}\big) + \phi p = \phi^{1/2} f \quad \text{in } \Omega, \tag{5.0.2}$$

$$b(\phi)\mathbf{u} \cdot \nu = \phi^{1/2} g_{\mathrm{N}} \qquad \text{on } \partial\Omega, \tag{5.0.3}$$

where $\mathbf{g}$ and f drive the system and Neumann boundary conditions have been applied for some g_{N} (we will also treat Robin boundary conditions (5.4.1)). The choice of scaling in (5.0.2)–(5.0.3) in terms of ϕ will become clear as we develop the ideas. The critical factor here is that ϕ may vanish on a set of positive measure. This leads to a loss of control on p (see (5.1.4) below), and a number of issues

arise for numerical approximation. In fact p may be unbounded off the support of ϕ, which is difficult to approximate numerically. Moreover, if ϕ vanishes, say everywhere for simplicity, it appears that the first equation implies that $\mathbf{u} = 0$, but the second equation trivializes to $0 = 0$ (when $b(0) = 0$), leading to more numerical difficulties.

To recover (3.1.1)–(3.1.2), set $a(\phi) = \frac{\mu_f}{k_0}\phi^{2(1+\Theta)}$, $b(\phi) = 1$, and $p = q_f$. Moreover, $\phi^{-1/2} f$ represents the matrix pressure.

5.1 A-priori estimates and a change of dependent variables

We proceed formally by assuming that there is a sufficiently smooth solution to the degenerate system (5.0.1)–(5.0.3) and that ϕ is reasonable. It will be convenient to define

$$c(\phi) = \sqrt{b(\phi)/a(\phi)} \quad \text{and} \quad d(\phi) = \sqrt{a(\phi)\, b(\phi)},$$

After an integration by parts we obtain the weak form

$$(c(\phi)^2\mathbf{u}, \psi) - \big(p, \nabla\cdot(b(\phi)\psi)\big) = (b(\phi)\mathbf{g}, \psi), \tag{5.1.1}$$

$$\big(\nabla\cdot(b(\phi)\mathbf{u}), w\big) + (\phi p, w) \qquad = (\phi^{1/2} f, w), \tag{5.1.2}$$

where the test function ψ satisfies the homogeneous boundary condition (5.0.3) with $g_{\mathrm{N}} = 0$ on $\partial\Omega$.

Suppose also that we can extend g_{N} to $\mathbf{u}_{\mathrm{N}}$ in Ω such that

$$b(\phi)\mathbf{u}_{\mathrm{N}}\cdot\nu = \phi^{1/2} g_{\mathrm{N}} \quad \text{on } \partial\Omega. \tag{5.1.3}$$

Taking $\psi = \mathbf{u} - \mathbf{u}_{\mathrm{N}}$ and $w = p$, and also taking $w = \phi^{-1}\nabla\cdot(b(\phi)\mathbf{u})$ in (5.1.1)–(5.1.2) results in the a-priori energy estimates

$$\begin{aligned} &\|c(\phi)\mathbf{u}\| + \|\phi^{1/2}p\| + \|\phi^{-1/2}\nabla\cdot(b(\phi)\mathbf{u})\| \\ &\quad \leq C\big\{\|f\| + \|d(\phi)\mathbf{g}\| + \|c(\phi)\mathbf{u}_{\mathrm{N}}\| + \|\phi^{-1/2}\nabla\cdot(b(\phi)\mathbf{u}_{\mathrm{N}})\|\big\}, \end{aligned} \tag{5.1.4}$$

Assuming the data are given so that the right-hand side is bounded, as ϕ vanishes we potentially lose control of p (and possibly $\mathbf{u}$). This makes sense, since p is the fluid pressure and there is no fluid phase. Nevertheless, we wish to have a well-posed two-phase mixture even as one phase disappears. We do this by making a change of dependent variables.

Let the *scaled velocity* and *pressure* be defined as

$$\mathbf{v} = c(\phi)\mathbf{u} = \sqrt{b(\phi)/a(\phi)}\,\mathbf{u}, \tag{5.1.5}$$

$$q = \phi^{1/2}p, \tag{5.1.6}$$

respectively, since we have control of these quantities. The system (5.0.1)–(5.0.3) becomes

$$\mathbf{v} = -d(\phi)\big(\nabla(\phi^{-1/2}q) - \mathbf{g}\big) \quad \text{in } \Omega, \tag{5.1.7}$$

$$\nabla\cdot(d(\phi)\mathbf{v}) + \phi^{1/2}q = \phi^{1/2}f \quad \text{in } \Omega, \tag{5.1.8}$$

$$d(\phi)\mathbf{v}\cdot\nu = \phi^{1/2}g_{\mathrm{N}} \quad \text{on } \partial\Omega. \tag{5.1.9}$$

If we divide the second equation by $\phi^{1/2}$, this system is antisymmetric, since the formal adjoint of $-d(\phi)\nabla(\phi^{-1/2}(\cdot))$ is $\phi^{-1/2}\nabla\cdot(d(\phi)(\cdot))$. Now the energy esti-

mates read more simply as

$$\begin{aligned} &\|\mathbf{v}\| + \|q\| + \|\phi^{-1/2}\nabla\cdot(d(\phi)\mathbf{v})\| \\ &\quad \le C\big\{\|f\| + \|d(\phi)\mathbf{g}\| + \|\mathbf{v}_{\mathrm{N}}\| + \|\phi^{-1/2}\nabla\cdot(d(\phi)\mathbf{v}_{\mathrm{N}})\|\big\}, \end{aligned} \tag{5.1.10}$$

where $\mathbf{v}_{\mathrm{N}} = c(\phi)\mathbf{u}_{\mathrm{N}}$.

5.2 The space $H_{\phi,d}(\mathbf{div},\Omega)$

We wish to define a space analogous to $H(\mathrm{div},\Omega)$ where the quantity $\phi^{-1/2}\nabla\cdot(d(\phi)\mathbf{v})$ is well-defined. Let

$$H_{\phi,d}(\mathrm{div};\Omega) = \big\{\mathbf{v}\in(L^2(\Omega))^d \,:\, \phi^{-1/2}\nabla\cdot(d(\phi)\mathbf{v})\in L^2(\Omega)\big\}, \tag{5.2.1}$$

and we assume that ϕ is well enough behaved to support the definition. To define $H_{\phi,d}(\mathrm{div})$, we interpret

$$\phi^{-1/2}\nabla\cdot(d(\phi)\mathbf{v}) = \phi^{-1/2}\nabla d(\phi)\cdot\mathbf{v} + \phi^{-1/2}d(\phi)\nabla\cdot\mathbf{v}, \tag{5.2.2}$$

and so we simply require that $\phi^{-1/2}\nabla d(\phi)$ is in $(L^\infty(\Omega))^d$ and $\phi^{-1/2}d(\phi)$ times the weak divergence of $\mathbf{v}$ lies in $L^2(\Omega)$. The natural conditions seem to be that

$$\phi^{-1/2}d(\phi)\in L^\infty(\Omega) \quad \text{and} \quad \phi^{-1/2}\nabla d(\phi)\in(L^\infty(\Omega))^d, \tag{5.2.3}$$

where $L^\infty(\Omega)$ is the space of functions with bounded essential supremum (thinking of bounded functions is sufficient). Moreover, to ensure that the formal adjoint operator $-d(\phi)\nabla(\phi^{-1/2}(\cdot))$ is well defined, we also ask that

$$\phi^{-3/2}d(\phi)\nabla\phi\in(L^\infty(\Omega))^d. \tag{5.2.4}$$

We remark that our conditions (5.2.3) and (5.2.4) are equivalent to the requirement that $\phi^{-1/2}d(\phi) \in W^{1,\infty}(\Omega) = \{u \in L^\infty(\Omega) : \nabla u \in L^\infty(\Omega)\}$ and $\phi^{-1/2}\nabla d(\phi) \in (L^\infty(\Omega))^d$.

Lemma 5.2.1. *If* (5.2.3) *and* (5.2.4) *holds, then* $H_{\phi,d}(\mathrm{div};\Omega)$ *is a Hilbert space with the inner-product*

$$(\mathbf{u},\mathbf{v})_{H_{\phi,d}(div)} = (\mathbf{u},\mathbf{v}) + \big(\phi^{-1/2}\nabla\cdot(d(\phi)\mathbf{u}), \phi^{-1/2}\nabla\cdot(d(\phi)\mathbf{v})\big). \tag{5.2.5}$$

Moreover, $H(\mathrm{div};\Omega) \subset H_{\phi,d}(\mathrm{div};\Omega)$.

Proof. Clearly $H_{\phi,d}(\mathrm{div};\Omega)$ is linear and $(\cdot,\cdot)_\phi$ is an inner product so we only have to show completeness. Let $\{\mathbf{u}_n\}_{n=1}^\infty \in H_{\phi,d}(\mathrm{div};\Omega)$ be a Cauchy sequence, that is

$$||\mathbf{u}_m - \mathbf{u}_n||^2_{H_{\phi,d}(\mathrm{div};\Omega)} = ||\mathbf{u}_m - \mathbf{u}_n||^2 + ||\phi^{-1/2}\nabla\cdot(d(\phi)(\mathbf{u}_m - \mathbf{u}_n))||^2 \to 0$$

as $m,n \to \infty$. This implies existence of $\mathbf{u} \in (L^2(\Omega))^d$ such that $\mathbf{u}_n \to \mathbf{u}$ in $(L^2(\Omega))^d$ and $\xi \in L^2(\Omega)$ such that $\xi_n = \phi^{-1/2}\nabla\cdot(d(\phi)\mathbf{u}_n) \to \xi$ in $L^2(\Omega)$, as $n \to \infty$. For a test function $\psi \in C_0^\infty(\Omega)$,

$$\begin{aligned}
\big(\phi^{-1/2}\nabla\cdot(d(\phi)\mathbf{u}_n), \psi\big) &= -\big(\mathbf{u}_n, d(\phi)\nabla(\phi^{-1/2}\psi)\big) \\
&= \tfrac{1}{2}\big(\mathbf{u}_n, \phi^{-3/2}d(\phi)\nabla\phi\,\psi\big) - \big(\mathbf{u}_n, \phi^{-1/2}d(\phi)\nabla\psi\big) \\
&\longrightarrow \tfrac{1}{2}\big(\mathbf{u}, \phi^{-3/2}d(\phi)\nabla\phi\,\psi\big) - \big(\mathbf{u}, \phi^{-1/2}d(\phi)\nabla\psi\big) \\
&= \big(\phi^{-1/2}\nabla\cdot(d(\phi)\mathbf{u}), \psi\big)
\end{aligned}$$

This shows that $\xi_n = \phi^{-1/2}\nabla\cdot(d(\phi)\mathbf{u}_n) \to \phi^{-1/2}\nabla\cdot(d(\phi)\mathbf{u})$ weakly in $L^2(\Omega)$ so $\xi = \phi^{-1/2}\nabla\cdot(d(\phi)\mathbf{u})$ and completeness is proved.

For any $\mathbf{v} \in H(\mathrm{div}, \Omega)$, both $\mathbf{v} \in (L^2(\Omega))^d$ and $\nabla \cdot \mathbf{v} \in L^2(\Omega)$, and so (5.2.2) implies that $\phi^{-1/2}\nabla \cdot (d(\phi)\mathbf{v}) \in L^2(\Omega)$, and the final assertion of the lemma holds as well. □

In order to apply the Neumann boundary condition we must define a way to interpret functions in $H_{\phi,d}(\mathrm{div}, \Omega)$ on the boundary. Define the normal trace operator $\gamma_{\phi,d} : H_{\phi,d}(\mathrm{div}; \Omega) \to H^{-1/2}(\partial\Omega)$ using the integration by parts formula

$$\begin{aligned}\langle \gamma_{\phi,d}(\mathbf{v}), w \rangle &= \big(\phi^{-1/2}\nabla \cdot (d(\phi)\mathbf{v}), w\big) + \big(\mathbf{v}, d(\phi)\nabla(\phi^{-1/2}w)\big) \\ &= \big(\phi^{-1/2}\nabla \cdot (d(\phi)\mathbf{v}), w\big) + \big(\mathbf{v}, \phi^{-1/2}d(\phi)\nabla w)\big) - \big(\mathbf{v}, \tfrac{1}{2}\phi^{-3/2}d(\phi)\nabla\phi w)\big),\end{aligned} \tag{5.2.6}$$

wherein $w \in H^{1/2}(\partial\Omega)$ has been extended to $w \in H^1(\Omega)$. Note that (5.2.3) and (5.2.4) imply that the operator is well-defined by the right-hand side of (5.2.6), and that we can interpret $\gamma_{\phi,d}(\mathbf{v}) = \phi^{-1/2}d(\phi)\mathbf{v} \cdot \nu$.

Lemma 5.2.2. *If* (5.2.3) *and* (5.2.4) *hold, then the normal trace operator* $\gamma_{\phi,d} : H_{\phi,d}(\mathrm{div}; \Omega) \to H^{-1/2}(\partial\Omega)$ *is well defined by* (5.2.6) *and there is a constant* $C > 0$ *such that*

$$\|\gamma_{\phi,d}(\mathbf{v})\|_{-1/2,\partial\Omega} = \|\phi^{-1/2}d(\phi)\mathbf{v} \cdot \nu\|_{-1/2,\partial\Omega} \leq C\|\mathbf{v}\|_{H_{\phi,d}(\mathrm{div};\Omega)} \tag{5.2.7}$$

for any $\mathbf{v} \in H_{\phi,d}(\mathrm{div}; \Omega)$.

Finally, to apply the homogeneous boundary condition define

$$H_{\phi,d,0}(\mathrm{div}; \Omega) = \big\{\mathbf{v} \in H_{\phi,d}(\mathrm{div}; \Omega) \ : \ \gamma_{\phi,d}(\mathbf{v}) = \phi^{-1/2}d(\phi)\mathbf{v} \cdot \nu = 0 \text{ on } \partial\Omega\big\}, \tag{5.2.8}$$

and we let the image of the normal trace operator be denoted by

$$H_{\phi,d}^{-1/2}(\partial\Omega) = \gamma_{\phi,d}\big(H_{\phi,d}(\mathrm{div};\Omega)\big) \subset H^{-1/2}(\partial\Omega). \tag{5.2.9}$$

5.3 A scaled weak formulation and unique existence of the solution

Replacing (5.1.3) is the requirement of a function $\mathbf{v}_\mathrm{N} \in H_{\phi,d}(\mathrm{div};\Omega)$ such that

$$\gamma_{\phi,d}(\mathbf{v}_\mathrm{N}) = \phi^{-1/2} d(\phi)\mathbf{v}_\mathrm{N} \cdot \nu = g_\mathrm{N}, \tag{5.3.1}$$

which can be found provided that $g_\mathrm{N} \in H_{\phi,d}^{-1/2}(\partial\Omega)$. In place of the weak system (5.1.1)–(5.1.2), we test (5.1.7) and $\phi^{-1/2}$ times (5.1.8) to obtain our scaled weak formulation: Find $\mathbf{v} \in H_{\phi,d,0}(\mathrm{div};\Omega) + \mathbf{v}_\mathrm{N}$ and $q \in L^2(\Omega)$ such that

$$(\mathbf{v},\psi) - \big(q, \phi^{-1/2}\nabla\cdot(d(\phi)\psi)\big) = (d(\phi)\mathbf{g},\psi) \quad \forall \psi \in H_{\phi,d,0}(\mathrm{div};\Omega), \tag{5.3.2}$$

$$\big(\phi^{-1/2}\nabla\cdot(d(\phi)\mathbf{v}), w\big) + (q,w) \ = (f,w) \qquad \forall w \in L^2(\Omega). \tag{5.3.3}$$

We require that $f \in L^2(\Omega)$ and $d(\phi)\mathbf{g} \in (L^2(\Omega))^d$.

The a-priori energy estimates (5.1.10) for (5.3.2)–(5.3.3), imply that if there is a solution to the problem, then it is unique. To prove existence of a solution, we let $\delta \geq 0$ and define the stabilized bilinear form $a_\delta : \big(H_{\phi,d,0}(\mathrm{div},\Omega) \times L^2(\Omega)\big) \times \big(H_{\phi,d,0}(\mathrm{div},\Omega) \times L^2(\Omega)\big) \to \mathbb{R}$ by

$$\begin{aligned} &a_\delta\big((\mathbf{v}_0,q),(\psi,w)\big) \\ &\quad = (\mathbf{v}_0,\psi) - \big(q,\phi^{-1/2}\nabla\cdot(d(\phi)\psi)\big) + \big(\phi^{-1/2}\nabla\cdot(d(\phi)\mathbf{v}_0),w\big) + (q,w) \\ &\qquad + \delta\big\{\big(\phi^{-1/2}\nabla\cdot(d(\phi)\mathbf{v}_0), \phi^{-1/2}\nabla\cdot(d(\phi)\psi)\big) + \big(q,\phi^{-1/2}\nabla\cdot(d(\phi)\psi)\big)\big\} \end{aligned} \tag{5.3.4}$$

and the linear form $b_\delta : H_{\phi,d,0}(\mathrm{div},\Omega)\times L^2(\Omega)\to\mathbb{R}$ by

$$b_\delta(\psi,w) = (d(\phi)\mathbf{g},\psi) - (\mathbf{v}_\mathrm{N},\psi) + \big(f-\phi^{-1/2}\nabla\cdot(d(\phi)\mathbf{v}_\mathrm{N}),w\big) \\ + \delta\big\{\big(f-\phi^{-1/2}\nabla\cdot(d(\phi)\mathbf{v}_\mathrm{N}),\phi^{-1/2}\nabla\cdot(d(\phi)\psi)\big)\big\}. \tag{5.3.5}$$

These two forms are clearly continuous, i.e., bounded.

We now have the problem: Find $(\mathbf{v}_0,q)\in H_{\phi,d,0}(\mathrm{div};\Omega)\times L^2(\Omega)$ such that

$$a_\delta\big((\mathbf{v}_0,q),(\psi,w)\big) = b_\delta(\psi,w) \quad \forall(\psi,w)\in H_{\phi,d,0}(\mathrm{div};\Omega)\times L^2(\Omega). \tag{5.3.6}$$

With $\mathbf{v}=\mathbf{v}_0+\mathbf{v}_\mathrm{N}$ and $\delta=0$, this problem is (5.3.2)–(5.3.3). In fact, since $\psi\in H_{\phi,d}(\mathrm{div},\Omega)$, $\phi^{-1/2}\nabla\cdot(d(\phi)\psi)\in L^2(\Omega)$, and

$$a_\delta\big((\mathbf{v}_0,q),(\psi,w)\big) - b_\delta(\psi,w) \\ = a_0\big((\mathbf{v}_0,q),(\psi,w+\delta\phi^{-1/2}\nabla\cdot(d(\phi)\psi))\big) - b_0\big(\psi,w+\delta\phi^{-1/2}\nabla\cdot(d(\phi)\psi)\big).$$

Since $w+\delta\phi^{-1/2}\nabla\cdot(d(\phi)\psi)$ is arbitrary in L^2, problems (5.3.6) are equivalent for any $\delta\geq 0$.

For any $\delta\in(0,2)$, the bilinear form a_δ is coercive. To see this, compute that

$$\begin{aligned} a_\delta\big((\mathbf{v}_0,q),(\mathbf{v}_0,q)\big) &= \|\mathbf{v}_0\|^2+\|q\|^2+\delta\|\phi^{-1/2}\nabla\cdot(d(\phi)\mathbf{v}_0)\|^2+\delta\big(q,\phi^{-1/2}\nabla\cdot(d(\phi)\mathbf{v}_0)\big) \\ &\geq \|\mathbf{v}_0\|^2+\big(1-\tfrac{1}{2}\delta\big)\|q\|^2+\tfrac{1}{2}\delta\|\phi^{-1/2}\nabla\cdot(d(\phi)\mathbf{v}_0)\|^2 \\ &\geq \tfrac{1}{2}\delta\|\mathbf{v}_0\|_{H_{\phi,d}(\mathrm{div})}+\big(1-\tfrac{1}{2}\delta\big)\|q\|^2. \end{aligned}$$

Therefore, we can apply the Lax-Milgram Theorem to conclude that (5.3.6) has a unique solution for $\delta\in(0,2)$. By the equivalence of the weak problems, we then

have a solution for any $\delta \geq 0$, and in particular for problem (5.3.6) with $\delta = 0$, i.e., (5.3.2)–(5.3.3) (which we already know is unique).

Theorem 5.3.1. *Let* (5.2.3) *and* (5.2.4) *hold,* $f \in L^2(\Omega)$, $d(\phi)\mathbf{g} \in (L^2(\Omega))^d$, *and* $g_{\mathrm{N}} \in H^{-1/2}_{\phi,d}(\partial\Omega)$. *If* $\mathbf{v}_{\mathrm{N}}$ *is defined by* (5.3.1)*, then there is a unique solution to the problem* (5.3.2)–(5.3.3)*, and the energy estimates* (5.1.10) *and* (5.1.4) *hold.*

5.4 Some extensions of the results

We can handle Dirichlet and Robin boundary conditions, and in some cases, we can show that $p \in L^2(\Omega)$.

5.4.1 Dirichlet and Robin boundary conditions

Instead of Neumann boundary conditions (5.0.3), we could impose Dirichlet or Robin boundary conditions of the form

$$\phi p - \kappa^2 b(\phi)\mathbf{u}\cdot\nu = \phi^{1/2} g_R \quad \text{on } \partial\Omega, \tag{5.4.1}$$

where $\kappa \geq 0$ is a bounded function and g_R is given. The scaled version is

$$q - \kappa^2 \phi^{-1/2} d(\phi)\mathbf{v}\cdot\nu = g_R \quad \text{on } \partial\Omega, \tag{5.4.2}$$

and the scaled weak form is: Find $\mathbf{v} \in H_{\phi,d}(\mathrm{div};\Omega)$ and $q \in L^2(\Omega)$ such that

$$\begin{aligned}(\mathbf{v},\psi) - \big(q, \phi^{-1/2}\nabla\cdot(d(\phi)\psi)\big) + \langle \kappa^2\phi^{-1} d(\phi)^2 \mathbf{v}\cdot\nu, \psi\cdot\nu\rangle \qquad & (5.4.3)\\ = (d(\phi)\mathbf{g},\psi) - \langle g_R, \phi^{-1/2} d(\phi)\psi\cdot\nu\rangle \qquad \forall \psi \in H_{\phi,d}(\mathrm{div};\Omega),& \\ \big(\phi^{-1/2}\nabla\cdot(d(\phi)\mathbf{v}), w\big) + (q,w) = (f,w) \qquad \forall w \in L^2(\Omega). \qquad & (5.4.4)\end{aligned}$$

We require that $g_R \in H^{1/2}(\partial\Omega)$ (actually, we could require merely that g_R is in the dual space $(H^{-1/2}_{\phi,d}(\partial\Omega))^*$) and, as before, $f \in L^2(\Omega)$ and $d(\phi)\mathbf{g} \in (L^2(\Omega))^d$. Using the Trace Lemma 5.2.2, the a-priori energy estimates are

$$\begin{aligned} &\|\mathbf{v}\| + \|q\| + \|\phi^{-1/2}\nabla\cdot(d(\phi)\mathbf{v})\| + \|\kappa\phi^{-1/2}d(\phi)\mathbf{v}\cdot\nu\|_{\partial\Omega} \\ &\quad \le C\big\{\|f\| + \|d(\phi)\mathbf{g}\| + \|g_R\|_{1/2,\partial\Omega}\big\}. \end{aligned} \tag{5.4.5}$$

To prove an analogue to Theorem 5.3.1 we need to modify a_δ by extending it to $\big(H_{\phi,d}(\mathrm{div}) \times L^2\big) \times \big(H_{\phi,d}(\mathrm{div}) \times L^2\big)$ and adding a term, obtaining

$$\tilde{a}_\delta\big((\mathbf{v},q),(\psi,w)\big) = a_\delta\big((\mathbf{v},q),(\psi,w)\big) + \langle \kappa^2\phi^{-1}d(\phi)^2\mathbf{v}\cdot\nu, \psi\cdot\nu\rangle.$$

We also define $\tilde{b}_\delta : H_{\phi,d}(\mathrm{div}) \times L^2 \to \mathbb{R}$ such that

$$\tilde{b}_\delta(\psi,w) = (d(\phi)\mathbf{g},\psi) + (f,w) - \langle g_R, \phi^{-1/2}d(\phi)\psi\cdot\nu\rangle + \delta\big(f, \phi^{-1/2}\nabla\cdot(d(\phi)\psi)\big).$$

Both $\tilde{a}_\delta$ and $\tilde{b}_\delta$ are continuous, proving coercivity remains unchanged since $\langle \kappa^2\phi^{-1}d(\phi)^2\mathbf{v}\cdot\nu, \psi\cdot\nu\rangle = \|\kappa\phi^{1/2}d(\phi)\mathbf{v}\cdot\nu\|_{\partial\Omega}$ is non-negative, and a-priori estimates (5.4.5) prove uniqueness.

Theorem 5.4.1. *Let* (5.2.3) *and* (5.2.4) *hold,* $f \in L^2(\Omega)$, $d(\phi)\mathbf{g} \in (L^2(\Omega))^d$, *and* $g_R \in H^{1/2}(\partial\Omega)$. *Then there is a unique solution to the problem* (5.4.3)–(5.4.4)*, and the energy estimates* (5.4.5) *hold.*

5.4.2 A condition for the pressure to be in L^2

In some cases the solution is more regular than implied by (5.1.4). Proceeding formally from (5.0.1)–(5.0.2), we have the single equation

$$-\nabla\cdot\big((d(\phi))^2\nabla p\big) + \phi p = \phi^{1/2}f - \nabla\cdot\big((d(\phi))^2\mathbf{g}\big). \tag{5.4.6}$$

We multiply by $\phi^{-1}p$ and integrate by parts using homogeneous Neumann boundary condition (5.0.3) to see that

$$\big((d(\phi))^2\nabla p,\nabla(\phi^{-1}p)\big)+\|p\|^2=(\phi^{-1/2}f,p)+\big((d(\phi))^2\mathbf{g},\nabla(\phi^{-1}p)\big).$$

After formally expanding the derivative terms, we obtain

$$\begin{aligned}
&\big(\phi^{-1}(d(\phi))^2\nabla p,\nabla p\big)+\|p\|^2\\
&\quad=(\phi^{-1/2}f,p)+\big(\phi^{-1}(d(\phi))^2\mathbf{g},\nabla p\big)-\big(\phi^{-2}(d(\phi))^2\nabla\phi\cdot\mathbf{g},p\big)\\
&\qquad+\big(\phi^{-2}(d(\phi))^2\nabla\phi\cdot\nabla p,p\big)\\
&\quad\le\|\phi^{-3/2}d(\phi)\nabla\phi\|_{L^\infty(\Omega)}\|\phi^{-1/2}d(\phi)\nabla p\|\,\|p\|\\
&\qquad+\varepsilon\big\{\|p\|^2+\|\phi^{-1/2}d(\phi)\nabla p\|^2\big\}\\
&\qquad+C_\varepsilon\big\{\|\phi^{-1/2}f\|^2+\|\phi^{-1/2}d(\phi)\mathbf{g}\|^2+\|\phi^{-2}(d(\phi))^2\nabla\phi\cdot\mathbf{g}\|^2\big\}
\end{aligned}$$

for any $\varepsilon>0$, and so

$$\|\phi^{-1/2}d(\phi)\nabla p\|+\|p\|\le C\big\{\|\phi^{-1/2}f\|+\|\phi^{-1/2}d(\phi)\mathbf{g}\|+\|\phi^{-2}(d(\phi))^2\nabla\phi\cdot\mathbf{g}\|\big\},\tag{5.4.7}$$

provided that $\|\phi^{-3/2}d(\phi)\nabla\phi\|_{L^\infty(\Omega)}<2$. For greater generality, we have chosen to work with the scaled pressure. However, it is interesting to note that p may in fact be stable in many cases, and then it is only the loss of an equation that is problematic for numerical approximation.

5.5 Mixed finite element methods

We now discuss discrete versions of our scaled systems (5.3.2)–(5.3.3) for Neumann and (5.4.3)–(5.4.4) for Dirichlet and Robin boundary conditions. We will

impose a finite element mesh as described in chapter 4 and approximate $(\mathbf{v}, q)$ in the lowest order Raviart-Thomas (RT_0) finite element space.

We will make use of the usual projection operators associated with RT_0. Let $\mathcal{P}_{W_h} = \hat{\cdot} : L^2(\Omega) \to W_h$ denote the $L^2(\Omega)$ projection operator, which projects a function into the space of piecewise constant functions. Moreover, let $\pi : H(\mathrm{div};\Omega) \cap L^{2+\varepsilon}(\Omega) \to \mathbf{V}_h$ (any $\varepsilon > 0$) denote the standard Raviart-Thomas or Fortin operator that preserves element average divergence and edge normal fluxes [18, 42, 43].

To simplify the treatment of boundary conditions, when using Neumann conditions, let $\beta_{\mathrm{N}} = 1$ and $\beta_R = 1 - \beta_{\mathrm{N}} = 0$, and when using Robin conditions, $\beta_{\mathrm{N}} = 0$ and $\beta_R = 1$. Also let $\tilde{\mathbf{V}}_h = \beta_{\mathrm{N}} \mathbf{V}_{h,0} + \beta_R \mathbf{V}_h$.

5.5.1 A formal method based on RT_0

The formal mixed finite element method for Neumann (5.3.2)–(5.3.3) or Robin (5.4.3)–(5.4.4) boundary conditions is: Find $\mathbf{v}_h \in \tilde{\mathbf{V}}_h + \beta_{\mathrm{N}} \mathbf{v}_{\mathrm{N}}$ and $q_h \in W_h$ such that

$$
\begin{aligned}
&(\mathbf{v}_h, \psi) - \left(q_h, \phi^{-1/2} \nabla \cdot (d(\phi)\psi)\right) + \beta_R \langle \kappa^2 \phi^{-1} (d(\phi))^2 \mathbf{v}_h \cdot \nu, \psi \cdot \nu \rangle && (5.5.1)\\
&\quad = (d(\phi)\mathbf{g}, \psi) - \beta_R \langle g_R, \phi^{-1/2} d(\phi) \psi \cdot \nu \rangle && \forall \psi \in \tilde{\mathbf{V}}_h,\\
&\left(\phi^{-1/2} \nabla \cdot (d(\phi)\mathbf{v}_h), w\right) + (q_h, w) = (f, w) && \forall w \in W_h. \quad (5.5.2)
\end{aligned}
$$

When using Neumann boundary conditions, we might choose to find $\mathbf{v}_h \in \mathbf{V}_{h,0} + \pi \mathbf{v}_{\mathrm{N}}$ instead. To show unique solvability and stability for the Robin case requires a discrete version of the Trace Lemma 5.2.2.

Lemma 5.5.1. *If* (5.2.3) *and* (5.2.4) *hold and the finite element mesh* $\mathcal{T}_h$ *is quasi-uniform, then there is a constant* $C > 0$ *such that*

$$\|\phi^{-1/2}\nabla\cdot(d(\phi)\mathbf{v}_h)\| \le C\big\{\|\mathbf{v}_h\| + \|\mathcal{P}_{W_h}[\phi^{-1/2}\nabla\cdot(d(\phi)\mathbf{v}_h)]\|\big\} \tag{5.5.3}$$

for any $\mathbf{v}_h \in \mathbf{V}_h$. *Moreover, for some possibly different constant* $C > 0$,

$$\begin{aligned}\|\gamma_{\phi,d}(\mathbf{v}_h)\|_{-1/2,\partial\Omega} &= \|\phi^{-1/2}d(\phi)\mathbf{v}_h\cdot\nu\|_{-1/2,\partial\Omega} \\ &\le C\big\{\|\mathbf{v}_h\| + \|\mathcal{P}_{W_h}[\phi^{-1/2}\nabla\cdot(d(\phi)\mathbf{v}_h)]\|\big\}\end{aligned} \tag{5.5.4}$$

for any $\mathbf{v}_h \in \mathbf{V}_h$.

Proof. The triangle inequality gives that

$$\begin{aligned}&\|\phi^{-1/2}\nabla\cdot(d(\phi)\mathbf{v}_h)\| \\ &\quad\le \|\mathcal{P}_{W_h}[\phi^{-1/2}\nabla\cdot(d(\phi)\mathbf{v}_h)]\| + \|\phi^{-1/2}\nabla\cdot(d(\phi)\mathbf{v}_h) - \mathcal{P}_{W_h}[\phi^{-1/2}\nabla\cdot(d(\phi)\mathbf{v}_h)]\|.\end{aligned}$$

We compute that

$$\begin{aligned}&\|\phi^{-1/2}\nabla\cdot(d(\phi)\mathbf{v}_h) - \mathcal{P}_{W_h}[\phi^{-1/2}\nabla\cdot(d(\phi)\mathbf{v}_h)]\| \\ &\quad= \|\phi^{-1/2}\nabla d(\phi)\cdot\mathbf{v}_h - \mathcal{P}_{W_h}[\phi^{-1/2}\nabla d(\phi)\cdot\mathbf{v}_h] \\ &\qquad\qquad + \phi^{-1/2}d(\phi)\nabla\cdot\mathbf{v}_h - \mathcal{P}_{W_h}[\phi^{-1/2}d(\phi)\nabla\cdot\mathbf{v}_h]\| \\ &\quad\le 2\|\phi^{-1/2}\nabla d(\phi)\cdot\mathbf{v}_h\| + \|\phi^{-1/2}d(\phi)\nabla\cdot\mathbf{v}_h - \mathcal{P}_{W_h}[\phi^{-1/2}d(\phi)\nabla\cdot\mathbf{v}_h]\| \\ &\quad\le C\|\mathbf{v}_h\| + \big\|\big(\phi^{-1/2}d(\phi) - \mathcal{P}_{W_h}[\phi^{-1/2}d(\phi)]\big)\nabla\cdot\mathbf{v}_h\big\|,\end{aligned}$$

since $\phi^{-1/2}\nabla d(\phi) \in (L^\infty(\Omega))^d$ by assumption (5.2.3), and the projection operator,

$\|\mathcal{P}_{W_h}\| = 1$. Further, for the last term,

$$\begin{aligned}
&\big\|\big(\phi^{-1/2}d(\phi) - \mathcal{P}_{W_h}[\phi^{-1/2}d(\phi)]\big)\nabla\cdot\mathbf{v}_h\big\| \\
&\quad\le \|\phi^{-1/2}d(\phi) - \mathcal{P}_{W_h}[\phi^{-1/2}d(\phi)]\|_{L^\infty(\Omega)}\|\nabla\cdot\mathbf{v}_h\| \\
&\quad\le Ch\|\phi^{-1/2}d(\phi)\|_{W^{1,\infty}(\Omega)}\|\nabla\cdot\mathbf{v}_h\| \\
&\quad\le C\|\phi^{-1/2}d(\phi)\|_{W^{1,\infty}(\Omega)}\|\mathbf{v}_h\|,
\end{aligned}$$

using [23] for the approximation of the L^2-projection in L^∞ and an inverse estimate, since the finite element mesh $\mathcal{T}_h$ is assumed to be quasi-uniform. Because $\phi^{-1/2}d(\phi) \in W^{1,\infty}(\Omega)$ by assumptions (5.2.3) and (5.2.4), the first result (5.5.3) is established. The discrete trace bound (5.5.4) then follows directly from the Trace Lemma 5.2.2. □

Substituting into (5.5.1)–(5.5.2) the discrete solution $\psi = \mathbf{v}_h - \beta_{\mathrm{N}}\mathbf{v}_{\mathrm{N}} \in \tilde{\mathbf{V}}_h$ and $w = q_h + \mathcal{P}_{W_h}[\phi^{-1/2}\nabla\cdot(d(\phi)\mathbf{v}_h)] \in W_h$ shows the stability result

$$\begin{aligned}
&\|\mathbf{v}_h\| + \|q_h\| + \|\mathcal{P}_{W_h}[\phi^{-1/2}\nabla\cdot(d(\phi)\mathbf{v}_h)]\| + \beta_R\|\kappa\phi^{-1/2}d(\phi)\mathbf{v}_h\cdot\nu\|_{\partial\Omega} \qquad (5.5.5)\\
&\quad\le C\big\{\|f\| + \|d(\phi)\mathbf{g}\| \\
&\qquad + \beta_R\|g_R\|_{1/2,\partial\Omega} + \beta_{\mathrm{N}}\big(\|\mathbf{v}_{\mathrm{N}}\| + \|\mathcal{P}_{W_h}[\phi^{-1/2}\nabla\cdot(d(\phi)\mathbf{v}_{\mathrm{N}})]\|\big)\big\}.
\end{aligned}$$

Uniqueness of the solution is therefore established, and existence follows because the discrete system over a basis is a square linear system.

5.5.2 A practical method based on $\mathbf{RT}_0$

The formal method gives rise to a linear system of saddle point form (see (7.1.15) below), which can be difficult to solve. Moreover, it is perhaps not com-

pletely clear how to evaluate the divergence terms involving division by ϕ when ϕ vanishes. We modify the formal method to make it easier to implement and solve, and also to obtain local mass conservation. Denote the local average of ϕ over element $E \in \mathcal{T}_h$ by

$$\phi_E = \frac{1}{|E|}\int_E \phi\, dx = \hat{\phi}|_E. \tag{5.5.6}$$

We present the practical method for Neumann ($\beta_{\mathrm{N}} = 1$) and Robin ($\beta_R = 1$) boundary conditions: Find $\mathbf{v}_h \in \tilde{\mathbf{V}}_h + \beta_{\mathrm{N}}\mathbf{v}_{\mathrm{N}}$ and $q_h \in W_h$ such that

$$\begin{aligned}
&(\mathbf{v}_h, \psi) - \big(q_h, \hat{\phi}^{-1/2}\nabla\cdot(d(\phi)\psi)\big) + \beta_R\langle \kappa^2\phi^{-1}(d(\phi))^2\mathbf{v}_h\cdot\nu, \psi\cdot\nu\rangle && (5.5.7)\\
&\quad = (d(\phi)\mathbf{g}, \psi) - \beta_R\langle g_R, \phi^{-1/2}d(\phi)\psi\cdot\nu\rangle && \forall \psi \in \tilde{\mathbf{V}}_h,\\
&\big(\hat{\phi}^{-1/2}\nabla\cdot(d(\phi)\mathbf{v}_h), w\big) + (q_h, w) = (\hat{\phi}^{-1/2}\phi^{1/2}f, w) && \forall w \in W_h, \qquad (5.5.8)
\end{aligned}$$

with the caveat that we set the divergence terms to zero on an element E that would otherwise include $\hat{\phi}^{-1/2}$ when $\hat{\phi}|_E = \phi_E = 0$, and in that case, $\hat{\phi}^{-1/2}\phi^{1/2}f = f$.

We then easily recover the discrete pressure $p_h \in W_h$ by setting for all $E \in \mathcal{T}_h$

$$p_h|_E = \begin{cases} 0 & \text{if } \phi_E = 0,\\ \phi_E^{-1/2} q_h|_E & \text{if } \phi_E \neq 0, \end{cases} \tag{5.5.9}$$

and the discrete velocity $\mathbf{u}_h \in \tilde{\mathbf{V}}_h + \beta_{\mathrm{N}}\mathbf{v}_{\mathrm{N}}$ is defined by setting for all $e \in \mathcal{E}_h$

$$\mathbf{u}_h\cdot\nu|_e = \begin{cases} 0 & \text{if } b_e \equiv \displaystyle\int_e b(\phi)\, ds = 0,\\ b_e^{-1}\displaystyle\int_e d(\phi)\, ds\, \mathbf{v}_h\cdot\nu|_e & \text{if } b_e \neq 0, \end{cases} \tag{5.5.10}$$

so that $\pi(b(\phi)\mathbf{u}_h) = \pi(d(\phi)\mathbf{v}_h)$. Note that $\int_e b(\phi)\, ds = 0 \Rightarrow \phi|_e = 0 \Rightarrow \int_e d(\phi)\, ds = 0$.

We now discuss in detail implementation of the method, restricted to Robin boundary conditions for simplicity of exposition. Using the degrees of freedom for RT_0, $\mathbf{V}_h$ and W_h in (4.1.3) and (4.1.4), the linear system corresponding to the method (5.5.7)–(5.5.8) is thus

$$\begin{pmatrix} A & -B \\ B^T & C \end{pmatrix} \begin{pmatrix} v \\ q \end{pmatrix} = \begin{pmatrix} a \\ b \end{pmatrix}, \tag{5.5.11}$$

wherein v and q represent the degrees of freedom for $\mathbf{v}$ and q, respectively. We compute

$$\begin{aligned} A_{e,f} &= (\mathbf{v}_e, \mathbf{v}_f) + \langle \kappa^2 \phi^{-1} d(\phi)^2 \mathbf{v}_e \cdot \nu, \mathbf{v}_f \cdot \nu \rangle \qquad (5.5.12) \\ &= \Big(\frac{1}{3}|E_e| + \int_{e \cap \partial\Omega} \kappa^2 \phi^{-1} d(\phi)^2 \, ds \Big) \delta_{e,f} + \frac{1}{6} |E_{e,f}| \nu_e \cdot \nu_f, \\ C_{E,F} &= (w_E, w_F) = |E| \, \delta_{E,F}, \qquad (5.5.13) \end{aligned}$$

where E_e is the support of $\mathbf{v}_e$ (i.e., the one or two elements adjacent to e), and $E_{e,f}$ is the intersection of the supports of $\mathbf{v}_e$ and $\mathbf{v}_f$. Moreover,

$$\begin{aligned} a_e &= (d(\phi)\mathbf{g}, \mathbf{v}_e) - \langle g_R, \phi^{-1/2} d(\phi) \mathbf{v}_e \cdot \nu \rangle \qquad (5.5.14) \\ &= \int_{E_e} d(\phi) \mathbf{g} \cdot \mathbf{v}_e \, dx - \mathbf{v}_e \cdot \nu \int_{e \cap \partial\Omega} g_R \phi^{-1/2} d(\phi) \, ds, \\ b_E &= (\hat{\phi}^{-1/2} \phi^{1/2} f, w_E) = \begin{cases} \displaystyle\int_E f \, dx & \text{if } \phi_E = 0, \\ \phi_E^{-1/2} \displaystyle\int_E \phi^{1/2} f \, dx & \text{if } \phi_E \neq 0. \end{cases} \qquad (5.5.15) \end{aligned}$$

The matrix B remains, but it is now clear how it is defined because we have avoided division by ϕ when $\phi = 0$. In terms of our projection operators,

$$B_{e,E} = \big(\hat{\phi}^{-1/2} \nabla \cdot (d(\phi)\mathbf{v}_e), w_E \big) = \langle \phi_E^{-1/2} d(\phi) \mathbf{v}_e \cdot \nu, w_E \rangle_{\partial E};$$

that is,

$$B_{e,E} = \begin{cases} 0 & \text{if } e \not\subset \partial E \text{ or } \phi_E = 0, \\ \phi_E^{-1/2} \mathbf{v}_e \cdot \nu_E \displaystyle\int_e d(\phi)\, dx & \text{if } e \subset \partial E \text{ and } \phi_E \neq 0. \end{cases} \tag{5.5.16}$$

5.5.3 Cell-centered finite difference

To simplify implementation, we could approximate the first integral in (5.5.7) by a trapezoidal quadrature rule $(\cdot,\cdot)_Q$ so that for RT_0 basis functions

$$(\mathbf{v}_e, \mathbf{v}_f)_Q = \frac{1}{2}|E_e|\delta_{e,f}. \tag{5.5.17}$$

This approximation leads to a cell-centered finite difference method [6, 44]. The Schur complement of (7.1.15) for q is

$$v = A^{-1}(Bq + a), \tag{5.5.18}$$

$$(B^T A^{-1} B + C)\, q = b - B^T A^{-1} a. \tag{5.5.19}$$

The matrix of the second equation can be formed as a 5-point finite difference stencil because A and C are diagonal and positive definite [6, 44]. Thus we solve the second equation (5.5.19) relatively efficiently as a cell-centered finite difference method for q, and then form v using q and the first equation (5.5.18). Moreover, $(\psi, \psi)_Q^{1/2}$ is a norm on $\mathbf{V}_h$ equivalent to $\|\psi\|$ with bounds independent of h [54].

5.5.4 Discrete representation of ϕ

We remark that, in practice, our problem is a subproblem of a larger system that determines ϕ (see appendix B), so ϕ will be represented in a discrete space Φ_h.

We might chose the space used by the Arbogast and Chen [3] to approximate the solution to a nondegenerate second order elliptic problem using a nonconforming method. The nonconforming method is equivalent to a mixed method based on RT_0. The solution variable is approximated with degrees of freedom defined by element average values $\phi_E \ \forall E \in \mathcal{T}_h$ in (5.5.6) and face (or edge) average values

$$\phi_e = \frac{1}{|e|} \int_e \phi \, ds \ \ \forall e \in \mathcal{E}_h. \tag{5.5.20}$$

The space is

$$\Phi_h = \left\{ \phi \, : \, \phi|_E \in \mathbb{P}_{2,0} + \mathbb{P}_{0,2} \ \forall E \in \mathcal{T}_h \text{ and } \phi_e \text{ is unique } \forall e \in \mathcal{E}_h \right\}.$$

In this case, we could define the method using only the degrees of freedom of $\phi \in \Phi_h$. To do so, we would simply replace ϕ by ϕ_e in (5.5.12), the second integral of (5.5.14), and (5.5.16), and replace ϕ by ϕ_E in the first integral of (5.5.14) and (5.5.15).

5.5.5 Local mass conservation of the practical method

The equation (5.5.8) implies that mass is conserved locally by the practical method. Taking test function $\phi_E^{1/2} w_E \in W_h$,

$$\int_E \nabla \cdot (d(\phi)\mathbf{v}_h)\, dx + \int_E \phi_E^{1/2} q_h \, dx = \int_E \phi^{1/2} f \, dx, \tag{5.5.21}$$

which is the same as

$$\int_E \nabla \cdot \pi(d(\phi)\mathbf{v}_h)\, dx + \int_E \phi \, \phi_E^{-1/2} q_h \, dx = \int_E \phi^{1/2} f \, dx.$$

Since (5.5.10) defines $\mathbf{u}_h \in \mathbf{V}_h$ such that $\pi(d(\phi)\mathbf{v}_h) = \pi(b(\phi)\mathbf{u}_h)$ and (5.5.9) defines $p_h \in W_h$, we have

$$\int_E \nabla \cdot (b(\phi)\mathbf{u}_h)\,dx + \int_E \phi\, p_h\,dx = \int_E \phi^{1/2} f\,dx, \tag{5.5.22}$$

which is the mass conservation equation (5.0.2) integrated over E.

5.5.6 Solvability and stability of the practical method

Substituting $\psi = \mathbf{v}_h - \beta_{\mathrm{N}}\mathbf{v}_{\mathrm{N}} \in \tilde{\mathbf{V}}_h$ and $w = q_h + \mathcal{P}_{W_h}[\hat{\phi}^{-1/2}\nabla\cdot(d(\phi)\mathbf{v}_h)] \in W_h$ into (5.5.7)–(5.5.8) gives

$$\begin{aligned}
&\|\mathbf{v}_h\|^2 + \|q_h\|^2 + \|\mathcal{P}_{W_h}[\hat{\phi}^{-1/2}\nabla\cdot(d(\phi)\mathbf{v}_h)]\|^2 + \beta_R\|\kappa\phi^{-1/2}d(\phi)\mathbf{v}_h\cdot\nu\|_{\partial\Omega}^2 \\
&\quad \le C\big\{\|\hat{\phi}^{-1/2}\phi^{1/2} f\|^2 + \|d(\phi)\mathbf{g}\|^2 + \beta_R|\langle g_R, \phi^{-1/2}d(\phi)\mathbf{v}_h\cdot\nu\rangle|^2 \\
&\qquad + \beta_{\mathrm{N}}\big(\|\mathbf{v}_{\mathrm{N}}\|^2 + \|\mathcal{P}_{W_h}[\hat{\phi}^{-1/2}\nabla\cdot(d(\phi)\mathbf{v}_{\mathrm{N}})]\|^2\big)\big\}.
\end{aligned}$$

Uniqueness and, therefore, existence of the solution is established.

Unfortunately, we do not have a discrete trace lemma involving $\hat{\phi}$. In many cases, we obtain the stability bound

$$\begin{aligned}
&\|\mathbf{v}_h\| + \|q_h\| + \|\mathcal{P}_{W_h}[\hat{\phi}^{-1/2}\nabla\cdot(d(\phi)\mathbf{v}_h)]\| + \beta_R\|\kappa\phi^{-1/2}d(\phi)\mathbf{v}_h\cdot\nu\|_{\partial\Omega} \\
&\quad \le C\big\{\|\hat{\phi}^{-1/2}\phi^{1/2} f\| + \|d(\phi)\mathbf{g}\| + \beta_R\|g_R\|_{0,\partial\Omega} \\
&\qquad + \beta_{\mathrm{N}}\big(\|\mathbf{v}_{\mathrm{N}}\| + \|\mathcal{P}_{W_h}[\hat{\phi}^{-1/2}\nabla\cdot(d(\phi)\mathbf{v}_{\mathrm{N}})]\|\big)\big\}.
\end{aligned} \tag{5.5.23}$$

This holds when we use Neumann boundary conditions ($\beta_{\mathrm{N}} = 1$, $\beta_R = 0$), or when we have either homogeneous Robin conditions, i.e., $g_R = 0$, or uniform Robin conditions, i.e., $\kappa \ge \kappa_* > 0$ for some constant κ_*.

In the case of nonhomogeneous, nonuniform Robin boundary conditions, we modify the treatment of g_R in (5.5.7) when $\beta_R = 1$. We base the method on a discrete version of the definition of the normal trace (5.2.6),

$$\langle g_R, \phi^{-1/2} d(\phi)\mathbf{v}_h \cdot \nu\rangle = \big(\hat{g}_R, \hat{\phi}^{-1/2}\nabla\cdot(d(\phi)\mathbf{v}_h)\big) + \big(d(\phi)\nabla(\phi^{-1/2}g_R), \mathbf{v}_h\big),$$

The modified practical method becomes

$$(\mathbf{v}_h, \psi) - \big(q_h, \hat{\phi}^{-1/2}\nabla\cdot(d(\phi)\psi)\big) + \langle \kappa^2\phi^{-1}(d(\phi))^2\mathbf{v}_h\cdot\nu, \psi\cdot\nu\rangle \tag{5.5.24}$$
$$= (d(\phi)\mathbf{g}, \psi) - \big(\hat{g}_R, \hat{\phi}^{-1/2}\nabla\cdot(d(\phi)\mathbf{v}_h)\big) - \big(d(\phi)\nabla(\phi^{-1/2}g_R), \mathbf{v}_h\big)\ \forall \psi \in \mathbf{V}_h,$$
$$\big(\hat{\phi}^{-1/2}\nabla\cdot(d(\phi)\mathbf{v}_h), w\big) + (q_h, w) = (\hat{\phi}^{-1/2}\phi^{1/2}f, w)\ \forall w \in W_h, \tag{5.5.25}$$

wherein we need any $H^1(\Omega)$-extension of g_R to the interior. In this case, we obtain the stability estimate (5.5.23) with the term $\beta_R\|g_R\|_{0,\partial\Omega}$ replaced by $\beta_R\|g_R\|_{1/2,\partial\Omega}$.

5.6 An analysis of the error of the formal method

A full analysis of the error of the practical method is an open question, and is complicated by the fact that ϕ may vanish at points of an element E, but ϕ_E may not vanish. Such an analysis is beyond the scope of this thesis. However, we can give an idea of the errors to be expected by analyzing the formal method that treats the integrals and ϕ exactly, i.e., (5.5.1)–(5.5.2). For simplicity of exposition, we continue the discussion for the Robin system ($\beta_N = 0$).

Since $\mathbf{V}_h \subset H(\mathrm{div}) \subset H_{\phi,d}(\mathrm{div})$, we can take the difference of the weak formulation (5.4.3)–(5.4.4) with discrete test functions and (5.5.1)–(5.5.2). This

leads to the system

$$
\begin{aligned}
&(\mathbf{v}-\mathbf{v}_h,\boldsymbol{\psi}) - \big(q-q_h,\phi^{-1/2}\nabla\cdot(d(\phi)\boldsymbol{\psi})\big) && (5.6.1)\\
&\quad + \langle \kappa^2\phi^{-1}(d(\phi))^2(\mathbf{v}-\mathbf{v}_h)\cdot\boldsymbol{\nu},\boldsymbol{\psi}\cdot\boldsymbol{\nu}\rangle \qquad = 0 \quad \forall \boldsymbol{\psi}\in\mathbf{V}_h,\\
&\big(\phi^{-1/2}\nabla\cdot(d(\phi)(\mathbf{v}-\mathbf{v}_h)),w\big) + (q-q_h,w) = 0 \quad \forall w\in W_h. && (5.6.2)
\end{aligned}
$$

We modify this system by introducing our two projection operators to see that

$$
\begin{aligned}
&(\boldsymbol{\pi}\mathbf{v}-\mathbf{v}_h,\boldsymbol{\psi}) - \big(\hat{q}-q_h,\mathcal{P}_{W_h}[\phi^{-1/2}\nabla\cdot(d(\phi)\boldsymbol{\psi})]\big) + \langle \kappa^2\phi^{-1}(d(\phi))^2(\boldsymbol{\pi}\mathbf{v}-\mathbf{v}_h)\cdot\boldsymbol{\nu},\boldsymbol{\psi}\cdot\boldsymbol{\nu}\rangle\\
&\quad = -(\mathbf{v}-\boldsymbol{\pi}\mathbf{v},\boldsymbol{\psi}) + \big(q-\hat{q},\phi^{-1/2}\nabla\cdot(d(\phi)\boldsymbol{\psi})\big) - \langle \kappa^2\phi^{-1}(d(\phi))^2(\mathbf{v}-\boldsymbol{\pi}\mathbf{v})\cdot\boldsymbol{\nu},\boldsymbol{\psi}\cdot\boldsymbol{\nu}\rangle,\\
&\big(\mathcal{P}_{W_h}[\phi^{-1/2}\nabla\cdot(d(\phi)(\boldsymbol{\pi}\mathbf{v}-\mathbf{v}_h))],w\big) + (\hat{q}-q_h,w)\\
&\quad = -\big(\mathcal{P}_{W_h}[\phi^{-1/2}\nabla\cdot(d(\phi)(\mathbf{v}-\boldsymbol{\pi}\mathbf{v}))],w\big).
\end{aligned}
$$

Assuming that $\mathbf{v}$ is sufficiently regular to compute $\boldsymbol{\pi}\mathbf{v}$, the test functions $\boldsymbol{\psi}=\boldsymbol{\pi}\mathbf{v}-\mathbf{v}_h\in\mathbf{V}_h$ and $w=\hat{q}-q_h+\mathcal{P}_{W_h}[\phi^{-1/2}\nabla\cdot(d(\phi)(\boldsymbol{\pi}\mathbf{v}-\mathbf{v}_h))]\in W_h$, lead us to

$$
\begin{aligned}
&\|\boldsymbol{\pi}\mathbf{v}-\mathbf{v}_h\|^2 + \|\hat{q}-q_h\|^2\\
&\qquad + \|\mathcal{P}_{W_h}[\phi^{-1/2}\nabla\cdot(d(\phi)(\boldsymbol{\pi}\mathbf{v}-\mathbf{v}_h))]\|^2 + \|\kappa\phi^{-1/2}d(\phi)(\boldsymbol{\pi}\mathbf{v}-\mathbf{v}_h)\cdot\boldsymbol{\nu}\|^2_{\partial\Omega}\\
&\quad \le C\big\{\|\mathbf{v}-\boldsymbol{\pi}\mathbf{v}\|^2 + \|q-\hat{q}\|^2\\
&\qquad + \|\mathcal{P}_{W_h}[\phi^{-1/2}\nabla\cdot(d(\phi)(\mathbf{v}-\boldsymbol{\pi}\mathbf{v}))]\|^2 + \|\kappa\phi^{-1/2}d(\phi)(\mathbf{v}-\boldsymbol{\pi}\mathbf{v})\cdot\boldsymbol{\nu}\|^2_{\partial\Omega}\\
&\qquad + \big|\big(q-\hat{q},\phi^{-1/2}\nabla\cdot(d(\phi)(\boldsymbol{\pi}\mathbf{v}-\mathbf{v}_h))\big)\big|\big\}.
\end{aligned}
$$

The last term on the right-hand side arises because we could not substitute the test function $\phi^{-1/2}\nabla\cdot(d(\phi)(\boldsymbol{\pi}\mathbf{v}-\mathbf{v}_h))\notin W_h$ for w.

We continue by estimating

$$
\begin{aligned}
&\left|\left(q-\hat{q}, \phi^{-1/2}\nabla\cdot(d(\phi)(\boldsymbol{\pi}\mathbf{v}-\mathbf{v}_h))\right)\right| \\
&\quad = \left|\left(q-\hat{q}, (I-\mathcal{P}_{W_h})\left[\phi^{-1/2}\nabla d(\phi)\cdot(\boldsymbol{\pi}\mathbf{v}-\mathbf{v}_h) + \phi^{-1/2}d(\phi)\nabla\cdot(\boldsymbol{\pi}\mathbf{v}-\mathbf{v}_h)\right]\right)\right| \\
&\quad \leq C\,\|q-\hat{q}\|\left\{\|\boldsymbol{\pi}\mathbf{v}-\mathbf{v}_h\| + \|(I-\mathcal{P}_{W_h})[\phi^{-1/2}d(\phi)\nabla\cdot(\boldsymbol{\pi}\mathbf{v}-\mathbf{v}_h)]\|\right\},
\end{aligned}
$$

and, since $\nabla\cdot(\boldsymbol{\pi}\mathbf{v}-\mathbf{v}_h)\in W_h$,

$$
\begin{aligned}
&\|(I-\mathcal{P}_{W_h})[\phi^{-1/2}d(\phi)\nabla\cdot(\boldsymbol{\pi}\mathbf{v}-\mathbf{v}_h)]\| \\
&\quad = \|[(I-\mathcal{P}_{W_h})\phi^{-1/2}d(\phi)]\nabla\cdot(\boldsymbol{\pi}\mathbf{v}-\mathbf{v}_h)\| \\
&\quad \leq \|(I-\mathcal{P}_{W_h})\phi^{-1/2}d(\phi)\|_{L^\infty(\Omega)}\|\nabla\cdot(\boldsymbol{\pi}\mathbf{v}-\mathbf{v}_h)\| \\
&\quad \leq Ch\,\|\phi^{-1/2}d(\phi)\|_{W^{1,\infty}(\Omega)}\|\nabla\cdot(\boldsymbol{\pi}\mathbf{v}-\mathbf{v}_h)\| \\
&\quad \leq C\|\boldsymbol{\pi}\mathbf{v}-\mathbf{v}_h\|,
\end{aligned}
$$

using [23] again for the approximation of the L^2-projection in L^∞ and an inverse estimate, assuming that the finite element mesh $\mathcal{T}_h$ is quasi-uniform.

Similar estimates can be shown to hold for the system using Neumann boundary conditions. In this case, the test function $\psi = \boldsymbol{\pi}\mathbf{v}-\mathbf{v}_h+\mathbf{v}_{\mathrm{N}}-\boldsymbol{\pi}\mathbf{v}_{\mathrm{N}}\in\mathbf{V}_{h,0}$ is required.

Theorem 5.6.1. *Let* (5.2.3) *and* (5.2.4) *hold,* $f\in L^2(\Omega)$, $d(\phi)\mathbf{g}\in(L^2(\Omega))^d$, *and assume that the finite element mesh* $\mathcal{T}_h$ *is quasi-uniform. Let* $(\mathbf{v},q)$ *be either the solution to* (5.3.2)–(5.3.3) *with* $\mathbf{v}_N\in H_{\phi,d}(\mathrm{div};\Omega)$ *(and set* $\beta_{\mathrm{N}}=1$, $\beta_R=0$*) or the solution to* (5.4.3)–(5.4.4) *with* $g_R\in H^{1/2}(\partial\Omega)$ *(and set* $\beta_{\mathrm{N}}=0$, $\beta_R=1$*). Let* $(\mathbf{v}_h,q_h)$ *be the solution to the formal method* (5.5.1)–(5.5.2). *Assume that* $\mathbf{v},\beta_{\mathrm{N}}\mathbf{v}_{\mathrm{N}}\in$

$H(\mathrm{div};\Omega)\cap L^{2+\varepsilon}(\Omega)$ *for some* $\varepsilon>0$. *Then*

$$\begin{aligned}
&\|\mathbf{v}-\mathbf{v}_h\|+\|q-q_h\|+\|\mathcal{P}_{W_h}[\phi^{-1/2}\nabla\cdot(d(\phi)(\mathbf{v}-\mathbf{v}_h))]\| \\
&\quad+\beta_R\|\kappa\phi^{-1/2}d(\phi)(\mathbf{v}-\mathbf{v}_h)\cdot\nu\|_{\partial\Omega} \\
&\le C\big\{\|\mathbf{v}-\pi\mathbf{v}\|+\|q-\hat{q}\|+\|\mathcal{P}_{W_h}[\phi^{-1/2}\nabla\cdot(d(\phi)(\mathbf{v}-\pi\mathbf{v}))]\| \\
&\quad+\beta_R\|\kappa\phi^{-1/2}d(\phi)(\mathbf{v}-\pi\mathbf{v})\cdot\nu\|_{\partial\Omega}+\beta_{\mathrm{N}}\|\mathbf{v}_{\mathrm{N}}-\pi\mathbf{v}_{\mathrm{N}}\|_{H_{\phi,d}(\mathrm{div};\Omega)}\big\} \\
&\le C\big\{\|\mathbf{v}-\pi\mathbf{v}\|_{H(\mathrm{div};\Omega)}+\|q-\hat{q}\| \\
&\quad+\beta_R\|\kappa(\mathbf{v}-\pi\mathbf{v})\cdot\nu\|_{\partial\Omega}+\beta_{\mathrm{N}}\|\mathbf{v}_{\mathrm{N}}-\pi\mathbf{v}_{\mathrm{N}}\|_{H(\mathrm{div};\Omega)}\big\}.
\end{aligned}\tag{5.6.3}$$

If the solution is sufficiently regular, the approximation is $\mathcal{O}(h)$. We might expect that the practical method (5.5.7)–(5.5.8) that we proposed also achieves $\mathcal{O}(h)$ convergence. Moreover, we might expect to see superconvergence of order $\mathcal{O}(h^2)$ for sufficiently regular solutions [54]. We see evidence of these assertions in the numerical results presented below.

5.7 Some closed form solutions in one dimension

Before presenting numerical results, we consider a group of closed form solutions in one dimension. Let $\Omega=(-1,1)$, $a(\phi)=b(\phi)=\phi$ (so $d(\phi)=\phi$, $c(\phi)=1$), $\mathbf{g}=0$, and $\tilde{f}=\phi^{-1/2}f$, and reduce the mixed system (5.0.1)–(5.0.3) to

$$-(\phi^2p')'+\phi p=\phi\tilde{f},\quad -1<x<1, \tag{5.7.1}$$

$$\phi^{3/2}(-1)\,p'(-1)=\phi^{3/2}(1)\,p'(1)=0. \tag{5.7.2}$$

This is a Sturm-Liouville problem. By our energy estimates (5.1.4), we require that $u=v=-\phi p'\in L^2(-1,1)$ when $\phi^{1/2}\tilde{f}\in L^2(-1,1)$.

For $\alpha > 0$, let us simplify to the porosity

$$\phi(x) = \begin{cases} 0, & x < 0, \\ x^{\alpha}, & x > 0. \end{cases} \tag{5.7.3}$$

The conditions (5.2.3) and (5.2.4) hold if and only if $\alpha \geq 2$. Now (5.7.1)–(5.7.2) becomes

$$-x^{\alpha} p'' - 2\alpha x^{\alpha-1} p' + p = \tilde{f}, \quad 0 < x < 1, \quad \text{and} \quad p'(1) = 0.$$

When $\alpha = 2$, we have the Euler equation

$$-x^2 p'' - 4x p' + p = \tilde{f}, \quad 0 < x < 1. \tag{5.7.4}$$

In this case the Euler exponents satisfy $r(r-1) + 4r - 1 = 0$, and so

$$r_1 = \frac{-3+\sqrt{13}}{2} \approx 0.3 > 0 \quad \text{and} \quad r_2 = \frac{-3-\sqrt{13}}{2} \approx -3.3 < 0, \tag{5.7.5}$$

and the solution to the homogeneous equation is $p_{\text{hom}}(x) = c_1 x^{r_1} + c_2 x^{r_2}$. The boundary condition and the requirement that $u = -\phi p' \in L^2(0,1)$ shows that the solution is unique. Variation of parameters gives the nonhomogeneous solution as

$$p(x) = \frac{-1}{r_1 - r_2} \left\{ x^{r_1} \left(\int \frac{\tilde{f}(y)}{y^{r_1+1}} \, dy + c_1 \right) - x^{r_2} \left(\int \frac{\tilde{f}(y)}{y^{r_2+1}} \, dy + c_2 \right) \right\}.$$

If we restrict to

$$\tilde{f}(x) = x^{\beta}, \quad 0 < x < 1,$$

then, provided $\beta \neq r_1, r_2$ and $0 < x < 1$, we have the closed form solutions

$$p(x) = \frac{-x^{\beta}}{(\beta - r_1)(\beta - r_2)} + C_1 x^{r_1} + C_2 x^{r_2}.$$

To get $f = \phi^{1/2}\tilde{f} = x^{1+\beta} \in L^2(0,1)$, restrict to $\beta > -3/2$. Then $u = -\phi p' \in L^2(0,1)$ implies that $C_2 = 0$, and the boundary condition determines C_1. The solution is

$$q(x) = x\,p(x) \quad \text{and} \quad p(x) = \begin{cases} 0, & -1 < x \le 0, \\ \dfrac{\beta x^{r_1} - r_1 x^{\beta}}{r_1(\beta - r_1)(\beta - r_2)}, & 0 < x < 1, \end{cases} \tag{5.7.6}$$

$$v(x) = u(x) = \begin{cases} 0, & -1 < x \le 0, \\ \dfrac{-\beta(x^{r_1+1} - x^{\beta+1})}{(\beta - r_1)(\beta - r_2)}, & 0 < x < 1. \end{cases} \tag{5.7.7}$$

5.8 Numerical results

In this section we test the convergence of our proposed numerical method (5.5.7)–(5.5.8) using the cell-centered finite difference scheme outlined in section 5.5.3. We impose Dirichlet boundary conditions *without* using the stabilizing variant (5.5.24). We fix the domain $\Omega = (-1,1)^2$ and use a uniform rectangular mesh of $n = 1/h$ elements in each coordinate direction.

We implement the tests in terms of manufactured solutions in which closed form expressions for ϕ and p are given, and from these f and Dirichlet boundary conditions (i.e., $\kappa = 0$) are computed. In all tests, we take $\mathbf{g} = 0$ and $a(\phi) = b(\phi) = \phi$ (so $d(\phi) = \phi$, $c(\phi) = 1$, and $\mathbf{u} = \mathbf{v}$).

We use discrete L^2-norms to measure the relative errors. For p and q, we use the midpoint quadrature rule applied to the L^2-norm, which gives an approximation to $\|\hat{q} - q_h\|$ and $\|\hat{p} - p_h\|$. For $\mathbf{v}$, we use the trapezoidal rule applied to the $(L^2)^2$-norm, which is effectively like the norm $\|\pi\mathbf{v} - \mathbf{v}_h\|$. In both cases, these are norms for which superconvergence might be expected.

5.8.1 A simple Euler's equation in one dimension

For a given ϕ, it is difficult to determine the exact regularity of the solution. We begin with a test case corresponding to our closed form solution (5.7.6)–(5.7.7) of the Euler equation (5.7.4). In this case, it is easy to see that in terms of the potential singularity near $x = 0$, $q \sim \mathbf{u} \sim |x|^{1.3} + |x|^{1+\beta}$ and $p \sim |x|^{0.3} + |x|^{\beta}$, and so, approximately,

$$q, u \in H^{\min(1.8,3/2+\beta)} \quad \text{and} \quad p \in H^{\min(0.8,1/2+\beta)}.$$

We consider four values of β (which is the parameter in the source function $\tilde{f} = x^{\beta}$ (or $f = x^{1+\beta}$), $0 < x < 1$), $\beta = 1/2$, $-1/2$, -1, and $-3/2$. The numerical results are presented in Table 5.1. Based on the regularity of the solution, if the solution exhibited superconvergence, we would expect the order of convergence for q and u to be $\mathcal{O}(h^{1.8})$ for $\beta = 1/2$, $\mathcal{O}(h^{1})$ for $\beta = -1/2$, $\mathcal{O}(h^{1/2})$ for $\beta = -1$, and no convergence for $\beta = -3/2$. These rates are seen, approximately, in the numerical results. Moreover, the order of convergence for p should be $\mathcal{O}(h^{0.8})$ for $\beta = 1/2$ and no convergence for the other values of β, which we also see approximately.

We remark that the convergence rate is slightly better if instead of using (5.5.15), we simply set $b_E = (f, w_E)$. This, of course, would lead to a loss of strict local mass conservation.

		scaled pressure q		pressure p		velocity $\mathbf{u}$	
β	n	error	rate	err	rate	err	rate
0.5	32	0.002043	—	0.006756	—	0.007438	—
	64	0.000642	1.669	0.004341	0.638	0.002387	1.640
	128	0.000199	1.691	0.002724	0.672	0.000754	1.663
	256	0.000061	1.709	0.001681	0.697	0.000235	1.681
	512	0.000018	1.723	0.001024	0.716	0.000073	1.695
-0.5	32	0.001913	—	0.040343	—	0.013276	—
	64	0.000802	1.254	0.039971	0.013	0.006749	0.976
	128	0.000358	1.166	0.039289	0.025	0.003426	0.978
	256	0.000167	1.101	0.038474	0.030	0.001731	0.985
	512	0.000080	1.060	0.037617	0.033	0.000872	0.990
-1.0	32	0.006379	—	0.155115	—	0.015402	—
	64	0.004849	0.396	0.164987	-0.089	0.010550	0.546
	128	0.003526	0.460	0.170768	-0.050	0.007338	0.524
	256	0.002521	0.484	0.173955	-0.027	0.005142	0.513
	512	0.001790	0.494	0.175645	-0.014	0.003618	0.507
-1.5	32	0.060245	—	0.273779	—	0.004816	—
	64	0.059596	0.016	0.278083	-0.023	0.003470	0.473
	128	0.058620	0.024	0.279416	-0.007	0.002856	0.281
	256	0.057593	0.026	0.279819	-0.002	0.002507	0.188
	512	0.056590	0.025	0.279939	-0.001	0.002281	0.137

Table 5.1: Euler's equation. Shown are the relative discrete L^2-norm errors of q, p, and $\mathbf{u}$ for various number of elements $n \times n$ and for four values of β. The convergence rate corresponds to a superconvergent approximation, restricted by the regularity of the true solution.

5.8.2 A smooth solution test in two-dimensions

For the next series of tests, we assume that $p = \cos(6xy^2)$ is smooth and that ϕ is given by

$$\phi = \begin{cases} 0 & x \leq -3/4 \text{ or } y \leq -3/4, \\ (x+3/4)^{\alpha}(y+3/4)^{2\alpha} & \text{otherwise.} \end{cases} \tag{5.8.1}$$

We note that $\phi^{-1/2}\nabla\phi \in \left(L^{\infty}((-1,1)^2)\right)^2$ if and only if $\alpha \geq 2$. Nevertheless, we consider the four values $\alpha = 2$, 1, $1/4$, and $1/8$. Results are given in Table 5.2. We see good convergence for $\alpha = 2$ and 1, and some degradation for the smaller values of α. It appears that condition (5.2.3) (the second part of which is precisely the condition (5.2.4) when $d(\phi) = \phi$) may be overly restrictive for convergence. In fact, it may be enough that $\phi^{-1/2}\nabla\phi \in \left(L^2((-1,1)^2)\right)^2$, which is true here if and only if $\alpha > 1$.

We depict the solution p and q in Figure 5.1. Although p was chosen to be smooth, we have displayed $p = 0$ in the one-phase region, since it is ill-defined there. Therefore, p is not smooth on the boundary between the one and two phase regions $\Gamma = \{x = -3/4, y \geq -3/4\} \cup \{x \geq -3/4, y = -3/4\}$. We also display the scaled pressure q, which is well-behaved for $\alpha \geq 1$ and degenerates near Γ as α decreases (i.e., as $\phi^{1/2}\nabla\phi$ loses its regularity).

The reader should note that Γ lies on a grid line. If we take an odd number of elements, we will avoid this. Results are shown in Table 5.3. When $\alpha = 2$, we see similar errors and rates of convergence as for the case of Γ being resolved by the grid in Table 5.2. However, the errors are worse for the more challenging case of $\alpha = 1/4$, although the convergence rates seem to settle to about the same values.

		scaled pressure q		pressure p		velocity $\mathbf{u}$	
α	n	error	rate	err	rate	err	rate
2	32	0.012878	—	0.020996	—	0.029391	—
	64	0.003260	1.982	0.007574	1.471	0.009392	1.646
	128	0.000825	1.983	0.002655	1.512	0.002791	1.751
	256	0.000209	1.979	0.000924	1.523	0.000795	1.811
	512	0.000054	1.966	0.000322	1.521	0.000221	1.849
1	32	0.007507	—	0.008594	—	0.023786	—
	64	0.001929	1.961	0.002941	1.547	0.007442	1.676
	128	0.000493	1.966	0.001001	1.555	0.002182	1.770
	256	0.000127	1.955	0.000343	1.545	0.000616	1.824
	512	0.000034	1.924	0.000119	1.533	0.000170	1.858
0.25	32	0.007443	—	0.009351	—	0.019810	—
	64	0.004953	0.588	0.006521	0.520	0.008355	1.246
	128	0.003549	0.481	0.004687	0.476	0.004913	0.766
	256	0.002528	0.490	0.003348	0.485	0.003429	0.519
	512	0.001788	0.500	0.002380	0.493	0.002469	0.474
0.125	32	0.066864	—	0.082809	—	0.048566	—
	64	0.053265	0.328	0.065477	0.339	0.038811	0.323
	128	0.042347	0.331	0.051784	0.338	0.032259	0.267
	256	0.033806	0.325	0.041165	0.331	0.026911	0.262
	512	0.027147	0.317	0.032935	0.322	0.022434	0.263

Table 5.2: Smooth p two-dimensional test. Shown are the relative discrete L^2-norm errors of q, p, and $\mathbf{u}$ for various number of elements $n \times n$ and for three values of α defining ϕ. The convergence rate is better than expected for low values of α.

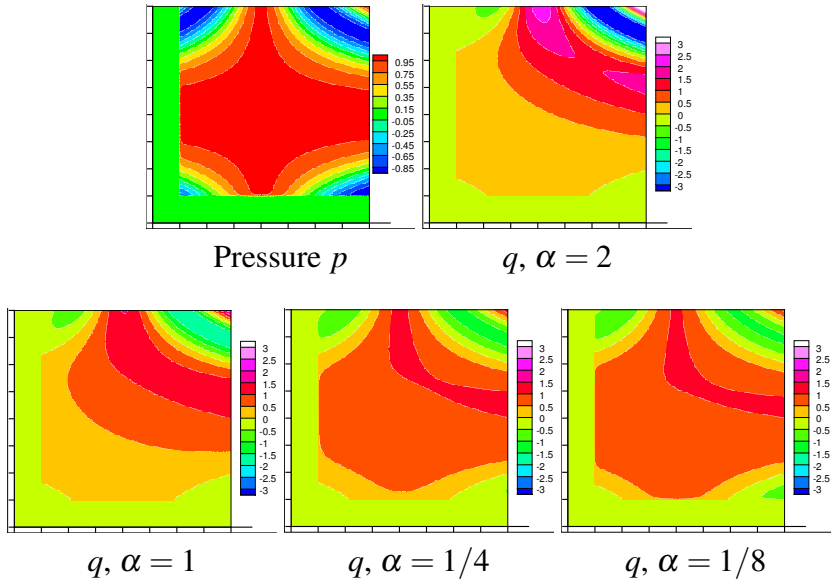

Figure 5.1: Smooth p two-dimensional test. Shown are the pressure p and scaled pressure q for various four values of α defining ϕ. The pressure is smooth, except on the boundary of the support of ϕ (i.e., $x = -3/4$ or $y = -3/4$. The scaled pressure becomes less regular near the boundary as α decreases.

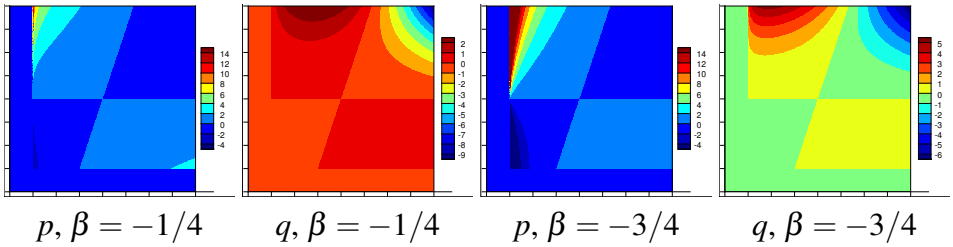

Figure 5.2: Nonsmooth p two-dimensional test. Shown are the pressure p and scaled pressure q for four values of α defining ϕ. The pressure is smooth, except on the boundary of the support of ϕ (i.e., $x = -3/4$ or $y = -3/4$. The scaled pressure becomes less regular near the boundary as α decreases.

		scaled pressure q		pressure p		velocity $\mathbf{u}$	
α	n	error	rate	err	rate	err	rate
2	33	0.012137	—	0.021447	—	0.028001	—
	65	0.003171	1.980	0.007832	1.486	0.009146	1.651
	129	0.000817	1.979	0.002769	1.517	0.002753	1.752
	257	0.000210	1.971	0.000969	1.523	0.000790	1.811
	513	0.000055	1.938	0.000339	1.520	0.000220	1.850
0.25	33	0.031315	—	0.047229	—	0.039155	—
	65	0.020907	0.596	0.029933	0.673	0.024967	0.664
	129	0.014105	0.574	0.019492	0.626	0.017147	0.548
	257	0.009588	0.560	0.012969	0.591	0.012062	0.510
	513	0.006566	0.548	0.008778	0.565	0.008545	0.499

Table 5.3: Smooth p two-dimensional test. Shown are the relative discrete L^2-norm errors of q, p, and $\mathbf{u}$ for various odd numbers of elements $n \times n$ and for $\alpha = 2$ and 0.25 defining ϕ. The convergence is similar to the case of grids that resolve the boundary between the one and two phase regions when $\alpha = 2$, but not for $\alpha = 1/4$.

5.8.3 A nonsmooth solution test in two-dimensions

For the final series of tests, we assume that ϕ is again given by (5.8.1), but we impose the nonsmooth pressure solution

$$p = y(y-3x)(x+3/4)^{\beta}, \quad \beta = -1/4 \text{ or } -3/4. \tag{5.8.2}$$

This pressure and the scaled pressure $q = \phi^{1/2}p$ are depicted in Figure 5.2, where one can see clearly the degeneracy in p near $x = -3/4$ and that q is better behaved. In the case $\beta = -1/4$, q and $\mathbf{u}$ lie in $H^{1.25}$ and are relatively smooth, whereas when $\beta = -3/4$, q and $\mathbf{u}$ lie only in $H^{0.75}$. We use grids that do *not* resolve the interface between the one and two-phase regions. The discrete errors and convergence rates are shown in Table 5.4. The scaled pressure converges as expected, and the velocity seems to be converging a bit better than expected. The pressure barely converges at all.

5.9 Summary and implications to the mantle equations

We began this chapter by considerting a linear degenerate elliptic boundary value problem, which can degenerate as the porosity ϕ vanishes. Energy estimates suggested that the pressure p is uncontrolled; moreover, an equation is lost when ϕ vanishes, making it difficult to handle the equations numerically. We changed variables to a scaled set that remain bounded in the energy estimates. To formulate a well-posed mixed weak problem in the scaled variables, we defined precisely the Hilbert space $H_{\phi,d}(\mathrm{div})$ within which the scaled velocity resides. The key hypotheses were that $\phi^{-1/2}d(\phi) \in W^{1,\infty}(\Omega)$ and $\phi^{-1/2}\nabla d(\phi) \in (L^{\infty}(\Omega))^d$. More-

β	n	scaled pressure q error	rate	pressure p err	rate	velocity $\mathbf{u}$ err	rate
$-1/4$	33	0.005050	—	0.045199	—	0.002885	—
	65	0.002193	1.231	0.034160	0.413	0.000786	1.918
	129	0.000944	1.230	0.027326	0.326	0.000211	1.919
	257	0.000402	1.239	0.022448	0.285	0.000056	1.925
	513	0.000171	1.237	0.018661	0.267	0.000015	1.906
$-3/4$	33	0.004155	—	0.193534	—	0.004991	—
	65	0.002554	0.718	0.184637	0.069	0.002113	1.268
	129	0.001608	0.675	0.179129	0.044	0.000935	1.190
	257	0.000991	0.702	0.175644	0.029	0.000432	1.120
	513	0.000601	0.724	0.173380	0.019	0.000210	1.044

Table 5.4: Nonsmooth p two-dimensional test. Shown are the relative discrete L^2-norm errors of q, p, and $\mathbf{u}$ for various odd numbers of elements $n \times n$ and for $\beta = -1/4$ and $-3/4$ defining p in (5.8.2).

over, a normal trace operator was defined to handle boundary conditions. Existence and uniqueness of a solution to the weak formulation was obtained from the Lax-Milgram Theorem.

We defined a theoretically simple, formal mixed finite element method based on lowest order Raviart-Thomas spaces. The method is stable, and an error analysis showed optimal rates of convergence for sufficiently smooth solutions. We modified the method to make it more practical in implementation, producing a cell-centered finite difference method that is stable and locally mass-conservative.

In a simple case in one dimension, the equations reduce to an Euler equation for which a closed form solution was computed. Numerical tests of this problem showed that the practical method achieved optimal rates of convergence with respect to the regularity of the solution; in fact, superconvergence of the velocity and

scaled pressure were observed. Convergence of the true pressure was relatively poor.

A numerical test for a two-dimensional problem using $d(\phi) = \phi$ also exhibited superconvergence. To see optimal convergence rates in this test, it was necessary that $\phi^{1/2}\nabla\phi \in L^2$, which is weaker than being in L^∞. Moreover, meshes that did not match the boundary of the one to two-phase region showed no degradation of results from cases with meshes that match this boundary.

We will see in chapter 6 that the same theory developed for the degenerate problem (5.0.1)–(5.0.2) can be applied to the full equations (3.1.1)–(3.1.4) to show uniqueness and solvability. In chapter 7, We will also extend the practical method to the full equations.

Chapter 6

Proof to the Full Equations

In order to prove the uniqueness and existence of a solution for the Darcy-Stokes system, we will mimic the concepts introduced in the previous chapter where a simpler degenerate problem is analyzed. First, we rewrite the symmetric equations (3.1.1)–(3.1.2) in terms of a scaled relative pressure $\tilde{q}_r \propto \phi^{1/2}(q_f - q_m)$. Second, we define the space $H_\phi(\mathrm{div})$ where the term $\phi^{-1/2}\nabla\cdot(\phi^{1+\Theta}\mathbf{v})$ makes sense. Third, we write a stabilized weak form of the equations as a saddle point problem. Finally, we prove the necessary conditions for the problem to have a unique solution, namely, coercivity and an inf-sup condition.

6.1 Scaled pressure equations

We would like to arrive at a saddle point system that is coercive and obeys an inf-sup condition. In order to achieve this goal, we manipulate the equations to extract positive terms and match symmetric terms in the corresponding weak form. Define the scaled relative pressure potential and scaled relative velocity by

$$\tilde{q}_r = \phi^{1/2}(q_f - q_m) = \phi^{1/2}(p_f - p_m),$$
$$\tilde{\mathbf{v}}_r = \phi^{-(1+\Theta)}\mathbf{u} = \phi^{-\Theta}(\mathbf{v}_f - \mathbf{v}_m).$$

Then Darcy's law (3.1.1) becomes

$$\tilde{\mathbf{v}}_r = -\frac{k_0}{\mu_f}\phi^{1+\Theta}\nabla(\phi^{-1/2}\tilde{q}_r + q_m)\,. \tag{6.1.1}$$

Adding (3.1.4) and (3.1.2) gives

$$\nabla\cdot\mathbf{v}_m + \nabla\cdot(\phi^{1+\Theta}\tilde{\mathbf{v}}_r) = 0\,. \tag{6.1.2}$$

Substituting (3.1.4) into (3.1.3) in terms of $\tilde{q}_r$ gives

$$\nabla q_m - \nabla\cdot(2\mu_m(1-\phi)\mathcal{D}\mathbf{v}_m) - \nabla\Big(\tfrac{5-2\phi}{3}\phi^{1/2}\tilde{q}_r\Big) = (1-\phi)\Delta\rho\mathbf{g}. \tag{6.1.3}$$

Adding (3.1.4) times $\frac{5-2\phi}{3}\phi^{1/2}$ and (3.1.2) times $\phi^{-1/2}$ gives

$$\tfrac{5-2\phi}{3}\phi^{1/2}\nabla\cdot\mathbf{v}_m + \phi^{-1/2}\nabla\cdot(\phi^{1+\Theta}\tilde{\mathbf{v}}_r) + \Big(1-\tfrac{5-2\phi}{3}\phi\Big)\tfrac{1}{\mu_m}\tilde{q}_r = 0\,. \tag{6.1.4}$$

6.2 Relative velocity space $H_\phi(\mathbf{div};\Omega)$

We wish to define a function space similar to $H(\mathrm{div};\Omega)$ where the quantity $\phi^{-1/2}\nabla\cdot(\phi^{1+\Theta}\tilde{\mathbf{v}}_r)$ is well defined. This is precisely the space defined in section 5.2, i.e.,

$$H_\phi(\mathrm{div};\Omega) = H_{\phi,\phi^{1+\Theta}}(\mathrm{div};\Omega) = \{\mathbf{v}\in L^2(\Omega)^d; \phi^{-1/2}\nabla\cdot(\phi^{1+\Theta}\mathbf{v})\in L^2(\Omega)\}. \tag{6.2.1}$$

The conditions on ϕ (5.2.3), and (5.2.4) reduce to

$$\phi^{1/2+\Theta}\in W^{1,\infty}(\Omega), \tag{6.2.2}$$

and lemmas 5.2.1 and 5.2.2 hold with $d(\phi)=\phi^{1+\Theta}$.

6.3 Stabilized weak formulation

We proceed assuming homogeneous boundary conditions. Note that for Neumann and Robin conditions the theory of chapter 5 generalizes as well. Define the spaces

$$\begin{aligned} V_r &= H_{\phi,0}(\mathrm{div};\Omega) = H_\phi(\mathrm{div};\Omega) \cap \{\gamma_\phi(\mathbf{v}) = \phi^{1/2+\Theta}\mathbf{v}\cdot\nu = 0 \text{ on } \partial\Omega\}, \\ V_m &= (H_0^1(\Omega))^d, \\ W_r &= W_m = L^2(\Omega), \\ X &= V_r \times V_m \times W_r, \end{aligned} \tag{6.3.1}$$

and equip X with its natural product space norm. For $\tilde{\mathbf{v}}_r \in H_\phi(\mathrm{div};\Omega)$, we need to control the quantity $\phi^{-1/2}\nabla\cdot(\phi^{1+\Theta}\tilde{\mathbf{v}}_r)$, so we add a stabilization term using (6.1.4) by testing with $w_r = \phi^{-1/2}\nabla\cdot(\phi^{1+\Theta}\Psi_r)$. The weak form of (6.1.1)–(6.1.4) becomes, for $\delta = 0$: Find $\mathbf{u} = (\tilde{\mathbf{v}}_r, \mathbf{v}_m, \tilde{q}_r) \in X$, $q_m \in W_m$ such that

$$a_\delta(\mathbf{u},\Psi) - b(q_m,\Psi) = f(\Psi) \qquad \forall \Psi \in X, \tag{6.3.2}$$

$$b(w_m,\mathbf{u}) = 0 \qquad \forall w_m \in W_m, \tag{6.3.3}$$

where

$$
\begin{aligned}
a(\mathbf{u},\Psi) &= \Big(\frac{\mu_f}{k_0}\tilde{\mathbf{v}}_r,\Psi_r\Big) + \big(2\mu_m(1-\phi)\mathcal{D}\mathbf{v}_m,\mathcal{D}\Psi_m\big) + \left(\left(1-\tfrac{5-2\phi}{3}\phi\right)\tfrac{1}{\mu_m}\tilde{q}_r,w_r\right)\\
&\quad - \big(\tilde{q}_r,\phi^{-1/2}\nabla\cdot(\phi^{1+\Theta}\Psi_r)\big) + \big(\phi^{-1/2}\nabla\cdot(\phi^{1+\Theta}\tilde{\mathbf{v}}_r),w_r\big)\\
&\quad - \Big(\tfrac{5-2\phi}{3}\phi^{1/2}\tilde{q}_r,\nabla\cdot\Psi_m\Big) + \Big(\tfrac{5-2\phi}{3}\phi^{1/2}\nabla\cdot\mathbf{v}_m,w_r\Big),\\
a_\delta(\mathbf{u},\Psi) &= a(\mathbf{u},\Psi)\\
&\quad + \delta\Big\{\big(\phi^{-1/2}\nabla\cdot(\phi^{1+\Theta}\tilde{\mathbf{v}}_r),\phi^{-1/2}\nabla\cdot(\phi^{1+\Theta}\Psi_r)\big)\\
&\quad\quad + \Big(\tfrac{5-2\phi}{3}\phi^{1/2}\nabla\cdot\mathbf{v}_m,\phi^{-1/2}\nabla\cdot(\phi^{1+\Theta}\Psi_r)\Big)\\
&\quad\quad + \left(\left(1-\tfrac{5-2\phi}{3}\phi\right)\tfrac{1}{\mu_m}\tilde{q}_r,\phi^{-1/2}\nabla\cdot(\phi^{1+\Theta}\Psi_r)\right)\Big\},\\
b(w,\Psi) &= \big(w,\nabla\cdot(\phi^{1+\Theta}\Psi_r)\big) + (w,\nabla\cdot\Psi_m),\\
f(\Psi) &= \big((1-\phi)\Delta\rho\mathbf{g},\Psi_m\big).
\end{aligned}
$$

Note that

$$
a(\mathbf{u},\Psi) = a_0(\mathbf{u},\Psi) = a_\delta(\mathbf{u},\Psi-(\mathbf{0},\mathbf{0},\phi^{-1/2}\nabla\cdot(\phi^{1+\Theta}\Psi_r))). \tag{6.3.4}
$$

Since $\Psi_r \in H_\phi(\mathrm{div};\Omega)$, $\phi^{-1/2}\nabla\cdot(\phi^{1+\Theta}\Psi_r) \in L^2(\Omega)$ so that (6.3.2)–(6.3.3) with $\delta = 0$ is equivalent to (6.3.2)–(6.3.3) with $\delta \neq 0$ since we test with arbitrary $w_r \in L^2(\Omega)$.

6.4 Conditions for the saddle point theory

Clearly $a_\delta(\cdot,\cdot)$ is continuous and bi-linear for every δ, $b(\cdot,\cdot)$ is continuous and bi-linear, and $f(\cdot)$ is continuous and linear. We only have left to prove coerciv-

ity of $a_\delta(\cdot,\cdot)$ and an inf-sup condition for $b(\cdot,\cdot)$.

Lemma 6.4.1. *Assume $\phi \le \phi^* \ll 1$. Then $a_\delta(\cdot,\cdot)$ is coercive on* $\ker b$ *for every $0 < \delta < \mu_m \phi^*$. That is, there exists $\alpha > 0$ such that*

$$a_\delta(\mathbf{u},\mathbf{u}) \ge \alpha ||\mathbf{u}||_X^2 \tag{6.4.1}$$

for all $\mathbf{u} \in \ker b = \{\mathbf{u} \in X;\, b(w,\mathbf{u}) = 0 \ \ \forall w \in W\}$.

Proof. For $\mathbf{u} \in \ker b$, $\nabla \cdot \mathbf{v}_m = -\nabla \cdot (\phi^{1+\Theta} \tilde{\mathbf{v}}_r)$ weakly in $L^2(\Omega)$. Then

$$\begin{aligned} a_\delta(\mathbf{u},\mathbf{u}) &= \left(\frac{\mu_f}{k_0}\tilde{\mathbf{v}}_r, \tilde{\mathbf{v}}_r\right) + \left(2\mu_m(1-\phi)\mathcal{D}\mathbf{v}_m, \mathcal{D}\mathbf{v}_m\right) \\ &+ \left(\left(1 - \tfrac{5-2\phi}{3}\phi\right)\tfrac{1}{\mu_m}\tilde{q}_r, \tilde{q}_r\right) + \delta ||\phi^{-1/2}\nabla\cdot(\phi^{1+\Theta}\tilde{\mathbf{v}}_r)||^2 \\ &+ \delta\left(\tfrac{5-2\phi}{3}\phi^{1/2}\nabla\cdot\mathbf{v}_m + \left(1 - \tfrac{5-2\phi}{3}\phi\right)\tfrac{1}{\mu_m}\tilde{q}_r, \phi^{-1/2}\nabla\cdot(\phi^{1+\Theta}\tilde{\mathbf{v}}_r)\right). \end{aligned} \tag{6.4.2}$$

The last term in (6.4.2) is bounded by

$$\begin{aligned} &\delta\left|\left(\frac{2}{3}\phi^{1/2}\nabla\cdot\mathbf{v}_m + \left(1 - \tfrac{5-2\phi}{3}\phi\right)\tfrac{1}{\mu_m}\tilde{q}_r, \phi^{-1/2}\nabla\cdot(\phi^{1+\Theta}\tilde{\mathbf{v}}_r)\right)\right| \\ &= \delta\left| - \left(\tfrac{5-2\phi}{3}\nabla\cdot(\phi^{1+\Theta}\tilde{\mathbf{v}}_r), \nabla\cdot(\phi^{1+\Theta}\tilde{\mathbf{v}}_r)\right) + \left(\left(1 - \tfrac{5-2\phi}{3}\phi\right)\tfrac{1}{\mu_m}\tilde{q}_r, \phi^{-1/2}\nabla\cdot(\phi^{1+\Theta}\tilde{\mathbf{v}}_r)\right)\right| \\ &\le \tfrac{5}{3}\delta\phi^* ||\phi^{-1/2}\nabla\cdot(\phi^{1+\Theta}\tilde{\mathbf{v}}_r)||^2 + \delta\left|\left|\left(1 - \tfrac{5-2\phi}{3}\phi\right)\tfrac{1}{\mu_m}\tilde{q}_r\right|\right| ||\phi^{-1/2}\nabla\cdot(\phi^{1+\Theta}\tilde{\mathbf{v}}_r)|| \\ &\le \tfrac{23}{12}\delta\phi^* ||\phi^{-1/2}\nabla\cdot(\phi^{1+\Theta}\tilde{\mathbf{v}}_r)||_0^2 + \tfrac{\delta}{\mu_m\phi^*}\left(1 - \tfrac{5-2\phi}{3}\phi\right)\left(\left(1 - \tfrac{5-2\phi}{3}\phi\right)\tfrac{1}{\mu_m}\tilde{q}_r, \tilde{q}_r\right), \\ &\le 2\delta\phi^* ||\phi^{-1/2}\nabla\cdot(\phi^{1+\Theta}\tilde{\mathbf{v}}_r)||_0^2 + \tfrac{\delta}{\mu_m\phi^*}\left(\left(1 - \tfrac{5-2\phi}{3}\phi\right)\tfrac{1}{\mu_m}\tilde{q}_r, \tilde{q}_r\right), \end{aligned}$$

using the inequality $\delta ab \le \frac{\delta}{\phi^*}a^2 + \frac{\delta\phi^*}{4}b^2$. Thus,

$$
\begin{aligned}
a_\delta(\mathbf{u},\mathbf{u}) &\geq \left(\frac{\mu_f}{k_0}\tilde{\mathbf{v}}_r,\tilde{\mathbf{v}}_r\right) + \left(2\mu_m(1-\phi)\mathcal{D}\mathbf{v}_m,\mathcal{D}\mathbf{v}_m\right) \\
&\quad + \left(1-\tfrac{\delta}{\mu_m\phi^*}\right)\left(\left(1-\tfrac{5-2\phi}{3}\phi\right)\tfrac{1}{\mu_m}\tilde{q}_r,\tilde{q}_r\right) \\
&\quad + \delta(1-\tfrac{2}{\phi}^*)||\phi^{-1/2}\nabla\cdot(\phi^{1+\Theta}\tilde{\mathbf{v}}_r)||^2 \\
&\geq C(||\tilde{\mathbf{v}}_r||^2 + ||\mathcal{D}\mathbf{v}_m||^2 + ||\tilde{q}_r||^2 + ||\phi^{-1/2}\nabla\cdot(\phi^{1+\Theta}\tilde{\mathbf{v}}_r)||^2,
\end{aligned}
$$

provided that $0 < \delta < \mu_m\phi^*$. Finally, Korn's lemma (3.2.5) completes the proof.

□

Lemma 6.4.2. *There exists $\gamma > 0$ such that*

$$
\sup_{\Psi\in X}\frac{b(w,\Psi)}{||\Psi||_X} \geq \gamma||w|| \;\; \forall w \in W \tag{6.4.3}
$$

Proof.

$$
\begin{aligned}
\sup_{\Psi\in X}\frac{b(w,\Psi)}{||\Psi||_X} &= \sup_{\Psi\in X}\frac{\left(w,\nabla\cdot(\phi^{1+\Theta}\Psi_r)\right)+(w,\nabla\cdot\Psi_m)}{\left(||\Psi_r||^2_{H_\phi(\mathrm{div})}+||\Psi_m||^2_1+||w_r||^2\right)^{1/2}} \\
&\geq \sup_{\Psi_m\in(H^1(\Omega))^d}\frac{(w,\nabla\cdot\Psi_m)}{||\Psi_m||_1} \geq \gamma_S||w||.
\end{aligned}
$$

where γ_S is the inf-sup constant for Stokes. □

Theorem 6.4.3. *There exists a unique solution to (6.3.2)–(6.3.3) $\forall\delta\in\mathbb{R}$. Moreover,*

$$
||\tilde{\mathbf{v}}_r||_{H_\phi(\mathrm{div})} + ||\mathbf{v}_m||_1 + ||\tilde{q}_r|| + ||q_m|| \leq C\Delta\rho. \tag{6.4.4}
$$

Proof. Apply the inf-sup theory for saddle point problems to (6.3.2)–(6.3.3) with $0 < \delta < \mu_m\phi^*$ then use the equivalence (6.3.4) to get existence for all $\delta\in\mathbb{R}$. To prove uniqueness, assume $(\mathbf{u},q_m)$ solves (6.3.2)–(6.3.3) with $f(\Psi)=\mathbf{0}$. Then

by (6.3.3) $b(w,\mathbf{u}) = 0\ \forall w \in W \Rightarrow a_\delta(\mathbf{u},\mathbf{u}) = 0$ by (6.3.2) and by (6.4.1), $\mathbf{u} = (\tilde{\mathbf{v}}_r, \mathbf{v}_m, \tilde{q}_r) = (\mathbf{0},\mathbf{0},0)$. So $a_\delta(\mathbf{u},\Psi) = 0\ \forall \Psi \in X$. This implies $b(q_m,\Psi) = 0\ \forall \Psi \in X$. Finally, the inf-sup condition gives

$$||q_m|| \leq \frac{1}{\gamma} \sup_{\Psi \in X} \frac{b(q_m,\Psi)}{||\Psi||_X} = 0\,.$$

Finally, the stability estimates in Theorem 3.2.1 give the stability estimate in (6.4.4).

□

Chapter 7

A Scaled Mixed Formulation

In this chapter we extend the practical mass-conservative mixed method for the linear degenerate elliptic problem (5.0.1)–(5.0.2) to the full equations (3.1.1)–(3.1.4). We obtain optimal convergence rates for sufficiently smooth solutions. Though the condition $\phi^{1/2+\Theta} \in W^{1,\infty}(\Omega)$ guarantees stability of the method, we will show several examples where we break this assumption and still retain stability and good convergence. We will also compare the behavior of the condition number for the new scaled method with the methods of chapter 4.

7.1 Extension of the practical method to the full system

To apply the degenerate problem (5.0.1)–(5.0.2), set $a(\phi) = \phi^{2(1+\Theta)}$ and $b(\phi) = 1$ $\left(c(\phi) = \phi^{-(1+\Theta)}\right.$, and $\left.d(\phi) = \phi^{(1+\Theta)}\right)$. Beginning with (3.1.1)–(3.1.4), make the substitutions

$$\tilde{q}_f = \phi^{1/2} q_f, \tag{7.1.1}$$

$$\tilde{\mathbf{v}}_r = \phi^{-(1+\Theta)} \mathbf{u}, \tag{7.1.2}$$

and multiply (3.1.2) by $\phi^{1/2}$ to get the new equations

$$\tilde{\mathbf{v}}_r = -\frac{k_0}{\mu_f}\phi^{1+\Theta}\nabla(\phi^{-1/2}\tilde{q}_f), \tag{7.1.3}$$

$$\phi^{-1/2}\nabla\cdot(\phi^{1+\Theta}\tilde{\mathbf{v}}_r) + \tfrac{1}{\mu_m}(\tilde{q}_f - \phi^{1/2}q_m) = 0. \tag{7.1.4}$$

$$\nabla q_m - \nabla\cdot(2\mu_m(1-\phi)\mathcal{D}\mathbf{v}_m) + \nabla\left(\tfrac{5-2\phi}{3}\mu_m\nabla\cdot\mathbf{v}_m\right) = (1-\phi)\Delta\rho\mathbf{g}, \tag{7.1.5}$$

$$\nabla\cdot\mathbf{v}_m - \tfrac{1}{\mu_m}(\tilde{q}_f - \phi^{1/2}q_m) = 0, \tag{7.1.6}$$

The boundary conditions for the the Darcy part (3.1.13) change to

$$\begin{cases} \phi^{1/2+\Theta}\tilde{\mathbf{v}}_r\cdot\nu = g_f^N, & \text{on } \Gamma_f^N, \\ \tilde{q}_f - \kappa_f^2\phi^{1/2+\Theta}\tilde{\mathbf{v}}_r\cdot\nu = g_f^R, & \text{on } \Gamma_f^R, \end{cases} \qquad \overline{\Gamma_f^N}\cup\overline{\Gamma_f^R} = \partial\Omega, \tag{7.1.7}$$

and analogously to (3.1.16), suppose we can extend g_f^N to $\tilde{\mathbf{v}}_r^N$ in Ω such that

$$\phi^{1/2+\Theta}\tilde{\mathbf{v}}_r^N\cdot\nu = g_f^N \quad \text{on } \Gamma_f^N, \tag{7.1.8}$$

Let the discrete search spaces be defined as in (4.2.1) on a rectangular mesh $\mathcal{T}_h$ defined in chapter 4. Then the discrete form of the mixed method becomes:

Find $\tilde{\mathbf{v}}_r \in V_{r,h} + \tilde{\mathbf{v}}_r^N$, $\mathbf{v}_m \in V_{m,h} + \mathbf{v}_m^{\nu,N} + \mathbf{v}_m^{\tau,N}$, $\tilde{q}_f \in W_{f,h}$, and $q_m \in W_{m,h}$ such that

$$\begin{aligned}\left(\frac{\mu_f}{k_0}\tilde{\mathbf{v}}_r, \Psi_r\right) - \left(\tilde{q}_f, \hat{\phi}^{-1/2}\nabla\cdot(\phi^{1+\Theta}\Psi_r)\right) + \langle \kappa_f \phi^{1+2\Theta}\tilde{\mathbf{v}}_r\cdot\nu, \Psi_r\cdot\nu\rangle_{\Gamma_f^R} \\ = -\langle \phi^{1/2+\Theta} g_f^R, \Psi_r\cdot\nu\rangle_{\Gamma_f^R} \qquad \forall \Psi_r \in V_{r,h},\end{aligned} \tag{7.1.9}$$

$$\begin{aligned}(\hat{\phi}^{-1/2}\nabla\cdot(\phi^{1+\Theta}\tilde{\mathbf{v}}_r), w_f) + \left(\tfrac{1}{\mu_m}\tilde{q}_f, w_f\right) - \left(\tfrac{\hat{\phi}^{-1/2}\phi}{\mu_m} q_m, w_f\right) = 0 \\ \forall w_f \in W_{f,h},\end{aligned} \tag{7.1.10}$$

$$\begin{aligned}-(q_m, \nabla\cdot\Psi_m) + \left(2\mu_m(1-\phi)\mathcal{D}\mathbf{v}_m, \mathcal{D}\Psi_m\right) - \left(\tfrac{5-2\phi}{3}\mu_m\nabla\cdot\mathbf{v}_m, \nabla\cdot\Psi_m\right) \\ + \langle \kappa_\nu^2 \mathbf{v}_m\cdot\nu, \Psi_m\cdot\nu\rangle_{\Gamma_m^{\nu,R}} + \langle \kappa_\tau^2 \mathbf{v}_m\cdot\tau, \Psi_m\cdot\tau\rangle_{\Gamma_m^{\tau,R}} \\ = \langle g_m^{\nu,R}, \Psi_m\cdot\nu\rangle_{\Gamma_m^{\nu,R}} + \langle g_m^{\tau,R}, \Psi_m\cdot\tau\rangle_{\Gamma_m^{\tau,R}} \\ + \left((1-\phi)\Delta\rho\mathbf{g}, \Psi_m\right) \qquad \forall \Psi_m \in V_{m,h},\end{aligned} \tag{7.1.11}$$

$$(\nabla\cdot\mathbf{v}_m, w_m) - \left(\tfrac{\hat{\phi}^{-1/2}\phi}{\mu_m}\tilde{q}_f, w_m\right) + \left(\tfrac{\phi}{\mu_m} q_m, w_m\right) = 0 \qquad \forall w_m \in W_{m,h}. \tag{7.1.12}$$

Following the practical method of section 5.5.2, $\hat{\phi}$ represents the projection of ϕ into W_h (constant on each element). In the last term in (7.1.10) and the middle term in (7.1.12), $\phi^{1/2}$ is replaced with $\hat{\phi}^{-1/2}\phi$ for the method to be mass-conservative. That is, using (5.5.9) and (5.5.10), the discrete solution (adding subscript h's for emphasis) satisfies

$$\int_E \mu_m \nabla\cdot\mathbf{u}_h\, dx + \int_E \phi(q_{f,h} - q_{m,h})\, dx = 0, \tag{7.1.13}$$

$$\int_E \mu_m \nabla\cdot\mathbf{v}_{m,h}\, dx - \int_E \phi(q_{f,h} - q_{m,h})\, dx = 0. \tag{7.1.14}$$

From the definitions in section 4.1, the degrees of freedom for RT_0 correspond to average edge fluxes with associated edge basis function $\mathbf{v}_e$. The degrees of freedom for BR correspond to edge fluxes with associated basis functions $\mathbf{v}_e$, and

nodal values with associated basis functions $\mathbf{v_p}$. Note that the edge basis functions $\mathbf{v}_e$ are constant on each edge for RT_0 but not for BR. The linear system corresponding to the method (7.1.9)–(7.1.12) is thus

$$\begin{pmatrix} A & -B_\phi & 0 & 0 \\ B_\phi^T & C & 0 & -C_{\sqrt{\phi}} \\ 0 & 0 & D & -B \\ 0 & -C_{\sqrt{\phi}} & -B^T & C_\phi \end{pmatrix} \begin{pmatrix} \tilde{v}_r \\ \tilde{q}_f \\ v_m \\ q \end{pmatrix} = \begin{pmatrix} a_\phi \\ 0 \\ a \\ 0 \end{pmatrix}, \tag{7.1.15}$$

where, for RT_0 basis functions,

$$\begin{aligned} A_{e,f} &= \Big(\frac{\mu_f}{k_0}\mathbf{v}_e, \mathbf{v}_f\Big) + \langle \kappa^2 \phi^{1+2\Theta} \mathbf{v}_e \cdot \nu, \mathbf{v}_f \cdot \nu \rangle \\ &= \Big(\frac{\mu_f}{3k_0}|E_e| + \int_{e\cap\partial\Omega} \kappa^2 \phi^{1+2\Theta}\, ds\Big)\delta_{e,f} + \frac{\mu_f}{6k_0}|E_{e,f}|\nu_e \cdot \nu_f, \end{aligned} \tag{7.1.16}$$

$$\begin{aligned} B_{\phi,e,E} &= \big(\hat{\phi}^{-1/2}\nabla\cdot(\phi^{1+\Theta}\mathbf{v}_e), w_E\big) \\ &= \begin{cases} 0 & \text{if } e \not\subset \partial E \text{ or } \phi_E = 0, \\ \phi_E^{-1/2}\mathbf{v}_e\cdot\nu_E \displaystyle\int_e \phi^{1+\Theta}\, ds & \text{if } e \subset \partial E \text{ and } \phi_E \neq 0, \end{cases} \end{aligned} \tag{7.1.17}$$

$$a_{\phi,e} = -\langle g_R, \phi^{1/2+\Theta}\mathbf{v}_e\cdot\nu\rangle = -\mathbf{v}_e\cdot\nu \int_{e\cap\Gamma_f^R} g_R \phi^{1/2+\Theta}\, ds. \tag{7.1.18}$$

For BR basis functions

$$\begin{aligned} D &= \big(2\mu_m(1-\phi)\mathcal{D}\mathbf{v}, \mathcal{D}\mathbf{v}\big) - \Big(\tfrac{5-2\phi}{3}\mu_m \nabla\cdot\mathbf{v}, \nabla\cdot\mathbf{v}\Big) \\ &\quad + \langle \kappa_\nu^2 \mathbf{v}\cdot\nu, \mathbf{v}\cdot\nu\rangle_{\Gamma_m^{\nu,R}} + \langle \kappa_\tau^2 \mathbf{v}\cdot\tau, \mathbf{v}\cdot\tau\rangle_{\Gamma_m^{\tau,R}}, \end{aligned} \tag{7.1.19}$$

$$B_{e,E} = (\nabla\cdot\mathbf{v}_e, w_E) = \begin{cases} 0 & \text{if } e \not\subset \partial E, \\ \pm|e| & \text{if } e \subset \partial E, \end{cases} \tag{7.1.20}$$

$$B_{\mathbf{p},E} = (\nabla\cdot\mathbf{v}_\mathbf{p}, w_E) = 0,$$

$$a = \langle g_m^{\nu,R}, \mathbf{v}\cdot\nu\rangle_{\Gamma_m^{\nu,R}} + \langle g_m^{\tau,R}, \mathbf{v}\cdot\tau\rangle_{\Gamma_m^{\tau,R}} + \big((1-\phi)\Delta\rho\mathbf{g}, \mathbf{v}\big). \tag{7.1.21}$$

The sign of $(\nabla \cdot \mathbf{v}_e, w_E)$ depends on the orientation of edge e with respect to element E. For piecewise constant basis functions

$$C_{E,F} = (\frac{w_E}{\mu_m}, w_F) = \frac{|E|}{\mu_m}\delta_{E,F}, \tag{7.1.22}$$

$$C_{\phi,E,F} = (\frac{\phi w_E}{\mu_m}, w_F) = \frac{|E|\phi_E}{\mu_m}\delta_{E,F}, \tag{7.1.23}$$

$$C_{\sqrt{\phi},E,F} = (\frac{\hat{\phi}^{-1/2}\phi w_E}{\mu_m}, w_F) = \begin{cases} 0 & \text{if } \phi_E = 0, \\ \frac{|E|\phi_E^{1/2}}{\mu_m}\delta_{E,F}, & \text{if } \phi_E \neq 0. \end{cases} \tag{7.1.24}$$

7.2 Benchmark test: compacting column with constant porosity

We apply our scaled method (hence called the scaled method) to a compacting column with constant porosity. Table 7.1 shows optimal convergence rates for the relative errors and Table 7.2 shows superconvergence for the interpolation errors.

7.3 Benchmark test: compacting column with zero porosity lid

We apply the scaled method with the following discontinuous porosity

$$\phi = \begin{cases} 0 & \text{if } z \leq 0, \\ \phi_+ & \text{if } z > 0. \end{cases} \tag{7.3.1}$$

Table 7.3 and Table 7.4 show optimal convergence rates and super-convergence with the exception of the H^1-error for the relative velocity. The convergence rate for the H^1-interpolation error dropped from 2 to 1.5, and the relative H^1-error does not converge at all.

	scaled relative velocity $\tilde{\mathbf{v}}_r$				scaled fluid pres. pot. $\tilde{q}_f$	
n	L^2-error	rate	H^1-error	rate	L^2-error	rate
10	1.0753e-2	—	3.2533e-1	—	4.9270e-2	—
20	2.8946e-3	1.8933	1.7295e-1	0.9115	2.4601e-2	1.0020
40	7.3837e-4	1.9709	8.7929e-2	0.9760	1.2288e-2	1.0015
80	1.8555e-4	1.9926	4.4152e-2	0.9939	6.1404e-3	1.0008
160	4.6447e-5	1.9981	2.2100e-2	0.9985	3.0695e-3	1.0003

	matrix velocity $\mathbf{v}_m$				matrix pres. pot. q_m	
n	L^2-error	rate	H^1-error	rate	L^2-error	rate
10	2.1506e-3	—	3.2533e-1	—	1.1987e-1	—
20	5.7891e-4	1.8933	1.7295e-1	0.9115	5.9796e-1	1.0034
40	1.4767e-4	1.9709	8.7929e-2	0.9760	2.9860e-2	1.0018
80	3.7110e-5	1.9926	4.4152e-2	0.9939	1.4921e-2	1.0009
160	9.2895e-6	1.9981	2.2100e-2	0.9985	7.4590e-3	1.0003

Table 7.1: Scaled method for a compacting column with constant porosity $\phi_0 = .04$. Relative L^2-errors and convergence rates for $\tilde{\mathbf{v}}_r$, $\tilde{q}_f$, $\mathbf{v}_m$, and q_m. Relative H^1-errors and convergence rates for $\tilde{\mathbf{v}}_r$ and $\mathbf{v}_m$. Solved on an $n \times 1$ ($\approx 6n$ DOF) mesh. $L = 3$, $\Theta = .1$.

	scaled relative velocity $\tilde{\mathbf{v}}_r$		scaled fluid pres. pot. $\tilde{q}_f$	
n	H^1-int-error	rate	L^2-int-error	rate
10	4.7401e-2	—	7.0795e-3	—
20	1.3203e-2	1.8441	2.9954e-3	1.2409
40	3.3985e-3	1.9579	1.0184e-3	1.5565
80	8.5596e-4	1.9893	3.0072e-4	1.7598
160	2.1439e-4	1.9973	8.1987e-5	1.8750

	matrix velocity $\mathbf{v}_m$		matrix pres. pot. q_m	
n	H^1-int-error	rate	L^2-int-error	rate
10	4.7401e-2	—	5.9736e-3	—
20	1.3203e-2	1.8441	2.7091e-3	1.1408
40	3.3985e-3	1.9579	9.4309e-4	1.5223
80	8.5596e-4	1.9893	2.8095e-4	1.7471
160	2.1439e-4	1.9973	7.6878e-5	1.8697

Table 7.2: Scaled method for a compacting column with constant porosity $\phi_0 = .04$. Relative L^2-interpolation-errors and convergence rates for $\tilde{q}_f$ and q_m. Relative H^1-interpolation-errors and convergence rates for $\tilde{\mathbf{v}}_r$ and $\mathbf{v}_m$. Solved on an $n \times 1$ ($\approx 6n$ DOF) mesh. $L = 3$, $\Theta = .1$.

	scaled relative velocity $\tilde{\mathbf{v}}_r$				scaled fluid pres. pot. $\tilde{q}_f$	
n	L^2-error	rate	H^1-error	rate	L^2-error	rate
10	1.2160e-2	—	1.7609	—	3.9981e-2	—
20	3.0303e-3	2.0045	1.8179	-0.0459	1.9999e-2	0.9994
40	7.1215e-4	2.0892	1.8340	-0.0127	1.0005e-2	0.9992
80	1.6710e-4	2.0914	1.8379	-0.0031	5.0035e-3	0.9998
160	3.9920e-5	2.0656	1.8388	-0.0007	2.5019e-3	0.9999

	matrix velocity $\mathbf{v}_m$				matrix pres. pot. q_m	
n	L^2-error	rate	H^1-error	rate	L^2-error	rate
10	3.7239e-3	—	3.6733e-1	—	1.1910e-1	—
20	1.0833e-3	1.7813	1.9536e-1	0.9110	5.9436e-2	1.0028
40	2.9145e-4	1.8942	9.9301e-2	0.9762	2.9704e-2	1.0007
80	7.5476e-5	1.9492	4.9856e-2	0.9940	1.4850e-2	1.0002
160	1.9194e-5	1.9754	2.4954e-2	0.9985	7.4248e-3	1.0000

Table 7.3: Scaled method for a compacting column with discontinuous porosity (7.3.1). Relative L^2-errors and convergence rates for $\tilde{\mathbf{v}}_r$, $\tilde{q}_f$, $\mathbf{v}_m$, and q_m. Relative H^1-errors and convergence rates for $\tilde{\mathbf{v}}_r$ and $\mathbf{v}_m$. Solved on an $n \times 1$ ($\approx 6n$ DOF) mesh. $L = 3$, $\Theta = .1$.

n	scaled relative velocity $\tilde{\mathbf{v}}_r$		scaled fluid pres. pot. $\tilde{q}_f$	
	H^1-int-error	rate	L^2-int-error	rate
10	8.8550e-2	—	3.9785e-3	—
20	3.5615e-2	1.3140	1.3287e-3	1.5822
40	1.3528e-2	1.3966	3.7337e-4	1.8314
80	4.9692e-3	1.4448	9.8967e-5	1.9156
160	1.7916e-3	1.4718	2.5504e-5	1.9562

n	matrix velocity $\mathbf{v}_m$		matrix pres. pot. q_m	
	H^1-int-error	rate	L^2-int-error	rate
10	3.7085e-2	—	2.4915e-4	—
20	1.2064e-2	1.6202	6.2017e-5	2.0063
40	3.3844e-3	1.8337	1.2503e-5	2.3104
80	8.9851e-4	1.9133	2.7779e-6	2.1702
160	2.3182e-4	1.9545	6.7587e-7	2.0392

Table 7.4: Scaled method for a compacting column with discontinuous porosity (7.3.1). Relative L^2-interpolation-errors and convergence rates for $\tilde{q}_f$ and q. Relative H^1-interpolation-errors and convergence rates for $\tilde{\mathbf{v}}_r$ and $\mathbf{v}_m$. Solved on an $n \times 1$ ($\approx 6n$ DOF) mesh. $L = 3$, $\Theta = .1$.

7.4 Discontinuous porosity

The symmetry preserving method failed to obtain a qualitatively reasonable solution for discontinuous porosity. Indeed, we were using continuous basis functions to fit a discontinuous solution. As shown in figure 7.1, the scaled method, solving for the same discontinuous velocity, is able to capture the jump in the relative velocity. The fluid pressure in the figure is generated from the scaled pressure using (5.5.9).

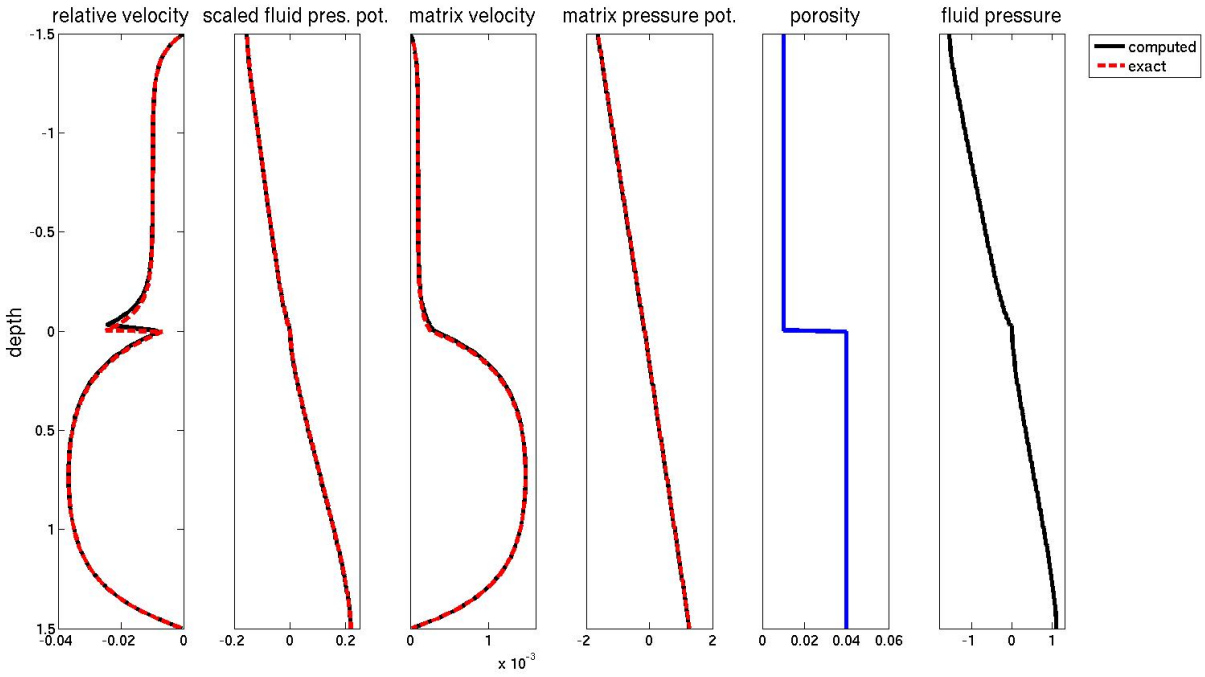

Figure 7.1: Computed solution using the scaled method for a compacting column with discontinuous porosity (4.3.23) and $\Theta = 0$.

7.5 Condition number for decreasing porosity

Following section 4.3.4 we test the scaled method for the three porosities in (4.3.24)–(4.3.26) and let $\phi_0 \to 0$. In terms of the condition (6.2.2), for $z \geq 0$

$$\phi_1(z)\nabla\phi_1(z) = (\phi_0 + z^2)z^2 \in L^\infty([0,L]), \tag{7.5.1}$$

$$\phi_2(z)\nabla\phi_2(z) = \frac{(\phi_0 + \sqrt{z})^{1/2}}{\sqrt{z}} \notin L^\infty([0,L]) \tag{7.5.2}$$

$$\phi_3(z)\nabla\phi_3(z) = \begin{cases} \infty & \text{if } z = 0, \\ 0 & \text{if } z > 0, \end{cases} \qquad \notin L^\infty([0,L]) \tag{7.5.3}$$

Figure 7.2 shows the condition number remains stable as $\phi \to 0$ and is unaffected by the regularity of ϕ.

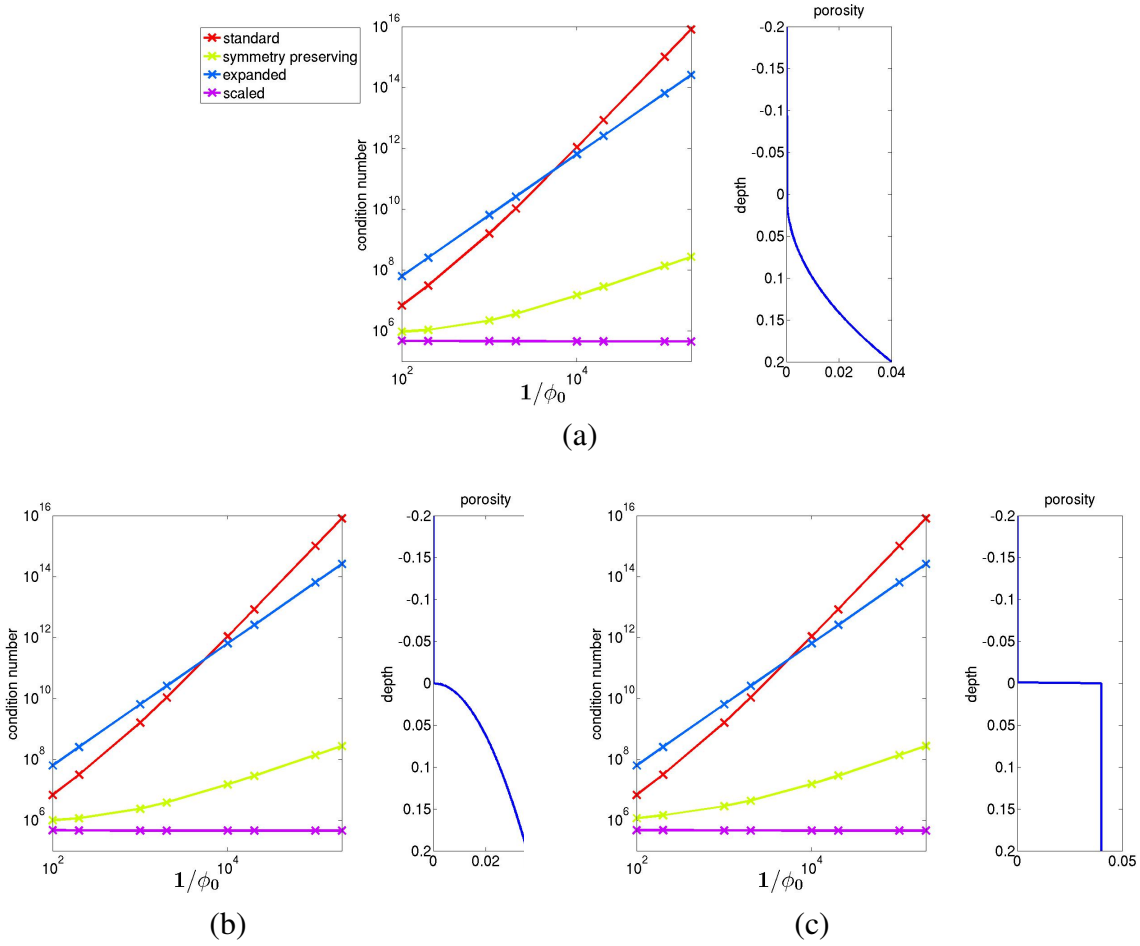

Figure 7.2: Condition number as $\phi_0 \to 0$, for porosities defined in (4.3.24)–(4.3.26) with $L = .2$. (a) ϕ_1. (b) ϕ_2. (c) ϕ_3, $\phi_+ = .04$.

Chapter 8

Conclusion

In this work I presented the equations of mantle dynamics with a focus on mid-ocean ridges. We began this project with a standard mixed finite element formulation but were unsatisfied because it can not confidently handle the one to two-phase transition and is ill-defined for the degenerate case of a single phase. We developed a new method for scaled variables that is stable and uniquely solvable for porosity $\phi \in W^{1,\infty}$. In practice, the method extends to much less regular porosities for compacting column tests. Moreover, the scaled method is guaranteed to be stable for any porosity.

The natural next step is to couple the scaled method with transport in a time-dependent problem and to observe the location of the one to two-phase boundary for mid-ocean ridges. It will be instructive to explore the regularity of the porosity as it evolves in a time-dependent problem.

Appendices

Appendix A

BR Spaces

The discussion below closely follows Arbogast and Wheeler [5], restricted to the lowest order spaces. We provide a characterization of the velocity space for *BR* and a derivation of a discrete inf-sup condition.

A.1 Characterization of the velocity space

On a rectangle $\mathcal{R} \in \mathbb{R}^2$ define,

$$V_h(\mathcal{R}) = Q_{1,2}(\mathcal{R}) \times Q_{2,1}(\mathcal{R}), \tag{A.1.1}$$

$$W_h(\mathcal{R}) = Q_{0,0}(\mathcal{R}) = \mathcal{P}_0(\mathcal{R}), \tag{A.1.2}$$

where $Q_{i,j}$ denotes the set of polynomials of degree at most i in x and at most j in y. Let $\mathcal{T}_h$ be a quasi-regular partitioning of a bounded domain Ω into closed rectangles and set

$$V_h = \{\mathbf{v} \in (C^0(\Omega))^2 : \mathbf{v}|_{\mathcal{R}} \in V_h(\mathcal{R}) \ \ \forall \mathcal{R} \in \mathcal{T}_h\}, \tag{A.1.3}$$

$$W_h = \{w \in L^2(\Omega) : w|_{\mathcal{R}} \in W_h(\mathcal{R}) \ \ \forall \mathcal{R} \in \mathcal{T}_h\}. \tag{A.1.4}$$

Lemma A.1.1. *For a rectangle $\mathcal{R}$, $\mathbf{u}_h \in V_h(\mathcal{R})$ is uniquely defined by the degrees of freedom:*

1. *For every corner point $P \in \partial\mathcal{R}$ and Cartesian direction $j = 1,2$,*

$$DOF_{P,j}(\mathbf{u}_h) = \mathbf{u}_h(P) \cdot \boldsymbol{e}_j. \tag{A.1.5}$$

2. *For every edge $e \in \partial\mathcal{R}$*

$$DOF_e(\mathbf{u}_h) = \int_e \mathbf{u}_h \cdot \nu_e \, ds, \tag{A.1.6}$$

where ν_e is the unit outward normal to e.

Proof. WLOG Let $\mathcal{R} = \hat{\mathcal{R}} = [-1,1]^2$. The degrees of freedom uniquely determine a function $\mathbf{u}_h \in V_h$ if and only if dim V_h equals the number of independent degrees of freedom. First consider $\mathbf{u}_h$ restricted to an edge e of $\mathcal{R}$. We have $\mathbf{u}_h \cdot \tau_e \in P_1(e)$, $\mathbf{u}_h \cdot \nu_e \in P_2(e)$ so the total number of dimensions on e is 5. Meanwhile, the number of degrees of freedom that act on an edge e are those associated with the two corner points on the edge e and the one associated with e itself, again totaling 5. Suppose the degrees of freedom restricted to e vanish. Then,

$$\mathbf{u}_h \cdot \tau_e(\xi) = 0,$$
$$\mathbf{u}_h \cdot \nu_e(\xi) = C(1-\xi^2),$$

since the corner degrees of freedom vanish. To determine the constant C we use the edge degree of freedom

$$\int_e C(1-s^2)\, ds = 0 \Rightarrow C = 0.$$

Thus $\mathbf{u}_h$ restricted to $\partial\mathcal{R}$ vanishes.

The total number of degrees of freedom for the entire rectangle $\mathcal{R}$ is 8 for the corner

points and 4 for the edges, making 12. Meanwhile the dimension of the space $V_h = 2 \times 2 \times 3 = 12$. Since $\mathbf{u}_h$ vanishes on $\partial\mathcal{R}$,

$$\mathbf{u}_h = (1-x^2)(1-y^2)\mathbf{v}(x,y) \Rightarrow \mathbf{v}(x,y) = 0,$$

since $\mathbf{u}_h \in V_h$. Thus $\mathbf{u}_h$ vanishes on the entire rectangle $\mathcal{R}$. □

A nodal basis for the first x-component of V_h on the reference element $\hat{\mathcal{R}} = [-1,1]^2$ is given by

$$\begin{aligned}
\mathbf{v}_{(-1,-1),1} &= \frac{1}{8}(1-x)(1-y)(1+3y)\mathbf{e}_1, \\
\mathbf{v}_{(1,-1),1} &= \frac{1}{8}(x+1)(1-y)(1+3y)\mathbf{e}_1, \\
\mathbf{v}_{(-1,1),1} &= \frac{1}{8}(1-x)(y+1)(1-3y)\mathbf{e}_1, \\
\mathbf{v}_{(-1,-1),1} &= \frac{1}{8}(x+1)(y+1)(1-3y)\mathbf{e}_1, \\
\mathbf{v}_{e_L} &= (3/4)(1-x)(1-y^2)\mathbf{e}_1, \\
\mathbf{v}_{e_R} &= (3/4)(x+1)(1-y^2)\mathbf{e}_1.
\end{aligned}$$

A nodal basis for the y-component of V_h can be constructed by flipping x and y above. See Figure A.1 and Figure A.2 for a visual representation.

A.2 The Clément interpolant

Let $P_{W_h} : L^2(\Omega) \to W_h$ denote the $L^2(\Omega)$-projection onto W_h defined by

$$P_{W_h}(w) = \{w_h \in W_h : (w - w_h, 1)_{\mathcal{R}} = 0 \ \ \forall \mathcal{R} \in \mathcal{T}_h\}. \tag{A.2.1}$$

When $\mathbf{u} \in (H^1(\Omega))^2$ the trace theorem implies $\mathbf{u} \cdot \nu|_e \in H^{1/2}(\Omega)$ ensuring the edge degrees of freedom are well-defined. The point degrees of freedom, however need

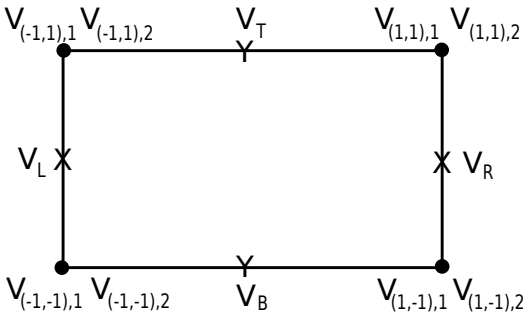

Figure A.1: Visual representation of the degrees of freedom on V_h

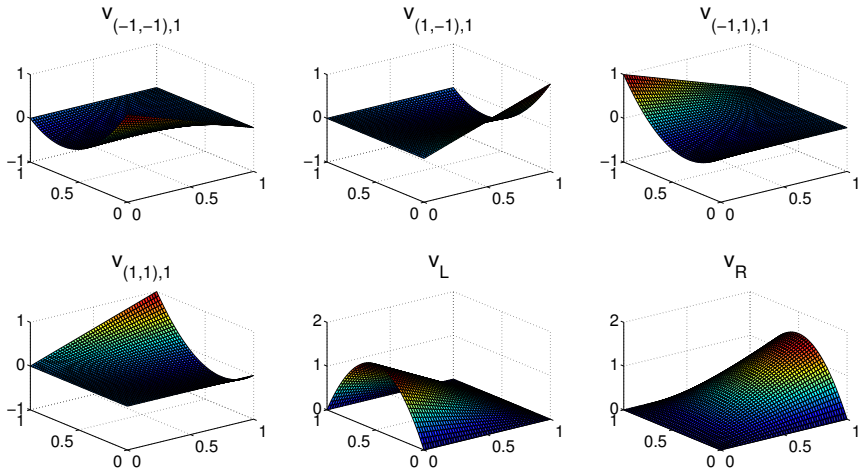

Figure A.2: Visual representation of BR basis functions for the x-component in V_h. The y-component for these functions is identically zero.

not be well-defined. To resolve this issue introduce the Clément [21] interpolant $\mathcal{I} : H^1(\Omega) \to Q_h$, where Q_h is the space of continuous functions with $Q_h|_{\mathcal{R}} = Q_{1,1}(\mathcal{R})\ \forall \mathcal{R} \in \mathcal{T}_h$. For $\phi \in L^2(\Omega)$ the Clément interpolant is defined at the the nodal points as the value of the local L^2-projection at those points. That is, for each nodal point P of $\mathcal{T}_h$ (i.e., the corner points of the rectangles) let

$$\Delta_P = \bigcup_{\mathcal{R} \in \mathcal{T}_h, P \in \mathcal{R}} \mathcal{R} \tag{A.2.2}$$

be the union of rectangles containing P. Then define $\phi_P \in Q_{1,1}(\Delta_P)$ by

$$(\phi - \phi_P, \psi)_{\Delta_P} = 0 \ \ \forall \psi \in Q_{1,1}(\Delta_P) \tag{A.2.3}$$

and set $\mathcal{I}\phi(P) = \phi_P(P)$. This uniquely defines $\mathcal{I}\phi \in Q_h$ since functions in $Q_{1,1}(\mathcal{R})$ are uniquely determined by their corner values. Moreover, we have the result from interpolation theory [17]

$$\|\phi - \mathcal{I}\phi\|_j \leq C\|\phi\|_r h^{r-j}, \ \ j \leq r \leq 2, \ j = 0, 1. \tag{A.2.4}$$

A.3 The π operator

Definition A.3.1. For $\mathbf{u} \in (H^1(\Omega))^2$ let $\pi\mathbf{u}$ be the interpolant of the degrees of freedom in the previous lemma, modified by the Clement interpolant $\mathcal{I}$. For each $\mathcal{R} \in \mathcal{T}_h$:

1. For every corner point $P \in \partial\mathcal{R}$ and Cartesian direction $j = 1, 2$,

$$\pi\mathbf{u}(P) \cdot \mathbf{e}_j = \mathcal{I}\mathbf{u}(P) \cdot \mathbf{e}_j. \tag{A.3.1}$$

2. For every edge $e \in \partial\mathcal{R}$,

$$\int_e \pi\mathbf{u} \cdot \nu_e \, ds = \int_e \mathbf{u} \cdot \nu_e \, ds \tag{A.3.2}$$

The operator π is clearly linear and well-defined, and $\pi\mathbf{u}$ can be written explicitly as

$$\pi\mathbf{u} = \mathcal{I}\mathbf{u} + \sum_{e \in \mathcal{T}_h} \left(\frac{1}{|e|} \int_e (\mathbf{u} - \mathcal{I}\mathbf{u}) \cdot \nu_e \, ds \right) \mathbf{v}_e, \tag{A.3.3}$$

which is indeed in V_h. Note also that after a change of variables,

$$\int_e \mathbf{v}_e \cdot \nu_e \, ds = |e| \int_{\hat{e}} \hat{\mathbf{v}}_{\hat{e}} \cdot \nu_{\hat{e}} \, d\hat{s}, \tag{A.3.4}$$

and the degrees of freedom of $\pi\mathbf{u}$ match those of $\mathbf{u}$.

Lemma A.3.1. *Let* $\mathbf{u} \in (H^1(\Omega))^2$. *Then*

1. *The operator* π *is linear and bounded in* $(H^1(\Omega))^2$ *and independent of h.*

2. *There exists a constant C independent of h such that for* $\mathbf{u} \in (H^r(\Omega))^2$

$$|\pi\mathbf{u} - \mathbf{u}|_j \leq C|\mathbf{u}|_r h^{r-j}, \;\; 1 \leq r \leq 2, \; j = 0, 1. \tag{A.3.5}$$

3.

$$P_W \nabla \cdot \mathbf{u} = P_W \nabla \cdot \pi\mathbf{u}, \tag{A.3.6}$$

where $|\cdot|_r$ denotes the $(H^r(\Omega))^2$ seminorm.

Proof. To show 1., using (A.3.3)

$$|\pi\mathbf{u}|^2 \leq |\mathcal{I}\mathbf{u}|^2 + \sum_{e \in \mathcal{T}_h} \left| \frac{1}{|e|} \left(\int_e (\mathbf{u} - \pi\mathbf{u}) \cdot \nu_e \, ds \right) \mathbf{v}_e \right|^2, \tag{A.3.7}$$

since at each point in Ω the sum above is finite and independent of h (each edge basis function is supported on at most two rectangles). Similarly for the gradient, after integrating,

$$\|\pi\mathbf{u}\|_1^2 = \|\mathcal{I}\mathbf{u}\|_1^2 + \sum_{e\in\mathcal{T}_h} \frac{1}{|e|^2}\left\|\left(\int_e (\mathbf{u}-\pi\mathbf{u})\cdot\nu_e\,ds\right)\mathbf{v}_e\right\|^2. \tag{A.3.8}$$

Recall that under an affine change variables to and from the reference element $\hat{\mathcal{R}}$, for any ϕ,

$$\|\phi\|_{0,\mathcal{R}} = |\mathcal{R}|^{1/2}\|\hat{\phi}\|_{0,\hat{\mathcal{R}}} \le Ch\|\hat{\phi}\|_{0,\hat{\mathcal{R}}} \le C\|\phi\|_{0,\mathcal{R}}, \tag{A.3.9}$$

$$|\phi|_{1,\mathcal{R}} \le C|\mathcal{R}|^{1/2}h^{-1}\|\hat{\phi}\|_{1,\hat{\mathcal{R}}} \le C\|\hat{\phi}\|_{1,\hat{\mathcal{R}}} \le C|\phi|_{1,\mathcal{R}} \tag{A.3.10}$$

since $\mathcal{T}_h$ is quasi-regular (i.e., $|\mathcal{R}|^{1/2}$ is $O(h)$). Then over Ω,

$$\|\mathbf{v}_e\| = \Big(\sum_{\mathcal{R}\in\mathcal{T}_h}\|\mathbf{v}_e\|_{0,\mathcal{R}}^2\Big)^{1/2} \le C\Big(\sum_{\mathcal{R}\in\mathcal{T}_h}|R|\|\hat{\mathbf{v}}_{\hat{e}}\|_{0,\hat{\mathcal{R}}}^2\Big)^{1/2} \le Ch \tag{A.3.11}$$

$$\|\mathbf{v}_e\|_1 = \Big(\sum_{\mathcal{R}\in\mathcal{T}_h}\|\mathbf{v}_e\|_{1,\mathcal{R}}^2\Big)^{1/2} \le C\Big(\sum_{R\in\mathcal{T}_h}\|\hat{\mathbf{v}}_{\hat{e}}\|_{1,\hat{\mathcal{R}}}^2\Big)^{1/2} \le C. \tag{A.3.12}$$

By the trace theorem, for every $v \in (H^1(\Omega))^2$

$$\begin{aligned}\frac{1}{|e|}\left|\int_e \mathbf{v}_e\cdot\nu_e\,ds\right| &= \left|\int_{\hat{e}}\hat{\mathbf{v}}_{\hat{e}}\cdot\nu_{\hat{e}}\,d\hat{s}\right|,\\ &\le C\|\hat{\mathbf{v}}\|_{1,\hat{R}}\\ &\le C\{h^{-1}\|\mathbf{v}\|_{0,\mathcal{R}} + |\mathbf{v}|_{1,\mathcal{R}}\}.\end{aligned}$$

Therefore,

$$\begin{aligned}\sum_e \frac{1}{|e|}\left\|\left(\int_e \mathbf{v}\cdot\nu_e\,ds\right)\mathbf{v}_e\right\|^2 &\le \sum_{e\in\mathcal{T}_h} C\{h^{-1}\|\mathbf{v}\|_{0,\mathcal{R}} + |\mathbf{v}|_{1,\mathcal{R}}\}\\ &\le C\{h^{-1}\|\mathbf{v}\|_0 + |\mathbf{v}|_1\}\end{aligned}$$

and we deduce by (A.2.4) that

$$\|\pi\mathbf{u}\|_1 \leq C\{\|\mathcal{I}\mathbf{u}\|_1 + h^{-1}\|\mathbf{u}-\mathcal{I}\mathbf{u}\| + |\mathbf{u}-\mathcal{I}\mathbf{u}|_1\} \leq C\|\mathbf{u}\|_1 \tag{A.3.13}$$

To prove 2., the case with $j=1$ follows from Bramble-Hilbert [17] since π preserves polynomials of order 1. For $j=0$,

$$\begin{aligned}
\|\mathbf{u}-\pi\mathbf{u}\| &\leq \|\mathbf{u}-\mathcal{I}\mathbf{u}\| + \sum_{e\in\mathcal{T}_h} \left\| \left(\int (\mathbf{u}-\mathcal{I}\mathbf{u})\cdot\nu_e\, ds \right)\mathbf{v}_e \right\|_0 \\
&\leq \|\mathbf{u}-\mathcal{I}\mathbf{u}\| + \sum_{e\in\mathcal{T}_h} \left| \int (\mathbf{u}-\mathcal{I}\mathbf{u})\cdot\nu_e\, ds \right| \|\mathbf{v}_e\|_0 \\
&\leq \|\mathbf{u}-\mathcal{I}\mathbf{u}\| + C\{h^{-1}\|\mathbf{u}-\mathcal{I}\mathbf{u}\|_0 + |\mathbf{u}-\mathcal{I}\mathbf{u}|_1\}h \\
&\leq Ch^r\|\mathbf{u}\|_r \;\; r=1,2.
\end{aligned}$$

For 3., let $w_h \in W_h$ (i.e., w_h is constant over $\mathcal{R}$). Then

$$(\nabla\cdot\mathbf{u}, w_h)_{\mathcal{R}} = \langle \mathbf{u}\cdot\nu, w_h\rangle_{d\mathcal{R}} = \langle \pi\mathbf{u}\cdot\nu, w_h\rangle_{d\mathcal{R}} = (\nabla\cdot\pi\mathbf{u}, w_h)_{\mathcal{R}}.$$

□

A.4 Discrete inf-sup condition

Theorem A.4.1. *The discrete spaces $V_h \times W_h$, also called BR, satisfy the inf-sup condition*

$$\inf_{w_h\in W_h} \sup_{\mathbf{v}_h\in V_h} \frac{(w_h, \nabla\cdot\mathbf{v}_h)}{\|w_h\|_W \|\mathbf{v}_h\|_V} \geq \gamma_h \tag{A.4.1}$$

for $V = (H^1(\Omega))^2$ (for the Stokes problem) or $V = H(\mathrm{div};\Omega)$ (for the Darcy problem) and $W = L^2(\Omega)$.

Proof. It is sufficient to show the inf-sup condition holds for the Stokes problem since for $\mathbf{v} \in (H^1(\Omega))^2$, $\|\mathbf{v}\|_{\text{div}} \leq \|\mathbf{v}\|_1$. As observed in the previous section, there exists an interpolation operator $\pi : (H^1(\Omega))^2 \to V_h$ with the properties:

1. For $\mathbf{v} \in (H^1(\Omega))^2$,

$$P_W \nabla \cdot \pi \mathbf{v} = P_W \nabla \cdot \mathbf{v}. \tag{A.4.2}$$

2. π is bounded on $(H^1(\Omega))^2$:

$$\|\pi \mathbf{v}\|_1 \leq C \|\mathbf{v}\|_1. \tag{A.4.3}$$

Moreover, the inf-sup condition holds on the continuous spaces [29]

$$\inf_{w \in L^2(\Omega)} \sup_{\mathbf{v} \in (H^1(\Omega))^2} \frac{(w, \nabla \cdot \mathbf{v})}{\|w\| \|\mathbf{v}\|_1} \geq \gamma. \tag{A.4.4}$$

Then, since $\pi : (H^1(\Omega))^2 \to V_h$, using (A.4.2)–(A.4.4)

$$\begin{aligned}
\sup_{\mathbf{v}_h \in V_h} \frac{(w_h, \nabla \cdot \mathbf{v}_h)}{\|\mathbf{v}_h\|_V} &\geq \sup_{\mathbf{v} \in (H^1(\Omega))^2} \frac{(w_h, \nabla \cdot \pi \mathbf{v})}{\|\pi \mathbf{v}\|_1} \\
&= \sup_{\mathbf{v} \in (H^1(\Omega))^2} \frac{(w_h, \nabla \cdot \mathbf{v})}{\|\pi \mathbf{v}\|_1} \\
&\geq \sup_{\mathbf{v} \in (H^1(\Omega))^2} \frac{(w_h, \nabla \cdot \mathbf{v})}{C \|\mathbf{v}\|_1} \\
&\geq \frac{\gamma}{C} \|w_h\|.
\end{aligned}$$

□

Appendix B

Time Evolution

Below we derive a closed set of equations that govern the time evolution of porosity. Conservation laws for energy and composition are derived. The enthalpy method [32] is then used to close the system.

B.1 Energy and composition equations

For conservation of energy, let bulk enthalpy be denoted by $H = \overline{\rho h}$ (h_m and h_f are the enthalpies of the matrix and fluid, respectively), let $\mathbf{x}$ be the coordinate vector, and take $\Psi = H - \overline{\rho}\mathbf{g}z \cdot \mathbf{x}$ in equation (2.2.1). Including diffusive flux gives

$$\int_\Omega \frac{\partial}{\partial t}(H - \overline{\rho}\mathbf{g}z \cdot \mathbf{x})d\mathbf{x} = -\int_{\partial\Omega} (\overline{\rho h \mathbf{v}} - \overline{\rho \mathbf{v}}(\mathbf{g}z \cdot \mathbf{x}) - \overline{k}\nabla T) \cdot \hat{\mathbf{n}}\, d\mathbf{x}, \qquad \text{(B.1.1)}$$

where $\overline{k}$ is the phase averaged thermal conductivity and T represents temperature. The terms on the right hand side of (B.1.1) can be interpreted from left to right as advection of enthalpy, advection of potential energy, and diffusion of sensible heat. Neglected from (B.1.1) are internal sources of heat, radioactive decay, and viscous dissipation of heat.

To reach a manageable differential equation for conservation of energy, we make several simplifications. Material properties (specific heat, thermal expansivity, and thermal conductivity) are taken to be constant and phase-independent. We

also apply the Boussinesq approximation, which states that variations in density are neglected (i.e., $\rho = \rho_f = \rho_m$) for terms not associated with buoyancy. In addition, we assume local thermal equilibrium everywhere within the domain. This allows the total differential of enthalpy for each phase to be decomposed in terms of differentials for temperature and pressure according to

$$dh = c_p\, dT + \rho^{-1}(1 - \alpha T)\, dP, \tag{B.1.2}$$

where c_p stands for specific heat and α represents thermal expansivity. Assuming lithostatic pressure, $P = P_l = \rho g z$, and $\alpha T \ll 1$, changes due to thermal expansion can be neglected. The enthalpy differential becomes

$$dh = c_p\, dT + (1 - \alpha T) g\, dz \approx c_p\, dT + g\, dz. \tag{B.1.3}$$

Using the divergence theorem as before and applying the above assumptions, (B.1.1) is transformed to the differential equation (the details appear in appendix A of Katz [32])

$$\frac{\partial H}{\partial t} + \rho c_p \nabla \cdot (\overline{\mathbf{v}} T) = \rho L \nabla \cdot \left((1 - \phi)\mathbf{v}_m\right) + k \nabla^2 T, \tag{B.1.4}$$

where the latent heat $L = h_f - h_m$ is assumed to be constant. Equation (B.1.4) states that changes in bulk enthalpy are caused by advection of sensible heat, advection of latent heat, and thermal diffusion.

If we limit composition to two thermodynamic components, mass conservation for bulk composition gives

$$\frac{\mathrm{d}}{\mathrm{d}t} \int_{\mathcal{V}} \overline{\rho C}\, d\mathcal{V} = - \int_{\mathcal{S}} (\overline{\rho C \mathbf{v}} - \rho_f \phi \mathcal{D} \nabla C_f) \cdot \nu\, d\mathcal{S}, \tag{B.1.5}$$

where C_f and C_m are the mass fractions of one of the components in the melt and matrix, respectively, and $\mathcal{D}$ is the chemical diffusivity of the melt. Taking $\rho = \rho_f = \rho_m$ and assuming constant diffusivity, we recast (B.1.5) as the differential equation

$$\frac{\partial \overline{C}}{\partial t} + \nabla \cdot \overline{C\mathbf{v}} = \mathcal{D}\nabla \cdot (\phi \nabla C_f). \tag{B.1.6}$$

B.2 The enthalpy method

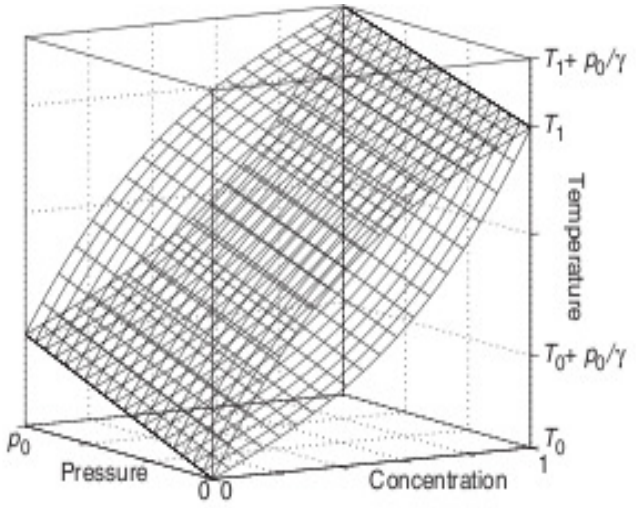

Figure B.1: Pressure-dependent binary phase diagram for a two-component system. Here $\gamma = \frac{\partial T}{\partial P}$ is the constant Clapeyron slope, T_0 is the lowest temperature at which melting can occur, and p_0 determines the pressure scale [32, p. 2104].

The enthalpy method depends on the crucial requirement that local thermodynamic equilibrium holds everywhere. This allows porosity, composition, and temperature to be determined directly from bulk enthalpy and bulk composition. Quantitatively, composition in each phase depends on lithostatic pressure and tem-

perature as shown in Figure B.1. Although it does not represent a rigorous derivation, Asimow [9] has shown that mantle melting is not eutectic and the continuous binary phase loop shown in the figure is reasonable. Moreover, leading-order features of the overall system are insensitive to the exact composition.

The total differential given in (B.1.2), neglecting local variations in pressure (i.e., $dP \approx 0$), can be integrated to give the enthalpy per unit mass for the melt and matrix. This gives

$$h_m = h_0 + c_p(T - T_0), \tag{B.2.1}$$

$$h_f = h_0 + c_p(T - T_0) + L, \tag{B.2.2}$$

where h_0, assigned to be zero, is the reference enthalpy at the reference temperature T_0, T_0 is the minimum melting temperature over all compositions (see Fig. B.1), and L is the latent heat of the fluid. As before, c_p is taken constant and phase-independent, $\rho = \rho_f = \rho_m$, and variations in latent heat with temperature are neglected (L is constant). The bulk enthalpy is then given by

$$H = \overline{\rho h} = \phi \rho L + \rho c_p(T - T_0). \tag{B.2.3}$$

From Figure B.1 we obtain two algebraic equations for the melt and matrix composition,

$$C_m = f_m(T, P_l), \tag{B.2.4}$$

$$C_f = f_f(T, P_l), \tag{B.2.5}$$

where $P_l = \rho g z$ is the lithostatic pressure. Recalling the definition of bulk composition, we combine (B.2.3)–(B.2.5) to obtain an equation for the porosity in terms

of H and $\overline{C}$,

$$\phi f_f\Big(\frac{H-\phi\rho L}{\rho c_p}+T_0,P_l\Big)+(1-\phi)f_m\Big(\frac{H-\phi\rho L}{\rho c_p}+T_0,P_l\Big)-\overline{C}=0. \qquad \text{(B.2.6)}$$

The porosity can then be substituted back into (B.2.3)–(B.2.5) to obtain T, C_m, and C_f.

Table B.1 lists the representative value of parameters for energy and composition in the mantle.

Quantity	Symbol	Value or Range	Units
Specific heat	c_p	1200	$J/kg/K$
Thermal diffusivity	κ	10^{-6}	m^2/s
Latent heat	L	4×10^5	J/kg
Clapeyron slope	γ	1.7×10^7	$Pa/^\circ C$
Reference temperature	T_0	1227	$^\circ C$
Reference temperature	T_1	1927	$^\circ C$

Table B.1: Representative value of parameters for energy and composition in the mantle.

Appendix C

Closed Form Solutions

C.1 Compacting column

Consider the mantle column shown in Figure 4.1(a) for $z \in [0, L]$ with no flow through the bottom or top boundary, i.e.,

$$v_m(-L) = v_m(L) = u(-L) = u(L) = 0, \tag{C.1.1}$$

Following the scaling in (4.3.3) we arrive at the dimensionless equations restricted to the vertical dimension given by

$$\phi_0^{-2(1+\Theta)} u = -q_f', \tag{C.1.2}$$

$$(q_m - \tfrac{1}{3}(1-4\phi_0)v_m')' = 1-\phi_0, \tag{C.1.3}$$

$$v_m' = \phi_0(q_f - q_m), \tag{C.1.4}$$

$$u' = -\phi_0(q_f - q_m). \tag{C.1.5}$$

C.1.1 Constant porosity

Take constant porosity $\phi = \phi_0$. Equations (C.1.2), (C.1.4), and (C.1.5) give

$$v_m'' = -u'' = \phi_0^{2(1+\Theta)} q_f''',$$

which, when substituted back into (C.1.4) gives

$$q_m' = -\tfrac{1}{\phi_0} v_m'' + q_f' = -\phi_0^{1+2\Theta} q_f''' + q_f'.$$

Finally, eliminating all variables but q_f in (C.1.3) gives

$$R^{-2}q_f''' - q_f' + 1 - \phi_0 = 0, \tag{C.1.6}$$

where

$$R = R(\phi_0) = \left(\tfrac{1-\phi_0+4\phi_0^2}{3}\phi_0^{1+2\Theta}\right)^{-1/2} \approx \sqrt{3}\phi_0^{-(1+2\Theta)/2}.$$

Solving (C.1.6) gives

$$q_f' = (1-\phi_0)\left(1 - C_1 e^{-R(z+L)} - C_2 e^{R(z-L)}\right),$$

and according to (C.1.2) and boundary conditions (C.1.1)

$$C_1 = C_2 = C = \frac{1}{1+e^{-2RL}} \approx 1\,.$$

Using the remaining equations, and setting the scale for the fluid pressure such that $q_f(0) = 0$, we have

$$v_m = -u = \phi_0^{2(1+\Theta)}(1-\phi_0)\left(1 - Ce^{-R(z+L)} - Ce^{R(z-L)}\right), \tag{C.1.7}$$

$$q_f = (1-\phi_0)\left(z + \tfrac{C}{R}\left(e^{-R(z+L)} - e^{R(z-L)}\right)\right), \tag{C.1.8}$$

$$q_m = (1-\phi_0)\left(z - \tfrac{1-4\phi_0}{1-\phi_0+4\phi_0^2}\phi_0\tfrac{C}{R}\left(e^{-R(z+L)} - e^{R(z-L)}\right)\right). \tag{C.1.9}$$

As the system evolves, the heavier matrix compacts downward while fluid is squeezed up, developing a boundary layer at both top and bottom boundaries as L increases or ϕ_0 (and thus R increases) decreases. The matrix and Darcy velocities are equal and opposite in sign. The two pressures are close to hydrostatic, but are affected by strong gradients in the flow near the boundaries. Plots of the solution for various domain lengths L can be seen in Figure C.1.

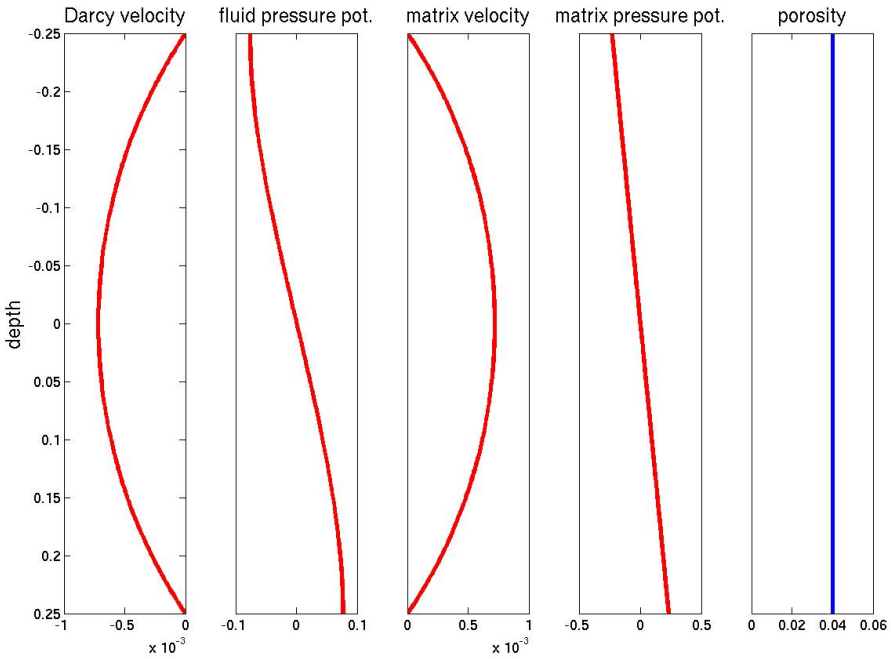

(a)

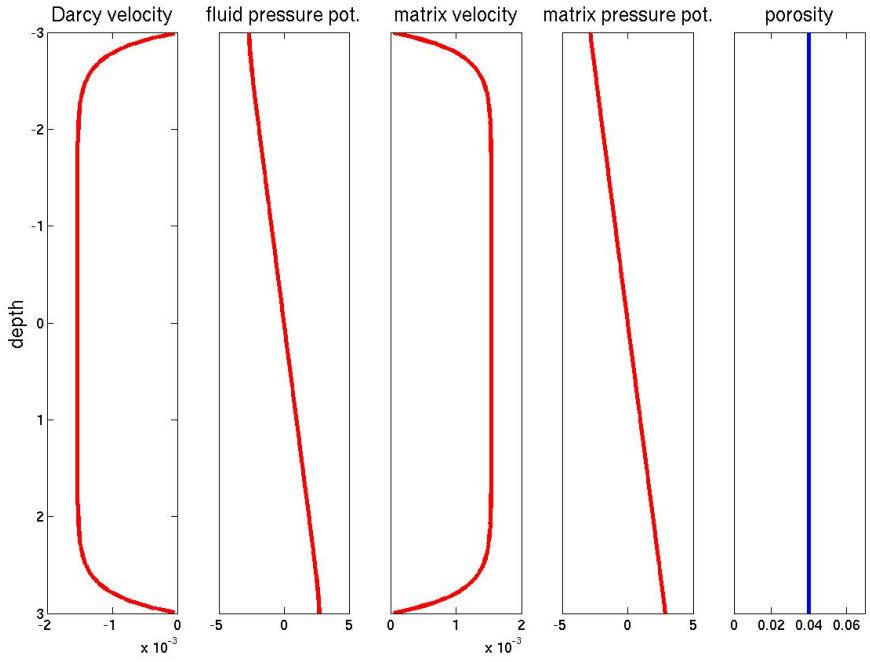

(b)

Figure C.1: Closed form solution in dimensionless variables (4.3.3) to a compacting column with constant porosity $\phi_0 = .04$, no flow boundary conditions, and $\Theta = 0$. (a) $L = .25L_c$. (b) $L = 3L_c$.

C.1.2 Discontinuous porosity

Take discontinuous porosity function on $z \in [-L, L]$,

$$\phi = \begin{cases} \phi_- & \text{if } z \leq 0, \\ \phi_+ & \text{if } z > 0. \end{cases} \tag{C.1.10}$$

solving (C.1.6) for $z \leq 0$ and $z > 0$ gives, respectively,

$$q_{f,-} = (1-\phi_-)\left(z + \frac{C_{1,-}}{R_-} e^{-R_-(z+L)} - \frac{C_{2,-}}{R_-} e^{R_- z}\right) + C_{int,-},$$
$$q_{f,+} = (1-\phi_+)\left(z + \frac{C_{1,+}}{R_+} e^{-R_+ z} - \frac{C_{2,+}}{R_+} e^{R_+(z-L)}\right) + C_{int,+}.$$

So there are six unknowns we must find, $C_{1,-}$, $C_{2,-}$, $C_{int,-}$, $C_{1,+}$,$C_{2,+}$, and $C_{int,+}$. Using boundary conditions (C.1.1) we have

$$u_-(-L) = 0, \qquad u_+(L) = 0. \tag{C.1.11}$$

Moreover, continuity of both pressures and the Darcy velocity (or alternatively the matrix velocity) as well as setting the fluid pressure scaling gives

$$q_{f,-}(0) = q_{f,+}(0) = 0, \qquad q_{m,-}(0) = q_{m,+}(0), \qquad u_-(0) = u_+(0), \tag{C.1.12}$$

and provides us with six independent equations.

Plots of the solution are shown in Figure C.2. For $\phi_+ \gg \phi_-$, the fluid pressure approaches a step function at $z = 0$. When ϕ_+ and ϕ_- are similar in magnitude, the relative velocity is discontinuous to balance the discontinuity in the porosity.

C.1.3 Quadratic porosity approximation

Combining (C.1.2), (C.1.4), and (C.1.5) gives

$$v_m' = -u' = \left(\phi^{2(1+\Theta)} q_f'\right)'$$

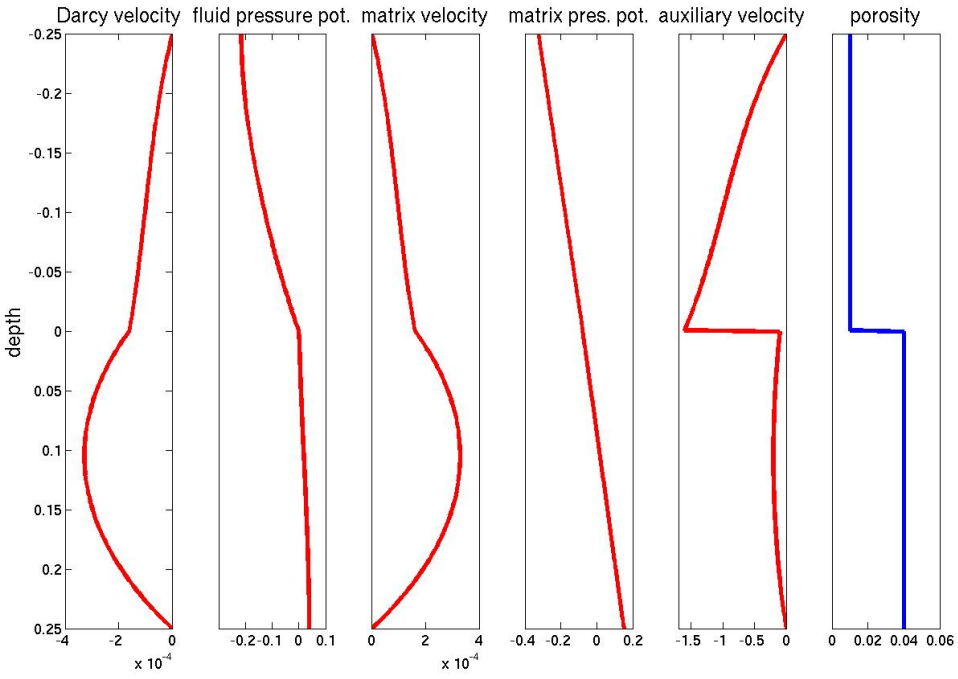
Darcy velocity
fluid pressure pot.
matrix velocity
matrix pres. pot.
auxiliary velocity
porosity
depth
x 10^-4
x 10^-4

(a)

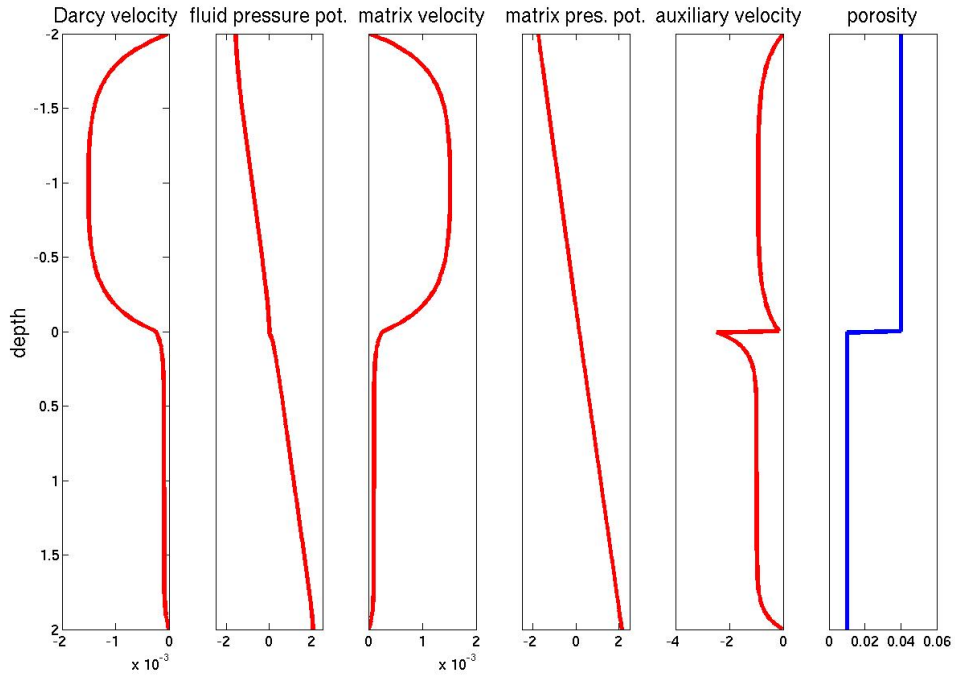
Darcy velocity
fluid pressure pot.
matrix velocity
matrix pres. pot.
auxiliary velocity
porosity
depth
x 10^-3
x 10^-3

(b)

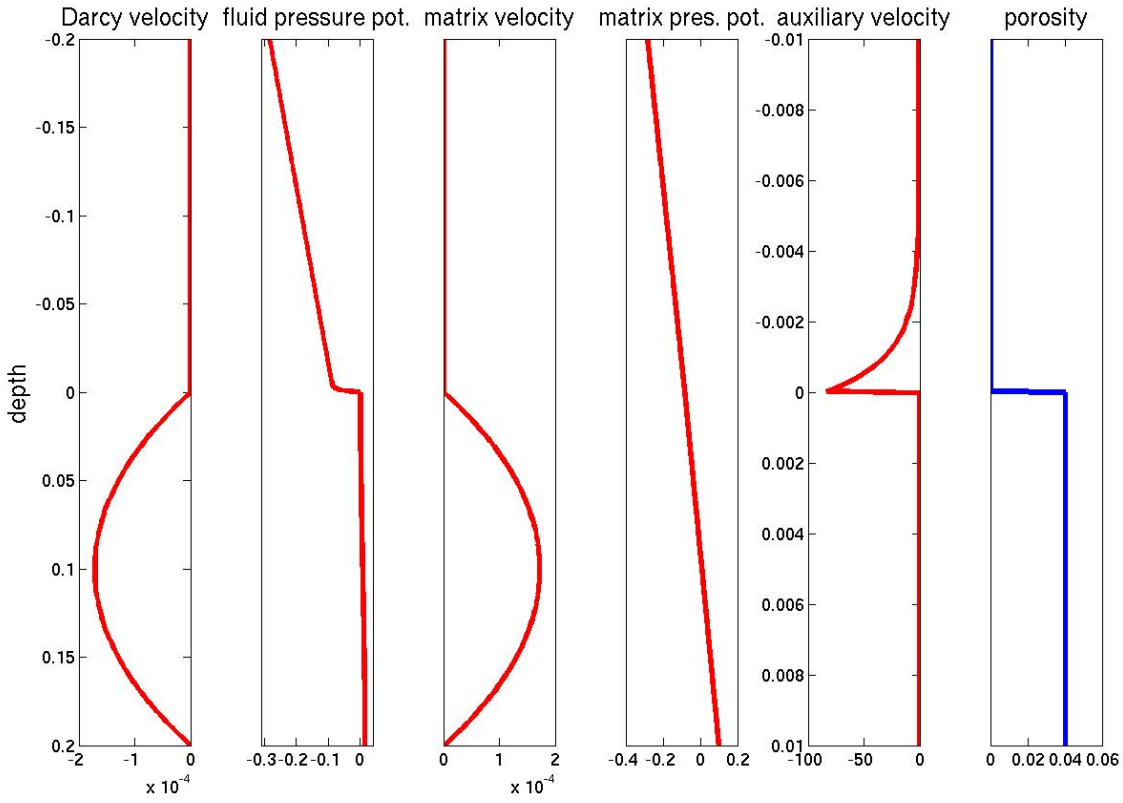

(c)

Figure C.2: Closed form solution in dimensionless variables (4.3.3) to a compacting column with no flow boundary conditions and $\Theta = 0$. Auxiliary velocity represents the velocity calculated by the expanded method. (a) $L = .25L_c$, $\phi_- = .01$, $\phi_+ = .04$. (b) $L = 2L_c$, $\phi_- = .04$, $\phi_+ = .01$. (c) $L = .25L_c$, $\phi_- = 10^{-6}$, $\phi_+ = .04$.

which, when substituted back into (C.1.4) gives

$$q_m = q_f - \tfrac{1}{\phi}\left(\phi^{2(1+\Theta)} q_f'\right)'.$$

Finally, eliminating all variables but q_f in (C.1.3) and integrating gives

$$q_f - \tfrac{3+\phi-4\phi^2}{3\phi}(\phi^{2(1+\Theta)} q_f')' = (1-\phi)z + C.$$

We assume porosity is much less than one, and set $\frac{3+\phi-4\phi^2}{3} \approx 1$. Then,

$$-\phi^{1+2\Theta} q_f'' - 2(1+\Theta)\phi^{2\Theta}\phi' q_f' + q_f = z + C.$$

Choosing

$$\phi(z) = \begin{cases} 0, & z \le 0, \\ z^{\alpha}, & z > 0. \end{cases} \tag{C.1.13}$$

then

$$-z^{\alpha(1+2\Theta)} q_f'' - 2\alpha(1+\Theta) z^{\alpha(1+2\Theta)-1} q_f' + q_f = z + C.$$

The fluid pressure scaling, $q_f(0) = 0$, implies $C = 0$. For simplicity take $\Theta = 0$. Set $\alpha = \dfrac{2}{1+2\Theta} = 2$ to get an Euler equation given by

$$-z^2 q_f'' - 4z q_f' + q_f = z \tag{C.1.14}$$

In this case the Euler exponents satisfy $r(r-1) + 4r - 1 = 0$, and so

$$r_1 = \frac{-3+\sqrt{13}}{2} \approx 0.3 > 0 \quad \text{and} \quad r_2 = \frac{-3-\sqrt{13}}{2} \approx -3.3 < 0, \tag{C.1.15}$$

and the solution to the homogeneous equation is $q_{f,hom}(z) = C_1 z^{r_1} + C_2 z^{r_2}$. Variation of parameters gives us the non-homogeneous solution for $z > 0$,

$$q_f(z) = \frac{-1}{r_1 - r_2}\left\{ z^{r_1}\left(\int \frac{y}{y^{r_1+1}}\, dy + c_1 \right) - z^{r_2}\left(\int \frac{y}{y^{r_2+1}}\, dy + c_2 \right) \right\}.$$

The Darcy velocity $u = -\phi^2 q_f \in L^2(0,1)$ implies $C_2 = 0$, and the boundary conditions determine C_1. For $z \leq 0$, $u = v_m = 0$, $q_m = z$, and we choose $q_f = 0$ (q_f is arbitrary when $\phi = 0$). For $z > 0$ the solution is

$$v_m = -u = \frac{-z^4 + L^{1-r_1} z^{r_1+3}}{(1-r_1)(1-r_2)}, \tag{C.1.16}$$

$$q_f = \frac{-r_1 z + L^{1-r_1} z^{r_1}}{r_1(1-r_1)(1-r_2)}, \tag{C.1.17}$$

$$q_m = z. \tag{C.1.18}$$

A plot of the approximate solution is shown in figure C.3. Note that it is qualitatively very similar to the solution for discontinuous porosity in figure C.2(c). The auxillary velocity is omitted since it blows up at $z = 0$.

C.2 Viscous corner flow

The viscous corner flow model with constant porosity $\phi = \phi_0$ and no melting, presented in section 4.3.2, with boundary conditions shown in figure 4.2(a) is given by the dimensionless equations

$$\nabla \cdot \mathbf{v}_m = \nabla \cdot \mathbf{u} = 0\,, \tag{C.2.1}$$

$$\nabla q - (1-\phi_0)\nabla^2 \mathbf{v}_m = (1-\phi_0)\hat{\mathbf{z}}\,, \tag{C.2.2}$$

$$\mathbf{u} = -\frac{w_0}{U_0}\nabla q\,, \tag{C.2.3}$$

where

$$w_0 = \frac{k_0 \phi_0^{2(1+\Theta)} \Delta\rho g}{\mu_f}, \tag{C.2.4}$$

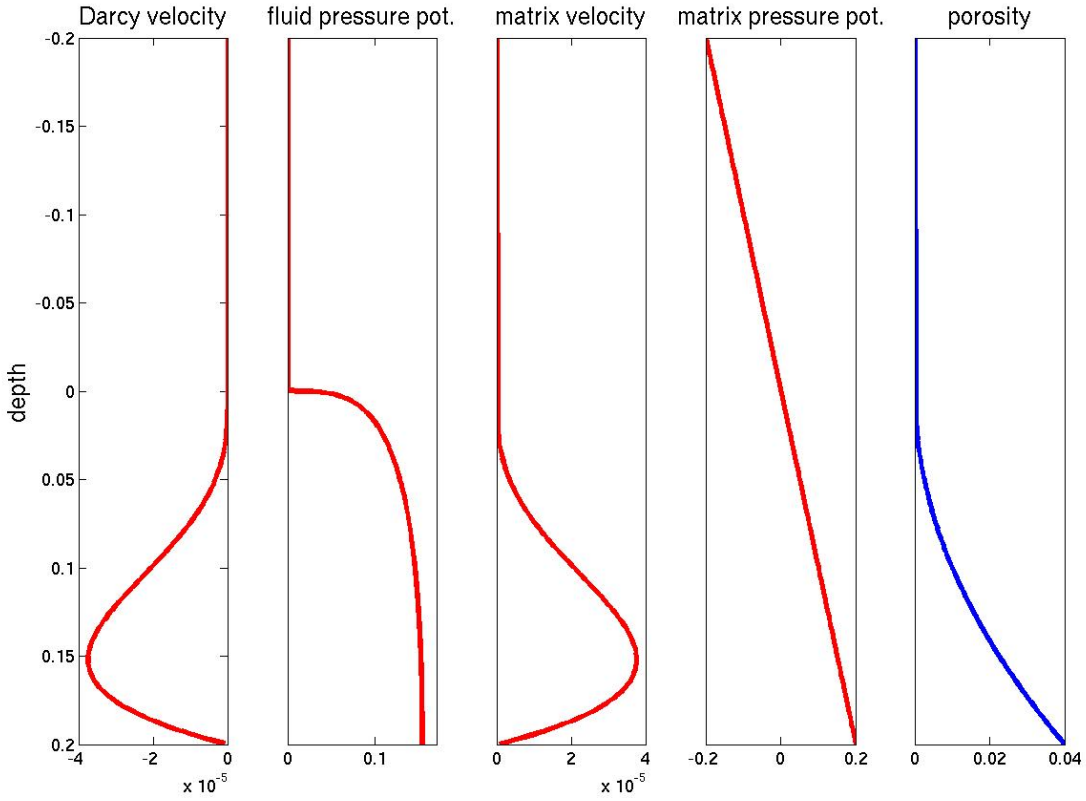

Figure C.3: Approximate solution to a compacting column with porosity given by (5.7.3) and no flow boundary conditions. $\Theta = 0$.

is the percolation velocity. Equation (C.2.1) implies a stream function solution

$$\mathbf{v}_m = \nabla \times (\Psi_m \hat{\mathbf{k}}),$$
$$\mathbf{u} = \nabla \times (\Psi_r \hat{\mathbf{k}}).$$

where $\hat{\mathbf{k}}$ is a vector perpendicular to the plane of the problem. Taking the cross product of (C.2.2) results in a biharmonic equation for Ψ_m given by

$$\nabla^4 \Psi_m = 0. \tag{C.2.5}$$

This equation is solved by inspection [11, 40] in polar coordinates with

$$\begin{aligned} \mathbf{v}_m &= \frac{1}{r}\frac{\partial \Psi_m}{\partial \theta}\hat{\mathbf{r}} - \frac{\partial \Psi_m}{\partial r}\hat{\boldsymbol{\theta}}, \\ \Psi_m &= r f(\theta), \\ f(\theta) &= C_1 \sin\theta + C_2 \cos\theta + C_3 \theta \sin\theta + C_4 \theta \cos\theta, \end{aligned} \tag{C.2.6}$$

where r is the distance from the corner, θ is the angle measured from the z-axis, and C_i are constants determined by the boundary conditions. The boundary conditions, in polar coordinates, imply the constraints

$$\mathbf{v}_{m,\theta}(r,0) = 0, \qquad \frac{\partial \mathbf{v}_{m,r}}{\partial \theta}(r,0) = 0, \qquad \mathbf{v}_m\big(r, \frac{\pi}{2}\big) = \hat{\mathbf{r}},$$

and so

$$f(\theta) = -\frac{2}{\pi}\theta \cos\theta.$$

By (C.2.6) we have $\mathbf{v}_m$, with q_m and $\mathbf{u}$ derived from (C.2.2)–(C.2.3). For $r > 0$,

$$\mathbf{v}_m = \frac{2}{\pi}((\theta \sin\theta - \cos\theta)\hat{\mathbf{r}} + \theta\cos\theta\hat{\boldsymbol{\theta}}) \tag{C.2.7}$$

$$q = (1-\phi_0)\Big(-\frac{4}{\pi r} + r\Big)\cos\theta = (1-\phi_0)\Big(-\frac{4\cos\theta}{\pi r} + z\Big), \tag{C.2.8}$$

$$\mathbf{u} = -\frac{w_0}{U_0}(1-\phi_0)\Big(\frac{4}{\pi r^2}(\cos\theta\hat{\mathbf{r}} + \sin\theta\hat{\boldsymbol{\theta}}) + \hat{\mathbf{z}}\Big). \tag{C.2.9}$$

As shown in Figure C.4, the matrix velocity is independent of r and ϕ_0. Near the corner, the pressure is dominated by the $1/r$-term and decreases as θ increases. The relative velocity is in the $(-\hat{\mathbf{r}})$-direction for small θ and in the $(-\hat{\boldsymbol{\theta}})$-direction for large θ, focusing the fluid toward the corner. Far away from the corner, the fluid moves upward relative to the matrix due to its buoyancy. Note that there is a stationary point in the relative (and thus fluid) velocity. The fluid pressure and relative velocity blow up at the corner.

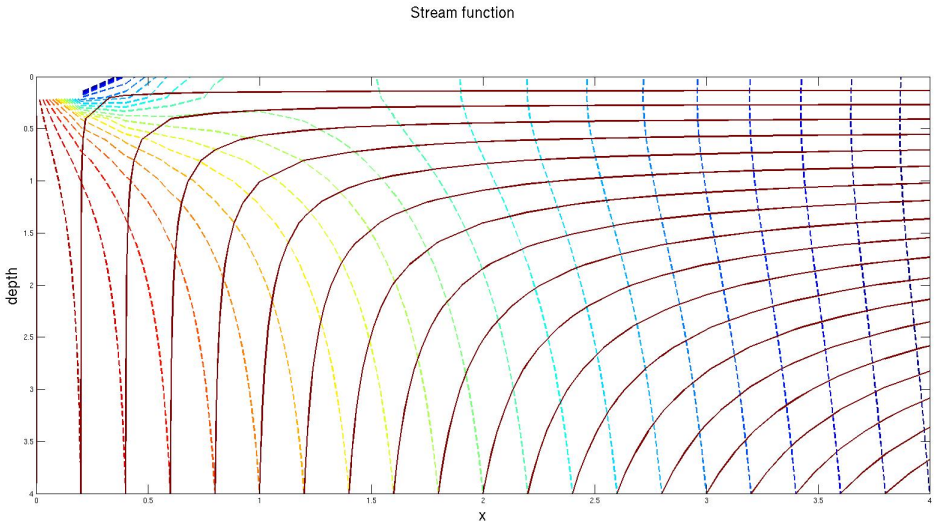

(a)

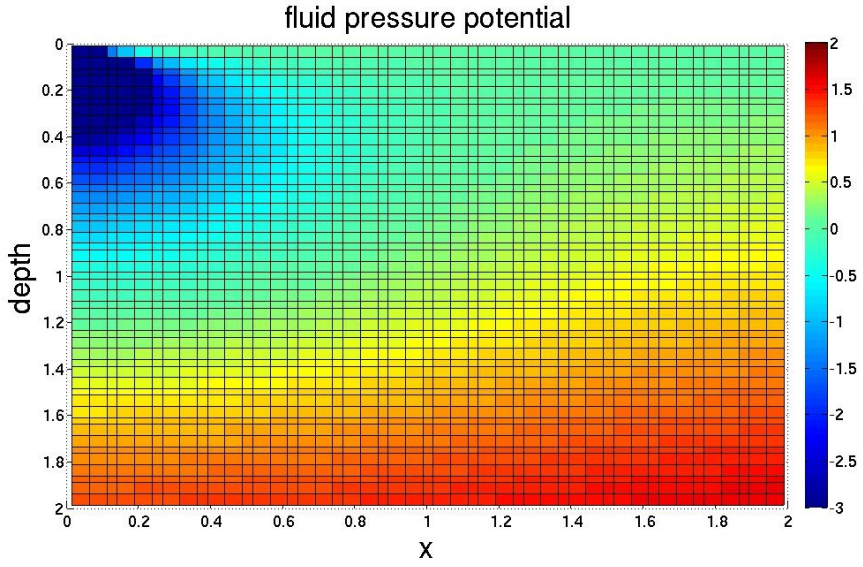

(b)

Figure C.4: Closed form solution in dimensionless variables (4.3.15) to viscous corner flow with boundary conditions given in figure 4.2(a) and $L = 2L_s$. (a) Solid lines represent matrix velocity stream lines. Dashed lines represent relative (fluid) velocity stream lines. (b) matrix (or fluid) pressure.

Appendix D

General Finite Element Code for Coupled Systems of Equations

D.1 Motivation

Presented in this document is a guide to a general finite element code for solving coupled nonlinear second order PDE's in 2D. I created this code with the intention of solving $2D$ problems in mantle convection using the mixed finite element method. This project began with a sincere attempt at a mixed method in PETSc, but ran out of steam party because PETSc documentation for my application is lacking, and partly due to my lack of necessity for and experience with parallel computing. I eliminated using standard finite element packages such as Deal.II and FEnICS and realized in a natural way that writing this code primarily in MATLAB (interfacing with C when necessary) was the right development direction. Undertaking the task of writing such an immense code from scratch requires justification. First, the multiphysics equations of mantle dynamics are not well-established especially in computational mathematics, and there appears to be no previous work in the finite element community. Even our own formulation of the equations remained in flux for much of the project's duration and the numerical interpretation of the porosity required significant tinkering and some non-standard techniques. This requires a general approach to implementing the variational form. Another key part of my

project is an investigation of the AW_0 basis functions. These basis functions are not easy to implement in standard finite element packages (PETSc, for example) because they do not form a tensor product space. Aside from interest in the improved performance of AW_0 over more standard elements for Stokes flow like Taylor-Hood, this is not a performance code. The code is entirely sequential, though the unstructured approach to the mesh does lend itself to convenient parallelization. There are no bells and whistles like adaptive mesh refinement, and the Newton method uses a direct solver for each iteration. The intention is only to demonstrate that the mixed method is a viable approach for the equations of mantle dynamics. Finally, this code is also intended for users in the geoscience community who are much more comfortable with MATLAB code over C++, for example.

D.2 Functionality and input file

I will outline here the different user inputs and functionality of the code to solve an arbitrary number of coupled non-linear PDE's. It uses an unstructured mesh defined by the user. The user can also pick the order of the Gaussian quadrature rule. The code includes functionality to enter new finite element basis, and many standard options as well as the AW_0 elements are already implemented. Most exciting about the code is its general approach to implementing the variational form and boundary condition as well as its approach to constructing the Jacobian. I will use Stokes corner flow on $\Omega = [0,1]^2$ as an example problem. Though this problem is linear and does not take full advantage of the functionality of the code, it will

sufficiently illustrate how it can be used. For velocity $\mathbf{u}$ and pressure p,

$$\begin{cases} -\nabla \cdot \nabla \mathbf{u} + \nabla p = \mathbf{0}, & \Omega, \\ -\nabla \cdot \mathbf{u} = 0, & \Omega. \end{cases} \tag{D.2.1}$$

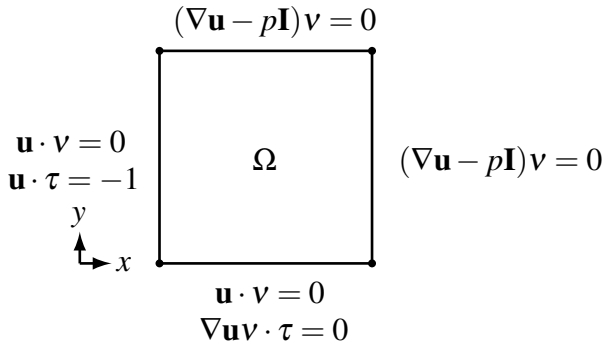

Figure D.1: Boundary conditions for Stokes symmetric corner flow.

Following Fig. D.1, ν and τ denote the outward pointing normal and tangent to the boundary $\partial\Omega$, respectively. The right and top boundary $\Gamma_1 = \{1\} \times [0,1] \cup [0,1] \times \{1\}$. Flow on these edges has normal stress equal to zero (recall, the stress is defined as $\sigma = \nabla \mathbf{u} - p\mathbf{I}$). The left boundary $\Gamma_2 = [0,1] \times \{0\}$ is moving with a velocity 1 to the right. The bottom boundary $\Gamma_3 = \{0\} \times [0,1]$ is a symmetry boundary (i.e. $u_y = \mathbf{u} \cdot \nu = 0$ and $\frac{\partial u_x}{\partial y} = \nabla \mathbf{u} \nu \cdot \tau = 0$) so we set zero normal flux and tangential component of the normal stress set to zero.

D.2.1 Mesh

Currently only rectangular meshes are implemented. To uniquely define the mesh, the input file must provide:

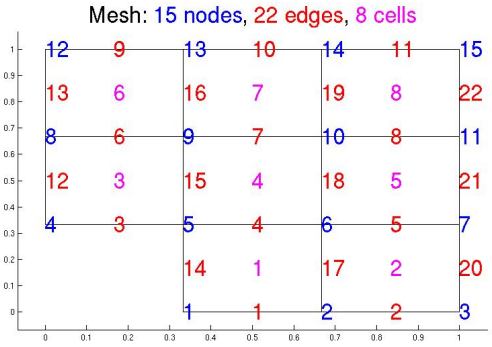

Figure D.2: Domain $[0,1]^2$ with the bottom-left cell removed. Blue indices represent nodes, red indices represent edges, and pink indices represent cells.

- `x` and `y` arrays representing the x-vertices and y-vertices of the mesh, OR
- `nx`, `Lx` representing the number of x elements between `Lx(1)` and `Lx(2)`, and `ny`, `Ly` representing the number of y elements between `Ly(1)` and `Ly(2)`.
- Optionally, `loc` is a function handle of two variables that eliminates vertices from the mesh where `loc(x,y)`≤ 0

For example, the following input would generate the mesh in Fig. D.2:

```
x = 0:1/3:1; y = 0:1/3:1;
loc = @(x,y) (x≥1/3)*(y≥1/3));
```

D.2.2 Problem variables

For the problem's variables, The user provides field names and number of components for each field. For the Stokes problem the velocity is a vector and the pressure is a scalar. Hence, with velocity first and pressure second,

```
field(1).name = 'velocity';
field(1).numComp = 2;
field(2).name = 'pressure';
field(2).numComp = 1;
```

This initializes the problem variable `u` which contains the degrees of freedom of the entire problem.

D.2.3 Quadrature

The user provides the precision of the Gauss quadrature rule for all interior and boundary integrals evaluated in the Jacobian and variational form. For example, for the AW_0 elements, `prec` = 5 would integrate the discrete variational form exactly.

D.2.4 Finite element basis

Each field requires the user to enter a finite element basis. Provided finite element spaces basis include basis functions shown in table D.1. For example, to

basis		command
vector fields	RT_0 Velocity	`RT0Velocity`
	$(\mathbb{P}^1)^2$	`P1Quad2`
	AW_0 velocity	`AWVelocity`
	Taylor-Hood velocity	`TaylorHoodVelocity`
scalar fields	$\mathbb{P}^0$	`piecewiseConst`
	$\mathbb{P}^1$	`P1Quad`

Table D.1: provided finite element options.

solve Stokes using the AW_0 finite elements, the input file must contain the lines:

```
field(1).basisType = @AWVelocity;
field(2).basisType = @piecewiseConst;
```

Moreover, the code has built-in functionality to quickly add new finite element basis.

D.2.5 Exact solution

Optionally, to check the finite element solution against an exact solution, the input file must define `uExact`. `uExact` is set by providing a function handle of 2 variables for every component of every field. To check the error in the H^1 or $H(\mathrm{div})$ norms, define `gradUExact` for every field, component, and derivative direction or use this provided routine to take symbolic derivatives of `uExact`:

```
field = symbolicDerivatives(field);
```

Note that this function is fragile because MATLAB's symbolic library is easily broken. For Stokes corner flow:

```
B = 2/pi;
r = @(x,y) sqrt(x^2+y^2);
r2 = @(x,y) x^2+y^2;
theta = @(x,y) atan(y/x);

% u_x = B*cos(theta)^2
field(1).uExact{1} = @(x,y) -B*cos(theta(x,y))^2;
% u_y = B*(theta - sin(theta)*cos(theta))
```

```
field(1).uExact{2} = @(x,y) B*(theta(x,y) - sin(2*theta(x,y))/2);
% p = -2*B*U_0*cos(theta)/r
field(2).uExact{1} = @(x,y) -2*B*cos(theta(x,y))/r(x,y);
```

D.2.6 Variational form

Let,

$$\mathbf{V} = \left\{ \mathbf{u} \in (H^1(\Omega))^2; \mathbf{u}|_{\Gamma_2} = \mathbf{0}; \mathbf{u}|_{\Gamma_3} \cdot \nu = 0 \right\}, \tag{D.2.2}$$

$$W = L_0^2(\Omega). \tag{D.2.3}$$

With an arbitrary lift $\mathbf{u}_N \in (H^1(\Omega))^2$ satisfying $\mathbf{u}_N|_{\Gamma_3} = \left(\begin{smallmatrix} 0 \\ -1 \end{smallmatrix}\right)$, and $\mathbf{u}_N|_{\Gamma_4} \cdot \nu = 0$, the variational form for Stokes becomes:

Find $\mathbf{u} \in \mathbf{V} + \mathbf{u}_N$, $p \in W$ such that,

$$\begin{aligned} &(\nabla \mathbf{u} : \nabla \mathbf{v}) - (p, \nabla \cdot \mathbf{v}) - \langle (\nabla \mathbf{u} - p\mathbf{I})\nu, \mathbf{v} \rangle_{\partial\Omega} \\ &= (\nabla \mathbf{u} : \nabla \mathbf{v}) - (p, \nabla \cdot \mathbf{v}) \qquad\qquad (\text{D.2.4}) \\ &\quad - \langle (\nabla \mathbf{u} - p\mathbf{I})\nu \cdot \nu, \mathbf{v} \cdot \nu \rangle_{\Gamma_3} - \langle \nabla \mathbf{u} \nu \cdot \tau, \mathbf{v} \cdot \tau \rangle_{\Gamma_2 \cup \Gamma_3} = 0 \quad \forall \mathbf{v} \in \mathbf{V} \\ &(\nabla \cdot \mathbf{u}, w) + (g, w) = 0 \qquad\qquad \forall w \in W \qquad (\text{D.2.5}) \end{aligned}$$

Next, consider the discrete system for finite element spaces $\mathbf{V}_h$ and W_h and test basis function $\mathbf{v}_i$ and w_i. Ignoring boundary terms for the moment, the discrete variational form becomes:

Find $\mathbf{u}_h \in V_h + \mathbf{u}_N$, $p_h \in W_h$ such that,

$$F_{\mathbf{u},i}(\mathbf{u}_h, p_h) = (\nabla \mathbf{u}_h : \nabla \mathbf{v}_i) - (p_h, \nabla \cdot \mathbf{v}_i) = 0 \qquad \forall \mathbf{v}_i \in \mathbf{V}_h \tag{D.2.6}$$

$$F_{p,i}(\mathbf{u}_h, p_h) = -(\nabla \cdot \mathbf{u}_h, q_i) = 0 \qquad \forall q_i \in W_h \tag{D.2.7}$$

Very useful observation: since the variational form is *always linear in the test functions*, it can be expressed generally for first order forms as, dropping subscript h's,

$$F_{\mathbf{u},i}(\mathbf{u},p) = (\mathbf{f}_{\mathbf{v}}(\mathbf{u},\nabla\mathbf{u},p,\nabla p),\mathbf{v}_i) + (\mathbf{f}_{\nabla\mathbf{v}}(\mathbf{u},\nabla\mathbf{u},p,\nabla p) : \nabla\mathbf{v}_i) = 0 \tag{D.2.8}$$

$$F_{p,i}(\mathbf{u},p) = (f_q(\mathbf{u},\nabla\mathbf{u},p,\nabla p),q_i) + (\mathbf{f}_{\nabla q}(\mathbf{u},\nabla\mathbf{u},p,\nabla p),\nabla q_i) = 0 \tag{D.2.9}$$

where, for Stokes,

$$\mathbf{f}_{\mathbf{v}}(\mathbf{u},\nabla\mathbf{u},p,\nabla p) = \mathbf{0}, \tag{D.2.10}$$

$$\mathbf{f}_{\nabla\mathbf{v}}(\mathbf{u},\nabla\mathbf{u},p,\nabla p) = \nabla\mathbf{u} - p\mathbf{I}, \tag{D.2.11}$$

$$f_q(\mathbf{u},\nabla\mathbf{u},p,\nabla p) = -\nabla\cdot\mathbf{u} - g, \tag{D.2.12}$$

$$\mathbf{f}_{\nabla q}(\mathbf{u},\nabla\mathbf{u},p,\nabla p) = \mathbf{0}. \tag{D.2.13}$$

To specify f_q the input file must set `field(2).varForm.v`. To specify $\mathbf{f}_{\nabla\mathbf{v}}$ set `field(1).varForm.gradV`. Using this general framework, the Stokes variational form is set by the following lines:

```
% (gradU , gradV) - (p , divV)
field(1).varForm.gradV{1,1} = @(u, gradU, x, y) ...
   gradU.field{1}(1,1) - u.field{2}(1);
field(1).varForm.gradV{1,2} = @(u, gradU, x, y) ...
   gradU.field{1}(1,2);
field(1).varForm.gradV{2,1} = @(u, gradU, x, y) ...
   gradU.field{1}(2,1);
field(1).varForm.gradV{2,2} = @(u, gradU, x, y) ...
   gradU.field{1}(2,2) - u.field{2}(1);
% -(divU , v)
field(2).varForm.v{1} = @(u, gradU, x, y) -gradU.field{1}(1,1) ...
   - gradU.field{1}(2,2);
```

where, for example, `u.field{1}` and `u.field{2}` represent the velocity and pressure trial functions, respectively, and `gradU.field{1}(i,j)` represents the derivative of the i^{th} component in the j^{th} direction.

D.2.7 Jacobian form

Since the Jacobian form is always bi-linear for the test functions, a similar approach to the formulation of the residual applies. For the discrete problem denote basis functions $\mathbf{w}_i$ and r_i for the velocity and pressure, respectively, so that $\mathbf{u} = \sum u_i \mathbf{w}_i$ and $p = \sum p_i r_i$.

$$\mathbf{J} = \begin{pmatrix} \frac{\partial F_{\mathbf{u}}}{\partial \mathbf{u}} & \frac{\partial F_{\mathbf{u}}}{\partial p} \\ \frac{\partial F_p}{\partial \mathbf{u}} & \frac{\partial F_p}{\partial p} \end{pmatrix} \tag{D.2.14}$$

For example, for the term $\frac{\partial F_{\mathbf{u}}}{\partial \mathbf{u}}$, by the chain rule,

$$\begin{aligned} \frac{\partial F_{\mathbf{u}}}{\partial \mathbf{u}}(i,j) = \frac{\partial F_{\mathbf{u},i}}{\partial u_j} = &\left(\frac{\partial \mathbf{f}_{\mathbf{v}}}{\partial \mathbf{u}}(\mathbf{u}, \nabla\mathbf{u}, p, \nabla p)\mathbf{w}_j : \mathbf{v}_i\right) \\ &+ \left(\frac{\partial \mathbf{f}_{\mathbf{v}}}{\partial (\nabla\mathbf{u})}(\mathbf{u}, \nabla\mathbf{u}, p, \nabla p)\nabla\mathbf{w}_j, \mathbf{v}_i\right) \\ &+ \left(\frac{\partial \mathbf{f}_{\nabla\mathbf{v}}}{\partial \mathbf{u}}(\mathbf{u}, \nabla\mathbf{u}, p, \nabla p)\mathbf{w}_j, \nabla\mathbf{v}_i\right) \\ &+ \left(\frac{\partial \mathbf{f}_{\nabla\mathbf{v}}}{\partial (\nabla\mathbf{u})}(\mathbf{u}, \nabla\mathbf{u}, p, \nabla p)\nabla\mathbf{w}_j : \nabla\mathbf{v}_i\right) \end{aligned} \tag{D.2.15}$$

with the three remaining terms ($\frac{\partial F_{\mathbf{u}}}{\partial p}$, $\frac{\partial F_p}{\partial \mathbf{u}}$, $\frac{\partial F_p}{\partial p}$) in the Jacobian derived analogously. In the input file, the coefficient corresponding to $\frac{\partial \mathbf{f}_p}{\partial (\nabla\mathbf{u})}(\mathbf{u}, \nabla\mathbf{u}, p, \nabla p)$ is set by `field(1).JacForm.field(2).gradW.v`. For the Stokes example:

```
% (gradW, gradV)
field(1).JacForm.field(1).gradW{1,1}.gradV{1,1} = ...
    @(u,gradU,x,y) 1;
```

```
field(1).JacForm.field(1).gradW{1,2}.gradV{1,2} = ...
    @(u,gradU,x,y) 1;
field(1).JacForm.field(1).gradW{2,1}.gradV{2,1} = ...
    @(u,gradU,x,y) 1;
field(1).JacForm.field(1).gradW{2,2}.gradV{2,2} = ...
    @(u,gradU,x,y) 1;
% -(w,divV)
field(2).JacForm.field(1).w{1}.gradV{1,1} = @(u,gradU,x,y) -1;
field(2).JacForm.field(1).w{1}.gradV{2,2} = @(u,gradU,x,y) -1;
% -(divW,v)
field(1).JacForm.field(2).gradW{1,1}.v{1} = @(u,gradU,x,y) -1;
field(1).JacForm.field(2).gradW{2,2}.v{1} = @(u,gradU,x,y) -1;
```

Alternately, the user can opt to use a finite difference Jacobian approximation by providing a nonzero parameter `h` to be used in a finite difference scheme. Since Stokes corner flow is a linear problem, the above Jacobian information need not be included and the finite difference scheme will calculate the Jacobian exactly with the input:

```
% finite difference parameter
h = 1;
```

Note that in the linear case `h` can be any non-zero constant.

D.2.8 Boundary conditions

The code handles Neumann and Robin boundary conditions of the form,

$$\alpha(\text{natural condition}) + \beta p = \eta \tag{D.2.16}$$

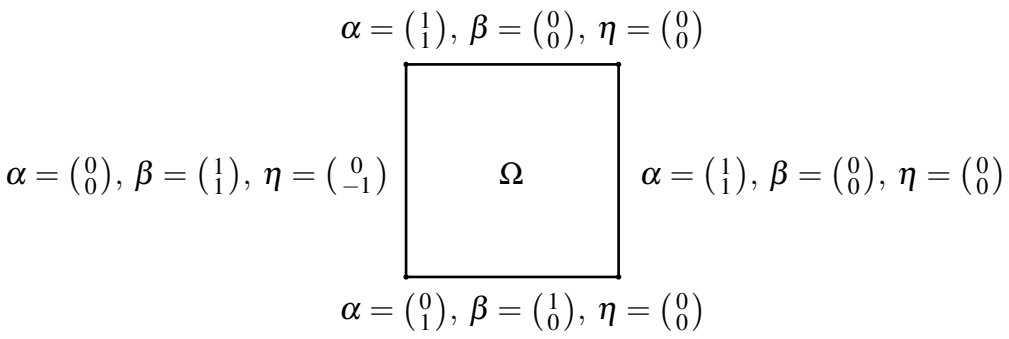

Figure D.3: Values of α, β, and η used to set the boundary conditions in Fig. D.1 for Stokes symmetric corner flow.

for scalar fields p. For vector fields $\mathbf{u}$, the Neumann and Robin boundary condition becomes

$$\alpha_1(\text{natural condition}) \cdot \nu + \beta_1 \mathbf{u} \cdot \nu = \eta_1, \tag{D.2.17}$$

$$\alpha_2(\text{natural condition}) \cdot \tau + \beta_2 \mathbf{u} \cdot \tau = \eta_2, \tag{D.2.18}$$

where the natural condition is defined by the boundary term in the variational form. By (D.2.4), theNeumann and Robin conditions for Stokes are defined by seting α, β, and η for boundary according to

$$\alpha_1((\nabla \mathbf{u} - p\mathbf{I})\nu) \cdot \nu + \beta_1 \mathbf{u} \cdot \nu = \eta_1, \tag{D.2.19}$$

$$\alpha_2(\nabla \mathbf{u}\, \nu) \cdot \tau + \beta_2 \mathbf{u} \cdot \tau = \eta_2. \tag{D.2.20}$$

Fig. D.3 shows the values of α, β, and η for each boundary Γ_i. The input file must contain:

```
% top and right edge
field(1).bndry(1).loc = @(x,y) (x-1)*(y-1);
field(1).bndry(1).alpha = [1 1];
field(1).bndry(1).beta = [0 0];
field(1).bndry(1).eta = {@(x,y) x , @(x,y) 0};
% bottom edge
field(1).bndry(2).loc = @(x,y) y;
field(1).bndry(2).alpha = [0 1];
field(1).bndry(2).beta = [1 0];
field(1).bndry(2).eta = {@(x,y) 0 , @(x,y) 0};
% left edge
field(1).bndry(3).loc = @(x,y) x;
field(1).bndry(3).alpha = [0 0];
field(1).bndry(3).beta = [1 1];
field(1).bndry(3).eta = {@(x,y) 0, @(x,y) -1};
```

D.2.9 Constant nullSpace

If one of the problem variables has a constant nullspace, the input file must supply the particular field (i.e. pressure for Stokes) by setting

```
field(2).nullSpace = 'true';
```

D.2.10 Newton iteration

To solve non-linear problems, the code uses a Newton method for which the user can enter the relative tolerance (`relTol`), absolute tolerance (`absTol`), and maximum number of iterations (`maxIter`).

D.2.11 Example input for Stokes corner flow

Putting it all together, to solve the homogeneous Stokes corner flow problem using AW_0 elements, the user must provide the following input file `StokesCornerFlow.m`:

```
%StokesCornerFlow.m
%% MESH------------------------------------------------------------------
% mesh on [0,1]^2 refince at bottom-left corner
x = [0 .025 .05 .1 .15 .25 .35 .45 .55 .65 .75 .85 .95 1];
y = [0 .025 .05 .1 .15 .25 .35 .45 .55 .65 .75 .85 .95 1];

%% VARIABLES-------------------------------------------------------------
field(1).name = 'velocity';
field(1).numComp = 2;
field(2).name = 'pressure';
field(2).numComp = 1;

%% GUASS QUADRATURE------------------------------------------------------
prec = 5;

%% FINITE ELEMENT BASIS--------------------------------------------------
field(1).basisType = @AWVelocity;
field(2).basisType = @piecewiseConst;

%% EXACT SOLUTION--------------------------------------------------------
B = 2/pi;
r = @(x,y) sqrt(x^2+y^2);
theta = @(x,y) atan(y/x);

% u_x = B*cos(theta)^2
field(1).uExact{1} = @(x,y) -B*cos(theta(x,y))^2;
% u_y = B*(theta - sin(theta)*cos(theta))
field(1).uExact{2} = @(x,y) B*(theta(x,y) - sin(2*theta(x,y))/2);
% p = -2*B*U_0*cos(theta)/r
field(2).uExact{1} = @(x,y) -2*B*cos(theta(x,y))/r(x,y);

%% VARIATIONAL FORM------------------------------------------------------
% (gradU , gradV) - (p , divV)
field(1).varForm.gradV{1,1} = @(u, gradU, x, y) ...
    gradU.field{1}(1,1) - u.field{2}(1);
field(1).varForm.gradV{1,2} = @(u, gradU, x, y) ...
```

```
    gradU.field{1}(1,2);
field(1).varForm.gradV{2,1} = @(u, gradU, x, y) ...
    gradU.field{1}(2,1);
field(1).varForm.gradV{2,2} = @(u, gradU, x, y) ...
    gradU.field{1}(2,2) - u.field{2}(1);
% -(divU , v)
field(2).varForm.v{1} = @(u, gradU, x, y) -gradU.field{1}(1,1) ...
    - gradU.field{1}(2,2);

%% JACOBAIN FORM-------------------------------------------------------------
% finite difference parameter
h = 1;

%% BOUNDARY CONDITIONS-------------------------------------------------------
% top and right edge
field(1).bndry(1).loc = @(x,y) (x-1)*(y-1);
field(1).bndry(1).alpha = [1 1];
field(1).bndry(1).beta = [0 0];
field(1).bndry(1).eta = {@(x,y) x , @(x,y) 0};
% bottom edge
field(1).bndry(2).loc = @(x,y) y;
field(1).bndry(2).alpha = [0 1];
field(1).bndry(2).beta = [1 0];
field(1).bndry(2).eta = {@(x,y) 0 , @(x,y) 0};
% left edge
field(1).bndry(3).loc = @(x,y) x;
field(1).bndry(3).alpha = [0 0];
field(1).bndry(3).beta = [1 1];
field(1).bndry(3).eta = {@(x,y) 0, @(x,y) -1};

%% SOLVER--------------------------------------------------------------------
% Solver uses Newton iteration
relTol = 1e-10;
absTol = 1e-10;
maxIter = 5;

%% NULLSPACE-----------------------------------------------------------------
% fields that have a constant nullSpace
field(2).nullSpace = 'true';
```

D.3 Running the code

In order to run the code simply execute

```
[u, norms, errors, appCtx] = ...
   driver(@StokesCornerFlow,DEBUGLEVEL,OUTPUTMODE);
```

Output:

- `u` - degrees of freedom of computed solution
- `norms` - L^2-norms, $H(\text{div})$-norms and H^1-norms (when available)
- `errors` - relative L^2-errors, $H(\text{div})$-errors and H^1-errors (when available) as well as relative interpolation errors in each norm, provided an exact solution is defined.
- `appCtx` - data structure storing all problem information

`DEBUGLEVEL` denoted the amount of tracking and output the user wants to see with each level adding onto the previous:

- `DEBUGLEVEL` $= 1$
    1. plot computed solution
    2. plot exact solution (if it exists)
    3. plot stream function for vector-valued fields
    4. output program processes during run-time

- DEBUGLEVEL $= 2$

    1. plot mesh
    2. plot locations of boundary condition
    3. plot initial guess
    4. plot residual of computed solution evaluated at quadrature points
    5. plot error evaluated at quadrature points
    6. plot interpolation error evaluated at quadrature points
    7. spy-plot of the Jacobian matrix
    8. summarize input file

- DEBUGLEVEL $= 3$

    1. plot shape functions for all finite element basis
    2. calculate Jacobian condition number

Setting OUTPUTMODE $= 1$ gives norms and errors (if exact solution exists):

```
velocity:
 L2 norm | L2 err | L2 int-err | H1 norm | H1 err | H1 int-err |
-------------------------------------------------------------------
  0.668  |  0.207 |   0.280    |   2.71  |  0.502 |   0.531    |


pressure:
  L2 norm |  L2 err |  L2 int-err |
-------------------------------------
    2.145 |  1.412  |     0.690   |
```

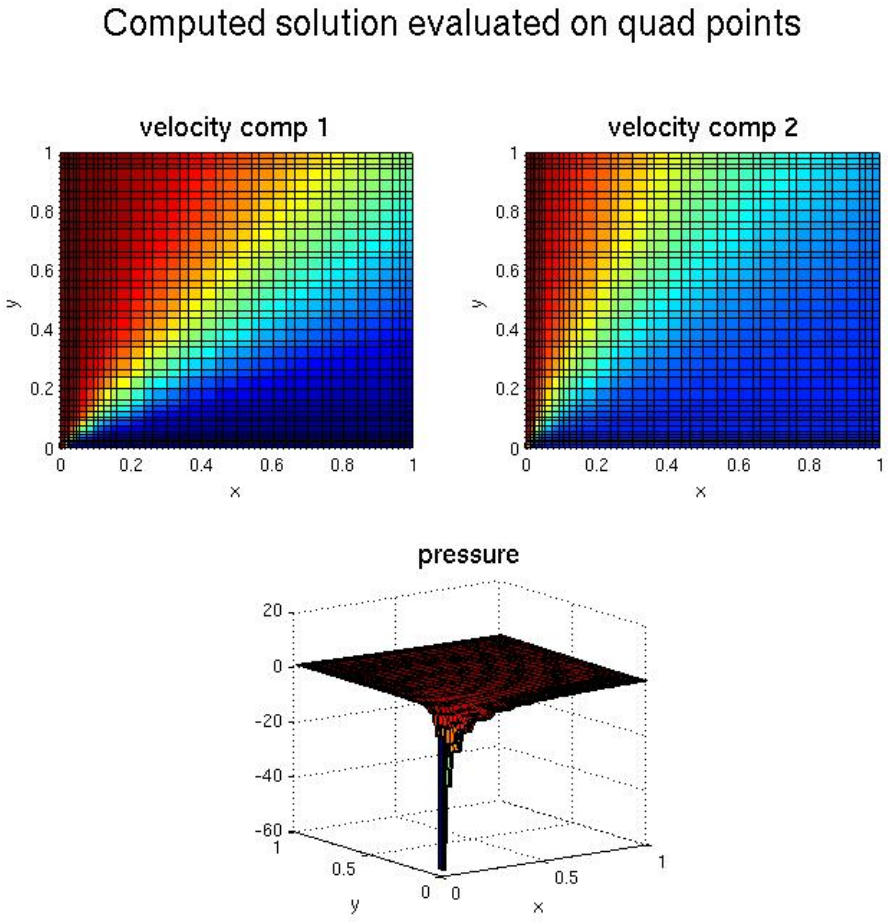

Figure D.4: Computed solution for Stokes corner flow. Velocity comp 1 denotes the x-velocity and velocity comp 2 denotes the y-velocity.

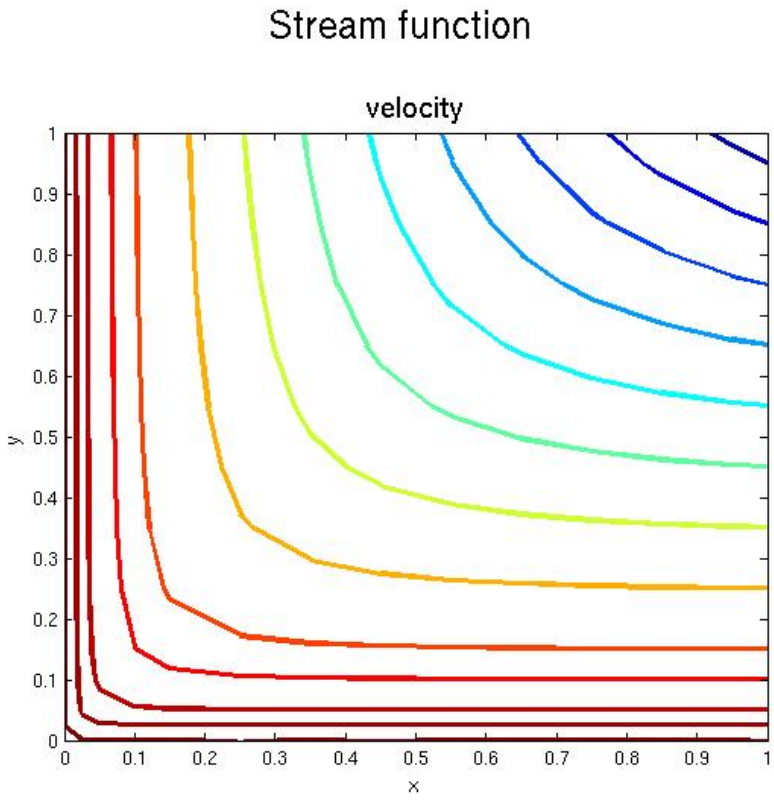

Figure D.5: Velocity stream lines for Stokes corner flow

Bibliography

[1] E. Aharonov, J. A. WhiteHead, P. B. Kelemen, and M. Spiegelman. Channeling instability of upwelling melt in the mantle. *J.Geophysical Research*, 100:20433–20450, 1995.

[2] T. Arbogast and J. Bona. *Methods of applied mathematics*. 2008.

[3] T. Arbogast and Z. Chen. On the implementation of mixed methods as nonconforming methods for second order elliptic problems. *Math. Comp.*, 64:943–972, 1995.

[4] T. Arbogast and A. Taicher. A linear degenerate elliptic equation arising from twho-phase mixtures. 2014.

[5] T. Arbogast and M. Wheeler. A family of rectangular mixed elements with a continuous flux for second order elliptic problems. *SIAM J. Numer. Anal.*, 42(5):1914–1931, 2005.

[6] T. Arbogast, M. F. Wheeler, and I. Yotov. Mixed finite elements for elliptic problems with tensor coefficients as cell-centered finite differences. *SIAM J. Numer. Anal.*, 34:828–852, 1997.

[7] D. Arroyo, A. Bespalov, and N. Heuer. On the finite element method for elliptic problems with degenerate and singular coeffiecients. *Math. Comp.*, 76:509–537, 2007.

[8] A. Aschwanden, E. Bueler, C. Khroulev, and H. Blatter. An enthalpy formulation for glaciers and ices sheets. *J. Glaciology*, 58:441–457, 2012.

[9] P. D. Asimow, M. M. Hirschmann, and E. M. Stopler. An analysis of variations in isentropic melt productivity. *Philosophical Transactions of the Royal Society of London, Searies A*, 355(1723):255–281, 1997.

[10] I. Babuska. The finite element method with Lagrange multipliers. *Num. Math.*, 20:179–192, 1973.

[11] G.K. Bachelor. *An Introdution to Fluid Dynamics*. Cambridge University Press, 1967.

[12] Satish Balay, Jed Brown, Kris Buschelman, William D. Gropp, Dinesh Kaushik, Matthew G. Knepley, Lois Curfman McInnes, Barry F. Smith, and Hong Zhang. PETSc Web page, 2012. http://www.mcs.anl.gov/petsc.

[13] J. Bear. *Dynamics of Fluids in Porous Media*. Elsevier, Amsterdam, 1972.

[14] J. Bear and D. Cheng. *Modeling groundwater flow and contaminant transport*. Springer, New York, NY, 2010.

[15] C. Bernardi and G. Raugel. Analysis of some finite elements for the Stokes problem. *math. comp.*, 169:71–79, 1985.

[16] S. Bidwell, M. E. Hassell, and C. R. Westphal. A weighted least squares finite element method for elliptic problems with degenerate and singular coefficients. *Math. Comp.*, 82:673–688, 2013.

[17] S. C. Brenner and L. R. Scott. *The mathematical theory of finite element methods*. Springer, New York, NY, 2008.

[18] F. Brezzi and M. Fortin. *mixed and hybrid finite elemnt methods*. Springer-Verlag, New York, 1991.

[19] J. Brown. Efficient nonlinear solvers for nodael high-order finite elemnts in 3D. *J. Sci. Comp.*, 45:48–63, 2010.

[20] Z. Chen, G. Huan, and Y. Ma. *Computational methods for multiphase flows in porous media*. SIAM, Philadelphia, PA, 2006.

[21] P. Clement. Approximation by finite element functions using local regualrization. *Anal. Numer.*, 9:77–84, 1975.

[22] J. Connolly, M. Schmidt, G. Soferino, and N. Bagdassarov. Permeability of asthenospheric mantle and melt extraction rates at mid-ocean ridges. *Nature*, 462(12), 2009.

[23] J. Jr. Douglas, T. Dupont, and L. Wajlbin. The stability in L^q of the L^2-projection into finite element function spaces. *Numer. Math.*, 23:193–197, 1975.

[24] D. A. Drew and L. A. Segel. Averaged equations for two-phase flows. *Stud. Appl. Maths.*, 50:205–231, 1971.

[25] K. Eriksson and V. Thomée. Galerkin methods for singular boundary value problems in one space dimension. *Math. Comp.*, 42:345–367, 1984.

[26] Alexandre Ern and Jean-Luc Guermond. *Theory and practice of finite elements*. Applied mathematical sciences. Springer, New York, 2004.

[27] C. Farhat and J. F. Gerbeau. The finite element method for fluid dynamics, 2009. Lecture Notes, Stanford University.

[28] A. C. Fowler. On the transport of moisture in polythermal glaciers. *Geophys. Astrophys. Fluid Dynamics*, 28:99–140, 1984.

[29] V. Girault and P.A. Raviart. *Finite element methods for Navier-Stokes equations: theory and algorithms*. Springer-Verlag, Berlin, 1986.

[30] M. A. Hesse, A. R. Schiemenz, and E. M. Parmentier. Compaction-dissolution waves in an upwelling mantle column. *Geophysical J. Int.*, 187:1057–1075, 2011.

[31] I. J. Hewitt and A. C. Fowler. Partial melting in an upwelling mantle column. *Proceedings of the Royal Society*, 464(2097):2467–2491, 2008.

[32] R. F. Katz. Magma dynamics with the enthalpy method: Benchmark solutions and magmatic focusing at mid-ocean ridges. *Journal of Petrology*, 49(12):2099–2121, 2008.

[33] P. B. Kelemen, G. Hirth, N. Shimizu, M. Spiegelman, and H.J.B. Dick. A review of melt migration processes in the adiabatically upwelling mantle beneath oceanic spreading ridges. *Phil. Trans. R. Soc. Lond.*, 355:283–318, 1997.

[34] M. Knepely and D. Karpeev. Mesh algorithms for PDE with sieve I: mesh distribution, 2009. Argonne National Labs.

[35] W. Lake. *Enhanced Oil Recovery*. Prentice Hall, Englewood Cliffs, NJ, 1989.

[36] H. Li. A-priori analysis and the finite element method for a class of degenerate elliptic equations. *Math. Comp.*, 78:713–737, 2009.

[37] D. Marini and P. Pietra. Mixed finite element approximation of a degenerate elliptic problem. *Numer. Math.*, 71:225–236, 1995.

[38] D. McKenzie. The generation and compaction of partially molten rock. *Journal of Petrology*, 25(3):713–765, 1984.

[39] D. McKenzie. Th-U disequilibrium and the melting processes beneath ridge axes. *Earth and Planetary Science Letters*, 72:149–157, 1985.

[40] H.K. Moffatt. Viscous and resistive eddies near a sharp corner. *J. Fluid Mechanics*, 18:1–18, 1963.

[41] J. Phipps Morgan. Melt migration beneach mid-ocean spreading centers. *Geophys. Res. Let.*, 14:1238–1241, 1987.

[42] T.A. Raviart and J.M. Thomas. A mixed finite element method for 2nd order elliptic problems. *math aspects of finite element methods*, 606:292–315, 1977.

[43] J. E. Roberts and J. M. Thomas. Mixed and hybrid methods.

[44] T. F. Russel and M. F. Wheeler. Finite element and finte difference methods for continuous flows in porous media. *SIAM*, 1:35–106, 1983.

[45] The MELT seismic team. Imaging the deep seismic structure beneath a mid-ocean ridge: the MELT experiement. *Science*, 280, 1998.

[46] N. Sleep. Tapping of melt by veins and dikes. *J. Geophys. Res.*, 93(10):255–272, 1988.

[47] E.A. Spiegel and G. Veronis. On the Boussinesq approximation for a compressible fluid. *Astophysical J.*, 131:442–447, 1960.

[48] M. Spiegelman. Flow in deformable porous media. *J. Fluid Mech.*, 247:17–38, 39–63, 1993.

[49] M. Spiegelman and D. McKenzie. Simple 2-D models for melt extraction at mid-ocean ridges and island arcs. *Earth and planetary science letters*, 83:137–152, 1987.

[50] B. Steinberger and A. R. Calderwood. Models of large-scale viscous flow in the earth's mantle with constraints from mineral physics and surface observations. *Geophysical J. International*, 167(3):1461–1481, 2006.

[51] A. L. Taicher, T. Arbogast, and M. A. Hesse. A mixed framework for two-phase Darcy-Stokes mixtures. *In preparation*, 14.

[52] C. J. Van Der Veen. Fundamentals of glacier dynamics. 2013.

[53] N. Vonbargen and H. S. Waff. Permeabilities, interfacial-areas and curvatures of partially molten systems - results of numerical computation of equilibrium microstructures. *J. Geophysical Res.*, 91(B9):9261–9276, 1986.

[54] A. Weiser and M. F. Wheeler. On convergence of block-centered finite-differences for elliptic problems. *SIAM. J. Numer. Anal.*, 25:351–375, 1988.

[55] W. Zhu, G. Gaetani, F. Fusseis, L Montesi, and F. De Carlo. Microtomography of partially molten rocks: three dimensional melt distribution in mantle peridotite. *Science*, 332, 2011.